

## **Developing a coral proxy system model to compare coral and climate model estimates of changes in paleo-ENSO variability**

**A. E. Lawman<sup>1,2\*</sup>, J. W. Partin<sup>1</sup>, S. G. Dee<sup>3</sup>, C. A. Casadio<sup>1</sup>, P. Di Nezio<sup>1</sup>, T. M. Quinn<sup>1,2</sup>**

<sup>1</sup>Institute for Geophysics, Jackson School of Geosciences, The University of Texas at Austin, Austin, TX, USA. <sup>2</sup>Department of Geological Sciences, Jackson School of Geosciences, The University of Texas at Austin, Austin, TX, USA. <sup>3</sup>Department of Earth, Environmental and Planetary Sciences, Rice University, Houston, TX, USA.

\*Corresponding author: Allison Lawman ([alawman@utexas.edu](mailto:alawman@utexas.edu))

**This is a preprint submitted to EarthArXiv. The citation for the published, peer-reviewed version is provided below:**

Lawman, A., Partin, J., Dee, S., Casadio, C., Di Nezio, P., Quinn, T. (2020), Developing a coral proxy system model to compare coral and climate model estimates of changes in paleo-ENSO variability. *Paleoceanography and Paleoclimatology*, 35, e2019PA003836. doi: 10.1029/2019PA003836.

### **Key Points:**

- We present a new coral proxy system model to facilitate comparison between proxy observations and climate model output
- Analytical and calibration errors, variable growth rates, and age modeling uncertainties all have measurable impacts on interannual variance
- The relative importance of different uncertainties on interannual variance are site-dependent

## 1 **Abstract**

2 Coral records of surface-ocean conditions extend our knowledge of interannual El Niño-Southern  
3 Oscillation (ENSO) variability into the pre-instrumental period. That said, the wide range of natural  
4 variability within the climate system as well as multiple sources of uncertainties inherent to the coral  
5 archive produce challenges for the paleoclimate community to detect forced changes in ENSO using  
6 coral geochemical records. We present a new coral proxy system model (PSM) of intermediate  
7 complexity, geared toward the evaluation of changes in interannual variance. Our coral PSM adds  
8 additional layers of complexity to previously published transfer functions of sensor models that  
9 describe how the archive responds to sea-surface temperature (SST) and salinity. We use SST and  
10 salinity output from the Community Earth System Model Last Millennium Ensemble 850 control to  
11 model coral oxygen isotopic ratios and SST derived from Sr/Ca. We present a detailed analysis of our  
12 PSM using climate model output for sites in the central and southwest Pacific before extending the  
13 analyses to span the broader tropical Pacific. We demonstrate how variable growth rates, analytical  
14 and calibration errors, and age model assumptions systematically impact estimates of interannual  
15 variance, and show that the relative magnitude of the change in interannual variance is location  
16 dependent. Importantly, however, we find that even with the added uncertainties in our PSM, corals  
17 from many circum-Pacific locations are broadly able to capture decadal and longer (decadal+)  
18 changes in ENSO variability. Our code is publicly available on GitHub to facilitate future  
19 comparisons between model output and coral proxy data.

## 20 21 **Plain Language Summary**

22 Climate scientists use the chemistry of coral skeletons to study past tropical climate conditions. The  
23 elemental ratio of strontium to calcium (Sr/Ca) and the oxygen isotopic composition ( $\delta^{18}\text{O}$ ) in the  
24 coral skeleton are used to reconstruct past sea-surface temperature and salinity. Coral Sr/Ca varies in  
25 response to changes in sea-surface temperature, whereas coral  $\delta^{18}\text{O}$  records both changes in  
26 temperature and salinity. Individual corals provide tens to hundreds of years of climate information  
27 from the tropical oceans. They are well-suited for studying variability related to the El Niño-Southern  
28 Oscillation (ENSO), a climate phenomenon that impacts global temperature and rainfall patterns  
29 every few years. We rely on both climate proxy data and simulations from global climate models to  
30 study changes in ENSO variability in the past. Nevertheless, it is difficult to directly compare proxy  
31 data with climate model output due to the imperfect nature of how the climate signal is recorded in  
32 the coral skeleton. Proxy system models are a tool designed to help bridge the gap between climate  
33 information recorded in corals and climate model output. In this study, we develop a coral proxy  
34 system model to demonstrate how different processes impact a coral's ability to record changes in  
35 ENSO variability.

## 36 37 **1 Introduction**

38 Geochemical records from massive corals provide decades to centuries of sub-annually resolved  
39 proxy climate data from the tropical oceans [Fairbanks *et al.*, 1997; Gagan *et al.*, 2000; Grottoli and  
40 Eakin, 2007; Lough, 2010]. The ratio of strontium to calcium (Sr/Ca) and the oxygen isotopic  
41 composition ( $\delta^{18}\text{O}$ ) of coral skeletal material are established climate proxies [Fairbanks *et al.*, 1997;  
42 Corrège, 2006; Lough, 2010; DeLong *et al.*, 2013]. Sea-surface temperature (SST) exerts the  
43 dominant climate control on coral Sr/Ca [Weber, 1973; Smith *et al.*, 1979; Beck *et al.*, 1992], whereas  
44 coral  $\delta^{18}\text{O}$  is jointly influenced by SST and the oxygen isotopic composition of seawater ( $\delta^{18}\text{O}_{\text{sw}}$ )  
45 [Weber and Woodhead, 1972; Gagan *et al.*, 1998; Ren *et al.*, 2003], the latter of which is impacted  
46 by similar processes as sea-surface salinity (e.g., rainfall, evaporation, advection of different water

47 masses, and freshwater runoff) [*LeGrande and Schmidt, 2006*]. One of the major climate applications  
48 of geochemical records from tropical Pacific corals is to provide insight about El Niño-Southern  
49 Oscillation (ENSO) variability during pre-instrumental times.

50

51 ENSO is the leading mode of interannual climate variability and has global impacts on temperature  
52 and precipitation patterns [*Bjerknes, 1969; Ropelewski and Halpert, 1987*]. SST anomalies (SSTA)  
53 averaged across the Niño 3.4 region in the central equatorial Pacific (5°N-5°S, 120-170°W) are  
54 canonically used to determine the occurrence of ENSO events [*Trenberth, 1997*]. Observed SSTA  
55 from the Niño 3.4 region shows an increase in the magnitude and frequency of extreme ENSO events  
56 over the last few decades [*Trenberth and Hoar, 1996; Bin Wang et al., 2019*]. That said, instrumental  
57 observations are of insufficient length [*Fairbanks et al., 1997; Deser et al., 2010*] to characterize the  
58 full range of natural variability in ENSO [*Wittenberg, 2009*]. Furthermore, tropical climate variability  
59 is a major source of uncertainty in climate model simulations that project how the Earth will respond  
60 to increasing greenhouse gas emissions [*Collins et al., 2013; Chung et al., 2019*]. Different model  
61 simulations of future changes in ENSO differ widely in their response to the external forcing of  
62 increasing greenhouse gas emissions, as well as in their simulated range of natural (unforced)  
63 variability within the climate system [*Collins et al., 2010; DiNezio et al., 2013; Bellenger et al., 2014;*  
64 *Cai et al., 2014; 2015*]. Uncertainties about ENSO projections for the future are a motivation to study  
65 ENSO under past climate conditions when the Earth experienced different background conditions.  
66 Coral-based climate records that overlap with, and extend beyond, the instrumental period provide  
67 important tests of climate model simulations of ENSO [*Gagan et al., 2000; Cobb et al., 2013; Schmidt*  
68 *et al., 2014; Emile-Geay et al., 2016*].

69

70 There are, however, several sources of uncertainty that impact our ability to understand past changes  
71 in ENSO variability. These sources of uncertainty include those due to the climate system as well as  
72 those from the coral archive. ENSO behavior can vary in the absence of forcings external to the  
73 climate system [*Wittenberg, 2009; Deser et al., 2012*], making it difficult to separate internally versus  
74 externally driven changes in variability from short coral records. Clear links between the climate  
75 variability experienced at an individual reef site and ENSO must be established through observational  
76 study. Lastly, the coral archive itself impacts how a climate signal is recorded. Sources of climate and  
77 coral-related uncertainties that impact our ability to characterize past changes in ENSO variability  
78 include, but are not limited to:

- 79 1. The fidelity of a point-source location to capture regional changes in ENSO variability
- 80 2. The range of natural variability within the climate system
- 81 3. The ability of coral Sr/Ca and  $\delta^{18}\text{O}$  to record ocean-climate variables
- 82 4. Uncertainties in the coral archive that may obscure the climate signal of interest (e.g., variable  
83 growth rates)
- 84 5. Proxy observation uncertainties (e.g., analytical, calibration, dating, and age-model errors)

85

86 A proxy system model (PSM) addresses points 3-5 of the uncertainties listed above, and serves as an  
87 important bridge between proxy data and observations or model output [and see *Evans et al., 2013;*  
88 *Dee et al., 2015* for a review]. PSMs mathematically model how different processes impact a climate  
89 signal that emerges from the proxy data. Typically, paleoclimate proxy data is used to reconstruct a  
90 climate variable (e.g., SST) using empirically determined calibration equations [*Corrège, 2006*].  
91 Conversely, forward modeling using a PSM broadcasts observations or climate model output into  
92 pseudoproxy time series, providing a forward estimate of the proxy signal [*Evans et al., 2013; Dee et*  
93 *al., 2015*]. Previous coral proxy system modeling work developed a transfer function of the sensor

94 model to forward model pseudocoral  $\delta^{18}\text{O}$  as a linear combination of SST and sea-surface salinity  
95 (SSS) [Brown *et al.*, 2008; Thompson *et al.*, 2011]:

$$\delta^{18}\text{O}_{\text{pseudocoral}} = a_1\text{SST} + a_2\text{SSS} \quad (\text{from [Thompson et al., 2011]})$$

96  
97  
98  
99 The coefficient  $a_1$  is based on the inverse SST dependence that arises from thermodynamic  
100 fractionation [Epstein *et al.*, 1953], and the coefficient  $a_2$  is based on observed  $\delta^{18}\text{O}_{\text{sw}}$ -SSS  
101 relationships [LeGrande and Schmidt, 2006]; (see section 2.3.1). Coral PSMs have been employed in  
102 previous work to compare a suite of coral  $\delta^{18}\text{O}$  records [Ault *et al.*, 2009] with pseudocorals generated  
103 from instrumental observations and climate model simulations for the 20<sup>th</sup> century [Thompson *et al.*,  
104 2011]. Coral PSMs have also been used to quantify uncertainties in climate signal interpretation [Dee  
105 *et al.*, 2015], including errors in coral-based ENSO amplitude [Russon *et al.*, 2015] or ENSO  
106 variability estimates [Stevenson *et al.*, 2013].

107  
108 In this study, we add additional layers of complexity to these previously published transfer functions  
109 that describe how the coral archive responds to SST and salinity [Thompson *et al.*, 2011; Dee *et al.*,  
110 2015]. We use surface temperature and salinity output from the Community Earth System Model Last  
111 Millennium Ensemble (CESM-LME) [Otto-Bliesner *et al.*, 2016] to model pseudocoral  $\delta^{18}\text{O}$  and  
112 SST derived from Sr/Ca ( $\text{SST}_{\text{Sr/Ca}}$ ). The model is applied to two sites in the central (Kiritimati) and  
113 southwest Pacific (Vanuatu) as case studies to demonstrate the subcomponents of our PSM, and then  
114 our pseudoproxy network is expanded to span the broader tropical Pacific.

115  
116 Our specific objective is to identify how uncertainties associated with 1) analytical and calibration  
117 errors, 2) variable growth rates, and 3) age modeling assumptions impact interannual variance and  
118 the ability of a pseudocoral to capture decadal and longer (decadal+) changes in ENSO variability.  
119 Although precise month-to-month SST variations in the Niño 3.4 region are a common target for  
120 ENSO studies, this is challenging for paleoclimate studies because of temporal uncertainties in proxy  
121 records [Emile-Geay *et al.*, 2013a; 2013b]. Thus, we focus on how various coral processes impact  
122 estimates of decadal+ changes in ENSO variability in coral paleoclimate reconstructions. Section 2  
123 describes the coral PSM framework and the various sub-models. Section 3 provides results and  
124 discusses the impact of the three coral uncertainties on interannual variance, as well as a coral's ability  
125 to capture changes in ENSO variability. The conclusions are provided in Section 4.

## 126 127 **2 A New Coral PSM**

128 Proxy system models are tools used to evaluate the contribution of local environmental signals and  
129 their variability on the measured proxy record, and have been widely employed to assess uncertainties  
130 in paleoclimate data for a variety of geological archives and proxy types [e.g., Herron and Langway,  
131 1980; Johnson *et al.*, 2013; Roden *et al.*, 2000; Evans *et al.*, 2007; Thompson *et al.*, 2011; Evans *et al.*,  
132 2013; Partin *et al.*, 2013; Comboul *et al.*, 2014; Dee *et al.*, 2015; Wong *et al.*, 2015; Dee *et al.*,  
133 2018]. This study introduces a coral PSM that builds upon previous work and adds new layers of  
134 complexity by incorporating uncertainties related to:

- 135 1. Variable growth rates experienced when sampling a coral along the maximum growth axis
- 136 2. Analytical and calibration errors
- 137 3. Seasonal chronological uncertainties associated with transforming coral geochemical data  
138 from the depth to the time domain (herein referred to as the age model)

139

140 The additions presented here adhere to the PSM sub-model framework described in *Evans et al.*  
141 [2013] where a PSM consists of environment, sensor, archive, and observation subcomponents  
142 (Figure 1). This is the first study to include an archive-based coral PSM with a variable growth rate  
143 algorithm. Analytical and calibration errors as well as the age model assumptions fall within the  
144 observation subcomponent of the PSM.

145  
146 Our coral PSM allows the user to run different permutations of the various archive and observation  
147 sub-models (Figure 1 arrows). For example, to isolate the impact of age modeling assumptions the  
148 user can solely perturb pseudocoral  $\delta^{18}\text{O}$  or SST derived from Sr/Ca ( $\text{SST}_{\text{Sr/Ca}}$ ) with the age model  
149 algorithm (Figure 1). The full coral PSM herein refers to first perturbing the coral sensor output with  
150 the variable growth rate algorithm, followed by analytical and/or calibration errors, and then the age  
151 modeling algorithm (follow the center arrows in Figure 1). With this framework we can also use  
152 Monte Carlo methods to generate many realizations of pseudocoral  $\delta^{18}\text{O}$  or  $\text{SST}_{\text{Sr/Ca}}$  in order to  
153 quantify the uncertainty in coral-inferred estimates of variance. This study focuses on how various  
154 uncertainties impact interannual variance, a leading timescale of interest for coral-based  
155 paleoclimatology.

## 156 157 **2.1 Coral PSM Input Variables**

158 In this study, we use surface temperature and salinity output from the CESM-LME 850 control [*Otto-*  
159 *Bliesner et al.*, 2016] as the environmental inputs to demonstrate how the new coral PSM quantifies  
160 how the coral archive affects interannual variance in coral climate reconstructions. The environmental  
161 inputs for the coral PSM are SST, sea-surface salinity (SSS), and  $\delta^{18}\text{O}_{\text{sw}}$  if available (Figure 1). These  
162 climate variables can be from instrumental observations or model output, though we choose to only  
163 use model output for this study. In this study, we use surface temperature and salinity output from the  
164 CESM-LME 850 control [*Otto-Bliesner et al.*, 2016] as the environmental inputs. The CESM-LME  
165 uses version 1.1 of CESM with the Community Atmospheric Model Version 5, CESM1(CAM5)  
166 [*Hurrell et al.*, 2013]. The CESM-LME has  $\sim 2^\circ$  resolution for the atmosphere and  $\sim 1^\circ$  resolution for  
167 the ocean. We use the 2-meter surface temperature output from the atmospheric model (CAM5),  
168 which will equal SST over the ocean. The surface salinity (0-10 m depth) output was gridded to the  
169 same  $\sim 2^\circ$  resolution as the atmospheric components to facilitate forward modeling coral  $\delta^{18}\text{O}$  as a  
170 linear combination of SST and SSS (Section 2.3.1).

171  
172 We focus on CESM as this model exhibits realistic ENSO dynamics [*DiNezio et al.*, 2017; *Wu et al.*,  
173 2019], and there are no changes in external forcing throughout the CESM-LME 850 control  
174 simulation [*Otto-Bliesner et al.*, 2016], hence all of the changes in interannual variability within the  
175 simulation are unforced. The 850 control is also sufficiently long (1156 years) to sample across a  
176 wide range of internal variability, which is not possible in the short instrumental record [*Wittenberg,*  
177 *2009; Stevenson et al.*, 2010]. Implementing our new coral PSM using CESM-LME allows us to  
178 quantify how different assumptions and uncertainties inherent to the coral archive impact interannual  
179 variance in a geochemical time series, while minimizing the impacts of a stationarity assumption by  
180 removing any effects that could result from external forcing. Here, the proxy uncertainties are  
181 evaluated within the simulated climate generated by the model, such that we constrain ourselves to  
182 the CESM-LME's simulation of tropical Pacific variability, including ENSO. Due to model biases,  
183 the spatial patterns observed using the CESM-LME may not be strictly comparable to other models  
184 or instrumental observations, but the general results about how the three coral uncertainties impact  
185 interannual variability within the framework of CESM are broadly applicable to other environmental  
186 inputs. Due to model biases, we caution future users of the PSM to avoid direct point-to-point



187 comparisons between coral observations and climate model output from a single grid point. Care must  
188 be taken to select a region in the model that best matches the climate conditions observed at the proxy  
189 site.

190

## 191 **2.2 Case Studies: Kiritimati and Vanuatu**

192 ENSO involves basin-scale atmospheric and oceanic interactions across the tropical Pacific, with the  
193 largest interannual signal occurring in the central and eastern equatorial Pacific. In contrast, coral  
194 heads are point-source locations (on the scale of meters) that are impacted by both regional and local  
195 climate processes. Thus, there needs to be a demonstrated link between climate variability at the  
196 individual reef site and ENSO. Modern and paleo-ENSO studies have targeted sites within the Niño  
197 3.4 region [Cobb *et al.*, 2013; Emile-Geay *et al.*, 2016], as well as sites in the eastern, western, and  
198 southwest Pacific that are sensitive to changes in ENSO variability [Hereid *et al.*, 2013a]. For  
199 example, the western and southwest Pacific contain a large number of islands that are home to  
200 abundant modern and fossil coral heads for paleoclimate studies [Cole *et al.*, 1993; Kilbourne *et al.*,  
201 2004; Linsley *et al.*, 2006; DeLong *et al.*, 2012; Gorman *et al.*, 2012; Hereid *et al.*, 2013b; Jimenez  
202 *et al.*, 2018; and many others].

203

204 We choose two end-member localities at Kiritimati (2°N, 157°W) and Vanuatu (16°S, 167°E) to  
205 apply our coral PSM for testing how different processes and uncertainties inherent to coral-based  
206 paleoclimatology impact interannual variance. Kiritimati, located in the central equatorial Pacific, has  
207 a small annual cycle and a large interannual response to ENSO, whereas Vanuatu, located within the  
208 South Pacific Convergence Zone, has a larger annual cycle and a smaller interannual response to  
209 ENSO. In all instances, when selecting the environmental input for the coral PSM, we use the model  
210 output from the grid point closest to the selected sites.

211

## 212 **2.3 Coral Sensor Models**

### 213 **2.3.1 Pseudocoral $\delta^{18}\text{O}$**

214 We use the coral sensor model of Thompson *et al.* [2011] to forward model mean-removed  
215 pseudocoral  $\delta^{18}\text{O}$  anomalies ( $\Delta\delta^{18}\text{O}_{\text{pseudocoral}}$ ) as a linear combination of SST and  $\delta^{18}\text{O}_{\text{sw}}$  or salinity  
216 anomalies:

217

$$\Delta\delta^{18}\text{O}_{\text{pseudocoral}} = a_1\Delta\text{SST} + \Delta\delta^{18}\text{O}_{\text{sw}} \text{ (Eq. 1)}$$

218

$$\Delta\delta^{18}\text{O}_{\text{pseudocoral}} = a_1\Delta\text{SST} + a_2\Delta\text{SSS} \text{ (Eq. 2)}$$

219

220

221 The  $\Delta$  symbol indicates the removal of the mean of the full-length SST and SSS/ $\delta^{18}\text{O}_{\text{sw}}$  input time  
222 series such that the resulting  $\delta^{18}\text{O}_{\text{pseudocoral}}$  anomalies are centered around zero. The coefficient  $a_1$  is  
223 based on the inverse SST dependence that arises from thermodynamic fractionation [Epstein *et al.*,  
224 1953]. The temperature dependence for  $\delta^{18}\text{O}$  at individual coral sites may range from -0.10 to -0.34  
225 ‰/°C [Evans *et al.*, 2000], whereas studies that synthesize the results from multiple locations report  
226 values of -0.20 [Evans *et al.*, 2000] and -0.22 [Lough *et al.*, 2004], that are close to the inorganic slope  
227 of -0.22 ‰/°C [Epstein *et al.*, 1953]. Here we use a slope -0.22 ‰/°C for  $a_1$  as used in Thompson *et al.*  
228 *et al.* [2011].

229

230 SSS and  $\delta^{18}\text{O}_{\text{sw}}$  are often assumed to be linearly proportional as they are impacted by similar  
231 precipitation, evaporation, and advection processes [LeGrande and Schmidt, 2006]. We use Eq. 2 and  
232 approximate  $a_2$  using observed  $\delta^{18}\text{O}_{\text{sw}}$ -SSS slopes determined from basin-scale regression analysis

233 [LeGrande and Schmidt, 2006]. Limited  $\delta^{18}\text{O}_{\text{sw}}$  and SSS observations [LeGrande and Schmidt, 2006],  
234 spatiotemporal variability in the  $\delta^{18}\text{O}_{\text{sw}}$ -SSS relationship [Conroy et al., 2017], or sub-grid processes  
235 affecting  $\delta^{18}\text{O}_{\text{sw}}$  [Stevenson et al., 2015] can lead to large errors on interannual variance [Stevenson  
236 et al., 2013; Russon et al., 2015] and hinder direct comparison between forward modeled  
237 pseudocorals and coral proxy observations. That said, since our study focuses on the impact of other  
238 processes on interannual variance we define  $a_2$  as 0.27 for tropical Pacific latitudes north of  $5^\circ\text{S}$  (e.g.,  
239 Kiritimati), and 0.45 for latitudes south of  $5^\circ\text{S}$  (e.g., Vanuatu) as defined in Legrande and Schmidt  
240 [2006].

241

### 242 **2.3.2 Pseudocoral SST Derived from Sr/Ca ( $\text{SST}_{\text{Sr/Ca}}$ )**

243 The inverse relationship between coral Sr/Ca and temperature is an established proxy for  
244 reconstructing SST [Beck et al., 1992; Gagan et al., 2000; Quinn and Sampson, 2002; Corrège, 2006;  
245 Lough, 2010]. Slope values for the linear Sr/Ca-SST transformation typically fall within the  $-0.06 \pm$   
246  $0.01$  ( $\pm 1\sigma$ ) mmol/mol/ $^\circ\text{C}$  range for the Indo-Pacific [Corrège, 2006]. Uncertainties in the Sr/Ca-SST  
247 calibration can yield errors in the SST reconstruction up to  $0.35^\circ\text{C}$  ( $\pm 2\sigma$ ) [Quinn and Sampson, 2002],  
248 although this uncertainty may be larger based on interlaboratory comparisons [Hathorne et al., 2013]  
249 and reproducibility studies [Sayani et al., 2019]. A published coral Sr/Ca sensor model does not exist  
250 at the time of this study but it could be incorporated into our coral PSM framework in the future.  
251 Given that a variety of slope values are published in the literature, in this study we assume that the  
252 original SST input to the coral PSM is a reasonable approximation of SST derived from coral Sr/Ca  
253 ( $\text{SST}_{\text{Sr/Ca}}$ ). This assumption helps circumnavigate some of the challenges associated with developing  
254 a universally applicable coral Sr/Ca sensor model. Importantly, this assumption also helps facilitate  
255 comparison between  $\text{SST}_{\text{Sr/Ca}}$  processed using the coral PSM algorithms and the original, unperturbed  
256 SST output from the model. The error in the Sr/Ca-SST calibration is considered in our PSM, as  
257 further discussed in Section 2.5.1.

258

### 259 **2.4 Coral Archive Model: Variation in Coral Growth Rates**

260 Sub-seasonal resolution is a goal of many coral paleoclimate studies that seek to quantify changes in  
261 interannual variance. However, a coral's growth rate may vary both within and between years. For  
262 example, a *Porites* coral growing an average of 1.2 cm/year would achieve approximately monthly  
263 resolution if sampled in 1 mm increments. Although monthly resolution is targeted, one sample of  
264 coral powder may average 2-3 weeks ( $-2\sigma$ ) of time when the coral is growing faster, or 5-6 weeks  
265 ( $+2\sigma$ ) when the coral is growing slower. Due to variable growth rates, the net effect of equal sampling  
266 in the depth domain will lead to unequal sampling in the time domain. We use our coral PSM to assess  
267 how variations in coral growth impact the variance of a resulting geochemical time series when the  
268 coral is sampled at a fixed sampling resolution (e.g., 1 mm).

269

270 High-precision calipers were used to measure the annual growth rates of 9 modern and fossil *Porites*  
271 cores from Vanuatu to generate a distribution of growth rates with a mean of  $1.2 \pm 0.2$  cm/year ( $\pm 1\sigma$ ).  
272 The measured growth rate values are consistent with the reported average values for *Porites* corals  
273 from other regions of the tropical Pacific [Cobb et al., 2013]. We incorporate variable growth rates  
274 into the coral PSM using an autoregressive order 2, AR(2), model since the measured annual growth  
275 rates are serially correlated and cannot be modeled with an independent error term. The lag 1 and 2  
276 correlation coefficients (0.25 and 0.20, respectively), and the standard deviation (0.2 cm/year) for the  
277 AR(2) model are based on the 9 measured *Porites* corals. The AR(2) model is used to generate a  
278 series of annual growth rates (Figure 2a). The distribution of simulated growth rates (Figure 2b) is  
279 consistent with the measured coral growth rates given a large  $n$ , as the simulated growth rates are

280 pulled from a distribution based on measured growth rates. The parameters for the AR(2) model can  
281 easily be adjusted for different species or for a different median and/or standard deviation of growth  
282 rates.

283

284 A single realization of the AR(2) model provides a transformation from the time to the depth domain.  
285 One random realization for SST and forward modeled  $\Delta\delta^{18}\text{O}_{\text{pseudocoral}}$  is provided at Kiritimati and  
286 Vanuatu as an illustrative example of how the algorithm works (Figure 3a-d). The pseudocoral annual  
287 growth rates are used to stretch and compress the original PSM inputs to mimic how equal sampling  
288 in the depth domain can yield to unequal sampling in the time domain. The net effect of the variable  
289 growth rate algorithm is that the pseudocoral output looks stretched and compressed relative to the  
290 original input. Monte Carlo methods are used to generate  $n$  number of random realizations of the  
291 AR(2) model that are then used to stretch and compress the original, unperturbed SST or  
292  $\Delta\delta^{18}\text{O}_{\text{pseudocoral}}$  input time series  $n$  number of times.

293

## 294 **2.5 Coral Observation Models**

### 295 **2.5.1 Analytical and Calibration Errors**

296 Monte Carlo methods are also used to randomly generate 1000  $\Delta\delta^{18}\text{O}_{\text{pseudocoral}}$  time series perturbed  
297 with analytical errors, and 1000 and SST<sub>Sr/Ca</sub> time series perturbed with the combined impact of  
298 analytical and calibration errors. The analytical and calibration errors are both modeled as Gaussian  
299 white noise, such that they sum accordingly (Figure 3e-h). For  $\Delta\delta^{18}\text{O}_{\text{pseudocoral}}$ , analytical errors are  
300 taken as 0.20‰ ( $\pm 2\sigma$ ), a value typical of laboratory analytical precision. For coral SST<sub>Sr/Ca</sub>, we  
301 incorporate the combined effect of the analytical instrument error, as well as the linear calibration  
302 error associated with transforming coral Sr/Ca into SST. Previous studies identified that the net effect  
303 of analytical and calibration errors can cause uncertainties of  $\sim 0.30^\circ\text{C}$  in Sr/Ca-SST reconstructions  
304 ( $\pm 2\sigma$ ) [Alibert and McCulloch, 1997; Schrag, 1999; Quinn and Sampson, 2002]. The original SST  
305 environmental inputs are thus perturbed with Gaussian white noise that includes the combined impact  
306 of analytical and calibration errors ( $0.30^\circ\text{C}$ ,  $\pm 2\sigma$ ). The error term for SST<sub>Sr/Ca</sub> can be changed within  
307 the PSM framework to account for larger analytical and calibration error terms [Corrège, 2006;  
308 DeLong et al., 2013; Hathorne et al., 2013; Sayani et al., 2019] based on user need.

309

### 310 **2.5.2 Monthly Coral Chronology**

311 The creation of an age model in coral paleoclimate studies requires the measured climate indicator  
312 (proxy) be transformed from the depth into the time domain. We investigate the impact of key age  
313 modeling assumptions on interannual variance. We note that the assumptions discussed here are  
314 different than the uncertainties that arise from missing or double counting years in annually banded  
315 archives [Comboul et al., 2014] that have been previously incorporated into existing PSM frameworks  
316 [Dee et al., 2015].

317

318 The chronology for coral data that has been sampled at approximately monthly resolution typically  
319 uses annual cyclicity in the data to constrain a relative chronology. For coral Sr/Ca, larger values  
320 indicate cooler temperatures, while smaller values indicate warmer temperatures [Weber, 1973; Smith  
321 et al., 1979; Beck et al., 1992]. For coral  $\delta^{18}\text{O}$ , surface conditions often constructively interfere such  
322 that more negative extrema indicate warmer and/or fresher conditions, while more positive extrema  
323 indicate cooler and/or more saline conditions [Fairbanks et al., 1997; Corrège, 2006; Lough, 2010],  
324 though exceptions may occur. When constructing an age model, the peaks and troughs in the coral  
325 geochemical data are assigned a specific calendar month based on knowledge about the climatology



326 at the site. For example, if the site on average experiences the warmest SST during June and the  
327 coolest SST during December, then the Sr/Ca minima are assigned the month of June and the Sr/Ca  
328 maxima are assigned the month of December. Coral  $\delta^{18}\text{O}$  is a function of SST and the  $\delta^{18}\text{O}_{\text{sw}}$  (SSS),  
329 so the input for the climatological extrema in  $\delta^{18}\text{O}$  may be dominated by temperature, salinity, or a  
330 combination of the two variables. Once identifying all the geochemical extrema, the coral data are  
331 interpolated to achieve evenly spaced monthly resolution. The resulting relative age model can be  
332 further refined by overlapping the coral record with instrumental observations (modern corals only)  
333 and with high-precision  $^{230}\text{Th}$  ages that serve as absolute chronological constraints with errors  $\sim 1\%$   
334 of the age [*Shen et al.*, 2012; *Cheng et al.*, 2013].

335  
336 We developed a MATLAB® algorithm to standardize coral age modeling and have made it publicly  
337 available. The age-model algorithm assumes that the coral was optimally sampled along the  
338 maximum growth axis [*DeLong et al.*, 2013] at sub-seasonal resolution. The coral geochemical data  
339 (in the depth or sample-number domain) is the first required input for the age model algorithm. There  
340 are several additional inputs supplied by the user based on their individual lab procedures. First, the  
341 user must provide the estimated sampling resolution of the coral (e.g., 10-14 samples per annual  
342 growth band). The user must also supply the calendar month that corresponds to the annual peaks and  
343 trough in the geochemical data. For Sr/Ca (or  $\text{SST}_{\text{Sr/Ca}}$  as in this study), this input would be the  
344 climatological warmest and coolest months at the coral site. The climatological month assignment  
345 can be determined from instrumental observations or model output for past time intervals when the  
346 annual cycle is not known. The target temporal resolution for the age modeled output defaults to  
347 monthly resolution (12 points/year), but this parameter can be changed by the user if desired.

348  
349 We demonstrate the utility of the age model algorithm using SST from the grid points nearest to  
350 Vanuatu and Kiritimati as illustrative examples (Figures 4-5). The age modeling approach for  
351  $\Delta\delta^{18}\text{O}_{\text{pseudocoral}}$  is identical and produces similar results (Supporting Figures 1-2). The age model uses  
352 a standard peak finding algorithm in the MATLAB® software (findpeaks) to identify local minima  
353 and maxima (i.e., inflection points) in the geochemical data (Figures 4c and 5c), herein referred to as  
354 critical points. To identify the critical points the input coral data is first 2-month low-pass filtered to  
355 smooth out high frequency noise and better-illuminate the annual cyclicity in the data. The peak  
356 finding algorithm then finds all of the peaks and troughs in the low-pass filtered data, and then ranks  
357 the critical points by their prominence (i.e., height) as well as their location relative to other prominent  
358 extrema. This ranking scheme ensures that the critical points are not spaced too closely or too far  
359 apart given the original sampling resolution of the data. The locations of the highest ranked  
360 peaks/troughs in the low-pass filtered time series are then mapped to the original input data set. The  
361 selected critical points are then assigned a calendar month based on the climatological input (Figure  
362 4a and Figure 5a). The data is then interpolated to monthly resolution using the geochemical extrema  
363 as tie points (Figures 4f and 5f). Our interpolation scheme uses a piecewise linear transformation  
364 [*Fritsch et al.*, 1980].

365  
366 The algorithm also contains an option to constrain the number of years based on an approximate  
367 number of annual density bands visible in a coral's X-ray image. The number of years constraint is  
368 often not necessary for sites with a clear annual cycle (e.g., the southwest Pacific), but may be  
369 necessary for sites with a small and/or noisy annual cycle (e.g., the equatorial Pacific). The age-model  
370 algorithm is deterministic, meaning that for a given Sr/Ca or  $\delta^{18}\text{O}$  input series the age model will find  
371 a single solution that meets the constraints provided by the user. In the context of the full coral PSM  
372 presented here, multiple realizations of age modeled pseudocoral output can be generated by first  
373 perturbing the PSM input with the variable growth rate algorithm (Section 2.4). Alternatively, the

374 user can follow the protocol of the *Comboul et al.* [2014] banded age model and perturb the number  
375 of years constraint within error.

376

### 377 **3 Results and Discussion**

378 After developing the sub-models of our coral PSM, including the three additions that model variable  
379 growth rates in the context of sampling, analytical and calibration errors, and age model assumptions,  
380 we now apply the model to constrain the climatic impacts. These three sources of uncertainty alter  
381 the input climate signals and impact estimates of interannual variance and ENSO variability inferred  
382 from the pseudocorals. Tropical reefs are point sources for paleoclimate reconstructions; by contrast,  
383 with climate model output the coral PSM can be run at every grid point in the tropical Pacific to  
384 identify regional patterns. Broad regions of the tropical Pacific exhibit distinct patterns when the  
385 original environmental inputs are perturbed using the coral PSM. We separate the identified patterns  
386 into three sub-sections: changes in the standard deviation of monthly anomalies as recorded by corals,  
387 decadal and longer changes in ENSO variability, and decadal and longer changes in ENSO variability  
388 as recorded by corals.

389

#### 390 **3.1 Quantifying Changes in Interannual Variability: Monthly Standard Deviation**

391 The percent change in standard deviation between the perturbed pseudocorals and the original  
392 (unperturbed) SST or  $\Delta\delta^{18}\text{O}_{\text{pseudocoral}}$  climatology-removed anomalies is a method used to quantify  
393 changes in interannual variance. The percent difference between the unperturbed anomalies and the  
394 anomalies that result from that PSM (Figure 6) is calculated using the median standard deviation  
395 value for  $n$  realizations of the perturbed pseudocoral monthly anomaly time series. The percent change  
396 in standard deviation highlights site dependencies in the results. The changes in interannual variance  
397 between the original environmental inputs and the coral PSM output at a given location is linked to  
398 both the amplitude of the interannual signal and the annual cycle. Analytical and calibration errors  
399 (Section 2.5.1) cause a systematic increase in interannual variance for pseudocoral SST<sub>Sr/Ca</sub> (Figure  
400 6b) and  $\Delta\delta^{18}\text{O}_{\text{pseudocoral}}$  (Figure 6f) compared to the original environmental inputs. Regions of the  
401 Pacific with a large interannual signal (Figure 6a, 6e) are less impacted by analytical/calibration errors  
402 compared to regions with a smaller interannual signal.

403

404 For the age modeling assumptions, we first assess how the algorithm (Section 2.5.2) impacts  
405 interannual variance locally at Kiritimati and Vanuatu before extending the analysis to the broader  
406 tropical Pacific. SST from the grid points nearest to Vanuatu and Kiritimati are provided as illustrative  
407 examples (Figures 4-5; Section 2.5.2). The results age for  $\Delta\delta^{18}\text{O}_{\text{pseudocoral}}$  are similar (Supporting  
408 Figures 1-2). Simulated SST at Vanuatu shows a clear annual cycle with the climatological warmest  
409 month occurring in February and the climatological coolest month in August (Figure 4a). The  
410 algorithm does well in identifying the timing of the austral warm/cool season peaks at Vanuatu  
411 (Figure 4c, black circles). The algorithm assigns the critical points the climatological warmest  
412 (February) and coolest (August) months, and the data is linearly interpolated between the critical  
413 points to generate the age modeled time series (Figure 4f). At Kiritimati, where the annual cycle is  
414 smaller (Figure 5a), the algorithm encounters more difficulties in identifying seasonal extrema due to  
415 the relatively large amplitude of interannual variability, as compared to the amplitude of the seasonal  
416 cycle (Figure 5b, Figure 5c). Uncertainty in the age model of a coral record results when the common  
417 assumption that the months of the climatological extrema do not change is violated.

418

419 To show how this uncertainty manifests, we show the spread in the distribution of the warmest and coolest  
420 months. Although February and August are climatologically the warmest and coolest months at Vanuatu, there

421 are years in which other months are the warmest or coolest (Figure 4b). That said, the overall spread in the  
422 distribution of the warmest and coolest months at Vanuatu (Figure 4b) is narrow. Since the distribution is  
423 narrow the age model algorithm has more success in identifying the correct calendar month in the extrema in  
424 the timeseries. That said, there is still an incorrect month assignment in the age model. For example, March is  
425 the actual warmest month in model year 4, but the age model algorithm assigns the month of February to the  
426 SST peak (Figure 4c). In contrast, the distribution of the simulated warmest/coolest months at Kiritimati  
427 (Figure 5b) is broad, such there is a large error in assigning the correct calendar month to the extrema. In worst-  
428 case scenarios, model years with strong El Niño events have a small, nearly absent annual cycle with SSTs  
429 during boreal winter (December-February) surpassing the climatological summertime maximum values  
430 typically experienced in June. Without constraining the approximate number of years, it is easy to miss weak  
431 troughs during boreal winters with El Niño events, and therefore miss years. These age model assumptions can  
432 yield large differences (~10-30%) in interannual variance when the climatology of the age modeled time series  
433 (Figure 5d, 5f) is removed from incorrectly assigned months to generate SST anomalies (Figure 5g).

434  
435 Globally, the increase in annual cycle regularity induced by the age model (Section 2.5.2) broadly  
436 tends to cause a decrease in interannual variance across most of the tropical Pacific (Figures 6d, 6h).  
437 The largest percent change in standard deviation occurs in the central Pacific and eastern Pacific cold  
438 tongue regions where ENSO events can lead to climatologically coolest months that are warmer than  
439 the climatologically warmest months. It is thus difficult to identify a trough in the geochemical data  
440 and accurately assign a month to the data when age modeling (Section 2.5.2). The age model effects  
441 are particularly exacerbated in the CESM-LME due to biases in the amplitude of ENSO events [Otto-  
442 Bliesner *et al.*, 2016]. Conversely, pseudocorals generated at sites with a larger annual cycle and less  
443 variable distribution of warmest and coolest months have a smaller reduction in interannual variance  
444 compared to the original environmental input (Figures 6d, 6h). Outside of the tropics, however, sites  
445 that have multiple consecutive months with approximately the same average SST value experience  
446 an increase in variance (Figure 6d). For a given site, the magnitude of the percent change is typically  
447 larger for  $\Delta\delta^{18}\text{O}_{\text{pseudocoral}}$  compared to SST given that  $\delta^{18}\text{O}$  is multivariate and may have contributions  
448 from SSS that may be a few months out of phase with SST [e.g., Gorman *et al.*, 2012] (Figure 6d  
449 versus 6h).

450  
451 The percent change in standard deviation for the full coral PSM (Figure 7) reveals the tradeoff  
452 between interannual variability and the amplitude of the annual cycle. At locations with the strongest  
453 interannual signal (equatorial sites), the loss of variance due to the age model assumptions, i.e.  
454 incorrect months assigned to extrema, exerts the dominant influence on interannual variance for  
455 pseudocoral SST<sub>Sr/Ca</sub> (Figure 7a) and  $\delta^{18}\text{O}$  (Figure 7b). Although age model uncertainty also causes  
456 a decrease in variance in regions like the southwest Pacific, the relative magnitude of the change is  
457 compensated by the increase in variance that results from analytical and calibration errors. Our results  
458 highlight that the different processes and assumptions inherent to coral-based studies exert sizable  
459 impacts on pseudocoral interannual variance, and that the relative contributions are site dependent.  
460 While changes in the monthly standard deviation of an individual anomaly time series can show  
461 longer term changes in ENSO [Wittenberg, 2009], uncertainties in coral climate reconstructions  
462 [Emile-Geay *et al.*, 2013a; 2013b] preclude such a reconstruction back in time, thus warranting an  
463 alternative metric for paleo-ENSO studies.

### 464 465 **3.2 Quantifying Changes in ENSO Variability: Decadal+**

466 This section evaluates the impact of coral uncertainties on reconstructing changes in ENSO variability  
467 through time. Although precise month-to-month variations of SST in the Niño 3.4 region are a sought-  
468 after target for ENSO studies, this is difficult to reconstruct back in time using a limited number of

469 coral proxy records with age uncertainties. Previous studies have used sophisticated statistical  
470 techniques on corals from the last millennium and still had an appreciable degree of uncertainty in  
471 the reconstruction [Emile-Geay *et al.*, 2013a; 2013b]. Fossil corals with absolute age errors on the  
472 order of 1% make a month-to-month reconstruction virtually impossible on  $10^3$ -year and longer  
473 timescales. We address this challenge by building upon the procedure suggested in Trenberth [1997]  
474 and use descriptive statistics and probability theory to quantify changes in ENSO variability on the  
475 timescale of decades. Indeed, the technique of looking at changes in ENSO over windows in the past  
476 has already been employed using corals from the central Pacific [Cobb *et al.*, 2013].

477  
478 We formalize this technique to quantify changes in ENSO variability using climatology-removed SST  
479 anomalies averaged across the Niño 3.4 region (Figure 6, box). The time series is restricted (Figure  
480 8a) to the first 200 years purely for discussion purposes; the entire control run (1156 years) is  
481 employed for the remainder of the analyses. During El Niño (La Niña) events, the Niño 3.4 region  
482 experiences positive (negative) SST anomalies that peak during boreal winter while the western  
483 Pacific experiences negative (positive) excursions [Trenberth, 1997]. Strong El Niño and La Niña  
484 events yield SST anomalies that fall into the tails of the SSTA distribution (Figure 8b, 8c). An increase  
485 in the frequency and/or magnitude of strong ENSO events will increase the width of the SSTA  
486 distribution, and result in a larger standard deviation, a result previously illustrated using corals from  
487 the southwest Pacific [Lawman *et al.*, 2020]. This technique is ideally suited for data that has small  
488 uncertainty in the time domain or in the interpretation.

489  
490 Longer-term changes in the amplitude and frequency of large SST anomalies can occur for decades  
491 or longer intervals (denoted here as decadal+ variability). For example, model years 100-120 (Figure  
492 8a) have smaller amplitude SSTA compared to the frequent large amplitude anomalies in model years  
493 125-150. These changes occur in the absence of external forcing, as this is an unforced model  
494 simulation, and they likely result from complex interactions between ENSO and other internally  
495 driven modes of variability [Wittenberg, 2009; Wittenberg *et al.*, 2014; Sun and Okumura, 2019]. We  
496 quantify decadal+ changes in ENSO variability using the running standard deviation of climatology-  
497 removed monthly SSTA of 20-year windows averaged across the Niño 3.4 region ( $\sigma_{\text{Niño3.4-SSTA}}$ ; Figure  
498 8d) [Okumura *et al.*, 2017]. Larger  $\sigma_{\text{Niño3.4-SSTA}}$  values indicate increased ENSO variability, whereas  
499 smaller  $\sigma_{\text{Niño3.4-SSTA}}$  values indicate decreased ENSO variability during a time interval. The wide range  
500 of internal ENSO variability within the CESM-LME 850 control is reflected in the width of the  
501  $\sigma_{\text{Niño3.4-SSTA}}$  distribution (Figure 8e, 8f). We suggest that longer term, decadal+ changes in ENSO  
502 variability, as reflected by  $\sigma_{\text{Niño3.4-SSTA}}$  and the distribution of standard deviation values (Figure 8f), is  
503 a feasible target for coral-based paleoclimate reconstructions since this metric reduces the influence  
504 of uncertainties, especially temporal uncertainty.

### 505 506 **3.3 Quantifying Changes in ENSO Variability using Corals: Decadal+ with PSM**

507 The coral PSM provides a tool to investigate how various uncertainties not only impact interannual  
508 variability locally, but also how the uncertainties broadly impact the ability of a pseudocoral to  
509 capture decadal+ changes ENSO variability. On interannual timescales, corals from circum-Pacific  
510 locations are influenced by ENSO, local variability, and how corals themselves records climate  
511 (Section 1). Our coral PSM addresses some of these confounding influences by quantifying how  
512 analytical and calibration errors, variable growth rates, and age modeling assumptions modify input  
513 climate signals and impact interannual variance (Section 2). The running standard deviation of  
514 climatology-removed anomalies is presented as an applicable metric in paleoclimate reconstructions  
515 for capturing temporal changes in interannual variability. This running standard deviation also



516 provides a means to provide constraints on the range of internal variability (Section 3.2). A running  
517 or windowed standard deviation is also advantageously poised to handle short (several decades or  
518 less) and/or discontinuous coral records, and has previously been employed for fossil coral records  
519 that are dated to cover snapshots of the last 7000 years (the mid- to late Holocene) [Cobb *et al.*, 2013].  
520

521 The 20-year running standard deviation of  $SST_{Sr/Ca}$  and  $\Delta\delta^{18}O_{pseudocoral}$  anomalies for Kiritimati and  
522 Vanuatu (Figure 9) demonstrate how the various PSM subcomponents impact interannual variance.  
523 This metric also encapsulates information about the range of simulated natural variability. As with  
524 Niño 3.4 monthly SSTA (Figure 8f), the median standard deviation value of the original  
525 environmental inputs (Figure 9 gray boxes) indicates the overall amplitude of interannual variance at  
526 a site, whereas the height of the box and whiskers indicate the range of internal variability. Kiritimati  
527 expectedly has a higher median standard deviation value and a larger spread compared to Vanuatu  
528 given that the site experiences larger interannual SST (Figure 6a) and  $\delta^{18}O$  (Figure 6e) signals.  
529 Perturbing the original SST and  $\Delta\delta^{18}O_{pseudocoral}$  time series at Kiritimati and Vanuatu with analytical  
530 and calibration errors (Section 2.5.1) systematically increases interannual variance (Figure 9 light  
531 blue) as quantified by the shift in the median standard deviation value compared to the original  
532 environmental inputs. Incorrect assumptions about the timing of the warmest and coolest month  
533 assignment in the age model (Section 2.5.2) decreases interannual variance (Figure 9 teal). We do not  
534 isolate the impact of variable growth rates as the algorithm generates a pseudodepth vector (Section  
535 4) that is not readily subset into 20-year windows. Instead, the original environmental input is  
536 perturbed with variable growth rates and then processed by the age model algorithm to generate  
537 multiple realizations (Figure 9 dark blue). The combined influence of variable growth rates and the  
538 age model assumptions causes a systematic decrease in interannual variance at both sites.  
539

540 Although each individual sub-model of the PSM causes a systematic change in interannual variance  
541 at both Kiritimati and Vanuatu, the relative increase or decrease in the interannual signal (median  
542 standard deviation) for the full PSM, or the summation of the effects from the sub-components, is site  
543 dependent. These site dependencies are revealed when expanding the pseudocoral network to the  
544 entire tropical Pacific (Figure 10). For similar reasons discussed in section 3.1, the interannual  
545 variance change is closely related to the ratio between the magnitude of the interannual signal and the  
546 amplitude of the annual cycle.  
547

548 We correlate Niño 3.4 SSTA with the pseudocoral realizations to demonstrate how corals from  
549 locations around the tropical Pacific record changes in ENSO, and begin with the familiar month-to-  
550 month correlation calculation. The month-to-month correlation of local SST or SSS anomalies with  
551 Niño 3.4 SSTA is canonically used to demonstrate the ENSO sensitivity at a site. A consistent pattern  
552 of response over the 1156-year-long control is the temperature relationship between the  
553 central/eastern and western tropical Pacific with monthly SSTA from the Niño 3.4 region (Figure  
554 11a). For example, SSTA in the Niño 3.4 region and the central/eastern Pacific are in phase, during  
555 ENSO events, meaning that when the Niño 3.4 region warms (cools), the central/eastern Pacific also  
556 warms (cools). For example, during an El Niño, SSTA in the Niño 3.4 region and the western Pacific  
557 are out of phase, such SSTA warm in the Niño 3.4 region while SSTA in the western Pacific cool.  
558 Forward modeled monthly  $\Delta\delta^{18}O_{pseudocoral}$ , a function of SST and SSS, also covaries with Niño 3.4  
559 SSTA (Figure 11b) with nearly the same pattern of response as SSTA (Figure 11a). For example,  
560 during El Niño events the central and eastern Pacific experience negative  $\Delta\delta^{18}O_{pseudocoral}$  anomalies  
561 indicating the combined impact of warmer and/or fresher conditions, while the western Pacific  
562 experiences positive  $\Delta\delta^{18}O_{pseudocoral}$  excursions indicative of cooler and/or more saline conditions  
563 [Fairbanks *et al.*, 1997]. As previously discussed, the month-to-month correlation with Niño 3.4



564 SSTA is more applicable for observations or model output with no uncertainty in the time domain.  
565 Some of the uncertainties in coral proxy data can be circumvented by instead shifting the focus to the  
566 ability of a coral to capture ENSO variability on decadal+ timescales (Section 3.2).

567

568 Unlike the month-to-month maps, Niño 3.4 SSTA and the running standard deviation of  $SST_{Sr/Ca}$  and  
569  $\Delta\delta^{18}O_{pseudocoral}$  anomalies on decadal+ timescales are positively correlated across much of the tropical  
570 Pacific (Figure 11c, 11d). The boomerang-shaped monthly SSTA correlation pattern that  
571 distinguishes the western Pacific from the central/eastern Pacific (Figure 11a) essentially disappears  
572 when examining how different regions of the Pacific track decadal+ changes in ENSO variability.  
573 The nodal structure (where the red color changes to blue in the month-to-month calculation), where  
574 the correlation is essentially zero (Figure 11a, 11b), is still apparent in decadal+. In the decadal+  
575 calculation of ENSO variability, a significant positive correlation coefficient between  $\sigma_{Ni\tilde{no}3.4-SSTA}$  and  
576 the running standard deviation of monthly SST (Figure 11c) or  $\Delta\delta^{18}O_{pseudocoral}$  (Figure 11d) anomalies  
577 indicates that when ENSO variability increases or decreases in the Niño 3.4 region, interannual  
578 variability at a given location tends to pace with those changes. The correlation with  $\sigma_{Ni\tilde{no}3.4-SSTA}$  for  
579 the pseudocorals perturbed by the full coral PSM are expectedly smaller than the original PSM inputs,  
580 but importantly, the temporal relationship with changes in SST variability in the Niño 3.4 region is  
581 broadly preserved for both pseudocoral  $SST_{Sr/Ca}$  (Figure 11e) and  $\Delta\delta^{18}O_{pseudocoral}$  (Figure 11f). Despite  
582 all of the calculated coral uncertainties, the correlation with decadal+ changes in ENSO remains  
583 statistically significant at many circum-Pacific locations, particularly those near coral atolls (Figure  
584 11e, 11f). This highlights the strength of corals in their ability to capture decadal+ changes in ENSO  
585 variability.

586

#### 587 **4 Conclusions**

588 The coral PSM presented here advances our knowledge of how corals modify interannual climate  
589 signals and how they record changes in ENSO variability via the decadal+ calculation. This study  
590 builds upon previous work by adding new archive and observation sub-models to the full PSM  
591 framework in order to quantitatively estimate the impact of various non-climatic processes on  
592 interannual variance in the final coral time series. Constraining such information is crucial given that  
593 quantitative estimates of interannual variance is one of the primary applications of coral  
594 paleoclimatology. Our process-based coral PSM explicitly incorporates an archive-based model  
595 (variable growth rates) as well as age modeling assumptions that are used when generating a coral  
596 geochemical time series. This study applies the new PSM framework to the CESM LME 850 control  
597 run, which serves as the environmental input. The long control run allows us to include the impact of  
598 a wide range of internal variability in our analyses, which is not possible using the short instrumental  
599 record. Although we note that the PSM is equally equipped to handle observational data or output  
600 from other climate models. Our tools and algorithms are publicly available to the broader community  
601 to facilitate the comparison of coral geochemical data and observational data or climate model output,  
602 as well as facilitate the reproducibility of our results, via a GitHub repository  
603 (<https://github.com/lawmana/coralPSM>).

604

605 Our results characterize and document the ability of pseudocorals to capture decadal and longer,  
606 which we call decadal+, changes in ENSO variability. Coral proxy records of past ENSO variability  
607 come from a suite of sites spanning the western, central, and eastern tropical Pacific, all of which  
608 have varying signal to noise ratios with respect to ENSO. In some regions of the tropical Pacific, the  
609 combination of different uncertainties can increase or decrease interannual  $SST_{Sr/Ca}$  and  $\delta^{18}O$  variance  
610 by 10-30% (Figures 7 and 10). We identify four broad conclusions from these analyses:

- 611 1. Analytical and calibration errors systematically increase interannual variance.
- 612 2. Seasonal chronological uncertainties associated with transforming coral geochemical data
- 613 from the depth to the time domain acts to decrease interannual variability.
- 614 3. Variable growth rates in conjunction with age modeling assumptions decreases interannual
- 615 variance.
- 616 4. The change in interannual variance at a given location is related to the relative magnitudes of
- 617 the interannual ENSO signal and the amplitude of the annual cycle.
- 618

619 Given that different processes exert sizable impacts on interannual variance, it is therefore most  
620 appropriate to compare coral geochemical data with instrumental observations or climate model  
621 output processed through the new coral PSM. Despite the three uncertainties investigated in this  
622 study, the temporal relationship with changes in SST variability in the Niño 3.4 region is preserved  
623 for both pseudocoral  $SST_{Sr/Ca}$  (Figure 11e) and  $\Delta\delta^{18}O_{pseudocoral}$  (Figure 11f). Importantly, decadal+  
624 changes in forward-modeled interannual  $SST_{Sr/Ca}$  and  $\delta^{18}O$  variability are positively correlated with  
625  $\sigma_{Ni\acute{o}3.4-SSTA}$  across much of the tropical Pacific. Despite all of the added uncertainties in our PSM, at  
626 many locations these processes do not obscure the target climate signal of decadal and longer changes  
627 in ENSO variability and yield statistically significant correlations with  $\sigma_{Ni\acute{o}3.4-SSTA}$ . This increases  
628 confidence that despite these major sources of uncertainties investigated herein, coral geochemical  
629 records from a suite of sites across the tropical Pacific are useful tools to reconstruct changes in ENSO  
630 variability back in time.

631  
632 Quantifying the range of ENSO variability experienced during different background climate states in  
633 the past is critical, as this data can help constrain models that provide projections of how ENSO  
634 variability may change in the future with anthropogenic warming. Paleoclimate reconstructions serve  
635 as important out-of-sample tests of ENSO variability, and climate models that are able to simulate  
636 past changes in ENSO may be better equipped to project how ENSO will change in the future. Proxy  
637 system modeling studies, such as this one that incorporates information from both models and proxy  
638 records, are necessary to compare model estimates of paleo-ENSO variability with coral geochemical  
639 data. By putting climate model output and proxy data on a level playing field, we can reconcile the  
640 agreement between climate models and proxy-inferred responses and take an important step toward  
641 predicting how ENSO will respond to future radiative forcing.

## 642 643 **Acknowledgements**

644 This research was supported by NSF grant #1805874 under the Paleoclimate Perspectives on Climate  
645 Change (P2C2) competition (to J.W.P) and the National Science Foundation Graduate Research  
646 Fellowship Program (to A.E.L). We thank Tim Shanahan and Rowan Martindale for their feedback  
647 on manuscript. We also thank Anthony Krupa for helping A.E.L. measure the annual coral growth  
648 rates used to develop the parameters for the growth rate AR(2) model. We thank the members of the  
649 PAGES Data Assimilation and Proxy System Modeling (DAPS) community for their feedback at the  
650 May 2019 working group meeting.

## 651 652 **Author Contributions**

653 A.E.L led the project and wrote the manuscript. A.E.L generated the figures and interpreted the results  
654 with input and feedback from all authors. A.E.L and C.A.C developed the MATLAB® code for the  
655 growth rate, analytical/calibration, and age model algorithms for the coral PSM with initial counsel  
656 from S.G.D. T.M.Q, J.W.P., S.G.D., and P.D.N. provided regular feedback on the analysis and

657 writing. J.W.P, S.G.D., and P.D.N contributed to the initial inception of the research ideas. All authors  
658 reviewed the manuscript.

659

### 660 **Data Availability**

661 The climate model output used in this study is from the Community Earth System Model Last  
662 Millennium Ensemble (CESM-LME) 850 control simulation [Otto-Bliesner *et al.*, 2016]. The output  
663 is publicly archived on the Earth System Grid as single variable time series:  
664 <https://www.earthsystemgrid.org/>. The monthly atmospheric components are available at:  
665 [https://www.earthsystemgrid.org/dataset/ucar.cgd.cesm4.CESM\\_CAM5\\_LME.atm.proc.monthly\\_a](https://www.earthsystemgrid.org/dataset/ucar.cgd.cesm4.CESM_CAM5_LME.atm.proc.monthly_a)  
666 [ve.html](https://www.earthsystemgrid.org/dataset/ucar.cgd.cesm4.CESM_CAM5_LME.atm.proc.monthly_a). The monthly oceanic components are available at:  
667 [https://www.earthsystemgrid.org/dataset/ucar.cgd.cesm4.CESM\\_CAM5\\_LME.ocn.proc.monthly\\_a](https://www.earthsystemgrid.org/dataset/ucar.cgd.cesm4.CESM_CAM5_LME.ocn.proc.monthly_a)  
668 [ve.html](https://www.earthsystemgrid.org/dataset/ucar.cgd.cesm4.CESM_CAM5_LME.ocn.proc.monthly_a).

669

### 670 **Code Availability**

671 The MATLAB® codes for the coral PSM algorithms that contributed to the analysis and results in  
672 this study are publicly available on the GitHub repository for the lead author:  
673 <https://github.com/lawmana/coralPSM>. We also acknowledge the use the Climate Data Toolbox  
674 (CDT) for MATLAB® [Greene *et al.*, 2019]. The CDT is publicly available on GitHub:  
675 <https://github.com/chadagreene/CDT>. We also acknowledge the use of the cmocean: colormaps for  
676 oceanography toolbox [Thyng *et al.*, 2016] that is available on the MathWorks® File Exchange:  
677 [https://www.mathworks.com/matlabcentral/fileexchange/57773-cmocean-perceptually-uniform-](https://www.mathworks.com/matlabcentral/fileexchange/57773-cmocean-perceptually-uniform-colormaps)  
678 [colormaps](https://www.mathworks.com/matlabcentral/fileexchange/57773-cmocean-perceptually-uniform-colormaps). We also acknowledge the use of M\_Map: A Mapping Package for MATLAB® available  
679 at: <https://www.eoas.ubc.ca/~rich/map.html>.

680

### 681 **Additional Information**

682 **Supporting information** is available for this paper.

683

684 **Competing Financial Interests:** The authors declare no competing financial interests.

685

### 686 **References**

687 Alibert, C., and M. T. McCulloch (1997), Strontium/calcium ratios in modern *Porites* corals from  
688 the Great Barrier Reef as a proxy for sea surface temperature: Calibration of the thermometer  
689 and monitoring of ENSO, *Paleoceanography*, 12(3), 345–363, doi:10.1029/97PA00318.

690 Ault, T. R., J. E. Cole, M. N. Evans, H. Barnett, N. J. Abram, A. W. Tudhope, and B. K. Linsley.  
691 (2009), Intensified decadal variability in tropical climate during the late 19<sup>th</sup> century.  
692 *Geophysical Research Letters*, 36(8), 2209, doi: 10.1029/2008GL036924.

693 Beck, J. W., R. L. Edwards, E. Ito, F. W. Taylor, J. Recy, F. Rougerie, P. Joannot, and C. Henin  
694 (1992), Sea-surface temperature from coral skeletal strontium/calcium ratios, *Science*,  
695 257(5070), 644–647, doi:10.1126/science.257.5070.644.

696 Bellenger, H., E. Guilyardi, J. Leloup, M. Lengaigne, and J. Vialard (2014), ENSO representation in  
697 climate models: from CMIP3 to CMIP5, *Clim Dyn*, 42(7-8), 1999–2018, doi:10.1007/s00382-  
698 013-1783-z.

- 699 Bin Wang, X. Luo, Y.-M. Yang, W. Sun, M. A. Cane, W. Cai, S.-W. Yeh, and J. Liu (2019),  
700 Historical change of El Niño properties sheds light on future changes of extreme El Niño, *Proc*  
701 *Natl Acad Sci USA*, 116(45), 22512–22517, doi:10.1073/pnas.1911130116.
- 702 Bjercknes, J. (1969), Atmospheric teleconnections from the equatorial pacific, *Mon. Weather Rev.*,  
703 97(3), 163–172, doi:10.1175/1520-0493(1969)097<0163:ATFTEP>2.3.CO;2.
- 704 Brown, J., A. W. Tudhope, M. Collins, and H. V. McGregor (2008), Mid-Holocene ENSO: Issues  
705 in quantitative model-proxy data comparisons, *Paleoceanography*, 23(3),  
706 doi:10.1029/2007PA001512.
- 707 Cai, W. et al. (2014), Increasing frequency of extreme El Niño events due to greenhouse warming,  
708 *Nature Climate Change*, 4(2), 111–116, doi:10.1038/nclimate2100.
- 709 Cai, W. et al. (2015), Increased frequency of extreme La Niña events under greenhouse warming,  
710 *Nature Climate Change*, 5(2), 132–137, doi:10.1038/nclimate2492.
- 711 Cheng, H. et al. (2013), Improvements in <sup>230</sup>Th dating, <sup>230</sup>Th and <sup>234</sup>U half-life values, and U–Th  
712 isotopic measurements by multi-collector inductively coupled plasma mass spectrometry, *Earth*  
713 *Planet. Sci. Lett.*, 371-372(C), 82–91, doi:10.1016/j.epsl.2013.04.006.
- 714 Chung, E.-S., A. Timmermann, B. J. Soden, K.-J. Ha, L. Shi, and V. O. John (2019), Reconciling  
715 opposing Walker circulation trends in observations and model projections. *Nature Climate*  
716 *Change*, 1–9, doi: 10.1038/s41558-019-0446-4.
- 717 Cobb, K. M., N. Westphal, H. R. Sayani, J. T. Watson, E. Di Lorenzo, H. Cheng, R. L. Edwards,  
718 and C. D. Charles (2013), Highly variable El Niño–Southern Oscillation throughout the  
719 Holocene, *Science*, 339(6115), 67–70, doi:10.1126/science.1228246.
- 720 Cole, J. E., R. G. Fairbanks, and G. T. Shen (1993), Recent variability in the Southern Oscillation:  
721 Isotopic results from a Tarawa Atoll coral, *Science*, 260(5115), 1790–1793,  
722 doi:10.1126/science.260.5115.1790.
- 723 Collins, M. et al. (2010), The impact of global warming on the tropical Pacific Ocean and El Niño,  
724 *Nature Geosci.*, 3(6), 391–397, doi:10.1038/ngeo868.
- 725 Collins, M., R. Knutti, J. Arblaster, J. Dufresne, T. Fichet, P. Friedlingstein, et al. (2013), Long-  
726 term climate change: Projections, commitments and irreversibility. *Climate Change 2013: The*  
727 *Physical Science Basis. Contribution of Working Group I to the Fifth Assessment Report of the*  
728 *Intergovernmental Panel on Climate Change*, 1–108.
- 729 Comboul, M., J. Emile-Geay, M. N. Evans, N. Mirnateghi, K. M. Cobb, and D. M. Thompson  
730 (2014), A probabilistic model of chronological errors in layer-counted climate proxies:  
731 applications to annually banded coral archives, *Clim. Past*, 10(2), 825–841, doi:10.5194/cp-10-  
732 825-2014.
- 733 Conroy, J. L., D. M. Thompson, K. M. Cobb, D. Noone, S. Rea, and A. N. LeGrande (2017),  
734 Spatiotemporal variability in the  $\delta^{18}\text{O}$ -salinity relationship of seawater across the tropical  
735 Pacific Ocean, *Paleoceanography*, 32(5), 484–497, doi:10.1002/2016PA003073.

- 736 Corrège, T. (2006), Sea surface temperature and salinity reconstruction from coral geochemical  
737 tracers, *Palaeogeogr. Palaeoclimatol. Palaeoecol.*, 232(2-4), 408–428,  
738 doi:10.1016/j.palaeo.2005.10.014.
- 739 Dawdy, D. and N. Matalas (1964), Statistical and Probability Analysis of Hydrologic Data, Part III:  
740 Analysis of Variance, Covariance and Time Series. McGraw-Hill.
- 741 Dee, S., J. Emile-Geay, M. N. Evans, A. Allam, E. J. Steig, and D. M. Thompson (2015), PRYSM:  
742 An open-source framework for PProxY System Modeling, with applications to oxygen-isotope  
743 systems, *J. Adv. Model. Earth Syst.*, 7(3), 1220–1247, doi:10.1002/2015MS000447.
- 744 Dee, S. G., J. M. Russell, C. Morrill, Z. Chen, and A. Neary (2018), PRYSM v2.0: A proxy system  
745 model for lacustrine archives. *Paleoceanography and Paleoclimatology*, 33(11), 1250–1269,  
746 doi: 10.1029/2018PA003413.
- 747 DeLong, K. L., T. M. Quinn, F. W. Taylor, C.-C. Shen, and K. Lin (2013), Improving coral-base  
748 paleoclimate reconstructions by replicating 350 years of coral Sr/Ca variations, *Palaeogeogr.*  
749 *Palaeoclimatol. Palaeoecol.*, 373(C), 6–24, doi:10.1016/j.palaeo.2012.08.019.
- 750 DeLong, K. L., T. M. Quinn, F. W. Taylor, K. Lin, and C.-C. Shen (2012), Sea surface temperature  
751 variability in the southwest tropical Pacific since AD 1649, *Nature Climate Change*, 2(11),  
752 799–804, doi:10.1038/nclimate1583.
- 753 Deser, C., A. S. Phillips, R. A. Tomas, Y. Okumura, M. A. Alexander, A. Capotondi, J. D. Scott,  
754 Y.-O. Kwon, and M. Ohba (2012), ENSO and Pacific decadal variability in the Community  
755 Climate System Model version 4, *J. Clim.*, 25, 2622–2651, doi:10.1175/JCLI-D-11-00301.1.
- 756 Deser, C., M. A. Alexander, S.-P. Xie, and A. S. Phillips (2010), Sea surface temperature  
757 variability: Patterns and mechanisms, *Annu. Rev. Marine. Sci.*, 2(1), 115–143,  
758 doi:10.1146/annurev-marine-120408-151453.
- 759 DiNezio, P. N., G. A. Vecchi, and A. C. Clement (2013), Detectability of changes in the Walker  
760 circulation in response to global warming, *J. Climate*, 26(12), 4038–4048, doi:10.1175/JCLI-D-  
761 12-00531.1.
- 762 DiNezio, P. N., C. Deser, A. Karspeck, S. Yeager, Y. Okumura, G. Danabasoglu, et al. (2017), A 2  
763 year forecast for a 60-80% chance of La Niña in 2017-2018. *Geophysical Research Letters*,  
764 44(22), 11,624–11,635, doi: 10.1002/2017GL074904.
- 765 Emile-Geay, J. et al. (2016), Links between tropical Pacific seasonal, interannual and orbital  
766 variability during the Holocene, *Nature Geosci.*, 9(2), 168–173, doi:10.1038/ngeo2608.
- 767 Emile-Geay, J., K. M. Cobb, M. E. Mann, and A. T. Wittenberg (2013a), Estimating Central  
768 Equatorial Pacific SST variability over the past millennium. Part I: Methodology and  
769 validation, *J. Climate*, 26(7), 2302–2328, doi:10.1175/JCLI-D-11-00510.1.
- 770 Emile-Geay, J., K. M. Cobb, M. E. Mann, and A. T. Wittenberg (2013b), Estimating Central  
771 Equatorial Pacific SST variability over the past millennium. Part II: Reconstructions and  
772 implications, *J. Climate*, 26(7), 2329–2352, doi:10.1175/JCLI-D-11-00511.1.



- 773 Epstein, S., R. Buchsbaum, H. A. Lowenstam, and H. C. Urey (1953), Revised carbonate-water  
774 isotopic temperature scale, *Geol. Soc. Am. Bull.*, *64*(11), 1315–1326, doi:10.1130/0016-  
775 7606(1953)64[1315:RCITS]2.0.CO;2.
- 776 Evans, M. N., A. Kaplan, M. C. P. and, 2000 (2000), Intercomparison of coral oxygen isotope data  
777 and historical sea surface temperature (SST): Potential for coral-based SST field  
778 reconstructions, *Paleoceanography*, *15*(5), 551–563, doi:10.1029/2000PA000498.
- 779 Evans, M. N. (2007), Toward forward modeling for paleoclimatic proxy signal calibration: A case  
780 study with oxygen isotopic composition of tropical woods. *Geochemistry, Geophysics,*  
781 *Geosystems*, *8*(7), doi: 10.1029/2006GC001406.
- 782 Evans, M. N., S. E. Tolwinski-Ward, D. M. Thompson, and K. J. Anchukaitis (2013), Applications  
783 of proxy system modeling in high resolution paleoclimatology, *Quat. Sci. Rev.*, *76*(c), 16–28,  
784 doi:10.1016/j.quascirev.2013.05.024.
- 785 Fairbanks, R. G., M. N. Evans, J. L. Rubenstone, R. A. Mortlock, K. Broad, M. D. Moore, and C.  
786 D. Charles (1997), Evaluating climate indices and their geochemical proxies measured in  
787 corals, *Coral Reefs*, *16*(1), S93–S100, doi:10.1007/s003380050245.
- 788 Fritsch, F. N., R. C. S. J. O. N. Analysis, 1980 (1980), Monotone piecewise cubic interpolation,  
789 *SIAM*, *17*(2), 238–246, doi:10.1137/0717021.
- 790 Gagan, M. K., L. K. Ayliffe, D. Hopley, J. A. Cali, G. E. Mortimer, J. Chappell, M. T. McCulloch,  
791 and M. J. Head (1998), Temperature and Surface-Ocean Water Balance of the Mid-Holocene  
792 Tropical Western Pacific, *Science*, *279*(5353), 1014–1018, doi:10.1126/science.279.5353.1014.
- 793 Gagan, M. K., L. K. Ayliffe, J. W. Beck, J. E. Cole, E. Druffel, R. B. Dunbar, and D. P. Schrag  
794 (2000), New views of tropical paleoclimates from corals, *Quat. Sci. Rev.*, *19*, 45–64,  
795 doi:10.1016/S0277-3791(99)00054-2.
- 796 Gorman, M. K., T. M. Quinn, F. W. Taylor, J. W. Partin, G. Cabioch, J. A. Austin Jr., B. Pelletier,  
797 V. Ballu, C. Maes, and S. Saustrup (2012), A coral-based reconstruction of sea surface salinity  
798 at Sabine Bank, Vanuatu from 1842 to 2007 CE, *Paleoceanography*, *27*(3),  
799 doi:10.1029/2012PA002302.
- 800 Greene, C. A., K. Thirumalai, K. A. Kearney, J. M. Delgado, W. Schwanghart, N. S. Wolfenbarger,  
801 et al. (2019), The Climate Data Toolbox for MATLAB. *Geochemistry, Geophysics, Geosystems*,  
802 *15*(3), 379–3781, doi: 10.1029/2019GC008392.
- 803 Grottoli, A. G., and C. M. Eakin (2007), A review of modern coral  $\delta^{18}\text{O}$  and  $\Delta^{14}\text{C}$  proxy records.  
804 *Earth Science Reviews*, *81*(1-2), 67–91, doi: 10.1016/j.earscirev.2006.10.001.
- 805 Hathorne, E. C. et al. (2013), Interlaboratory study for coral Sr/Ca and other element/Ca ratio  
806 measurements, *Geochem. Geophys. Geosyst.*, *14*(9), 3730–3750, doi:10.1002/ggge.20230.
- 807 Hereid, K. A., T. M. Quinn, and Y. M. Okumura (2013a), Assessing spatial variability in El Niño-  
808 Southern Oscillation event detection skill using coral geochemistry, *Paleoceanography*, *28*(1),  
809 14–23, doi:10.1029/2012PA002352.

- 810 Hereid, K. A., T. M. Quinn, F. W. Taylor, C. C. Shen, R. Lawrence Edwards, and H. Cheng  
811 (2013b), Coral record of reduced El Niño activity in the early 15<sup>th</sup> to middle 17<sup>th</sup> centuries,  
812 *Geology*, *41*(1), 51–54, doi:10.1130/G33510.1.
- 813 Herron, M. M. and C. C. Langway (2017), Firn densification: An empirical model. *Journal of*  
814 *Glaciology*, *25*(93), 373–385, doi: 10.3189/S0022143000015239
- 815 Hu, J., J. Emile-Geay, and J. Partin (2017), Correlation-based interpretations of paleoclimate data –  
816 where statistics meet past climates. *Earth and Planetary Science Letters*, *459*, 362–371, doi:  
817 10.1016/j.epsl.2016.11.04.
- 818 Hurrell, J. W. et al. (2013), The Community Earth System Model: A Framework for Collaborative  
819 Research, *Bull. Amer. Meteor. Soc.*, *94*(9), 1339–1360, doi:10.1175/BAMS-D-12-00121.1.
- 820 Jimenez, G., J. E. Cole, D. M. Thompson, and A. W. Tudhope (2018), Northern Galápagos Corals  
821 Reveal Twentieth Century Warming in the Eastern Tropical Pacific, *Geophys. Res. Lett.*, *45*(4),  
822 1981–1988, doi:10.1002/2017GL075323.
- 823 Johnsen, S. J., H. B. Clausen, K. M. Cuffey, G. Hoffmann and T. T. Creyts (2000), Diffusion of  
824 stable isotopes in polar firn and ice: the isotope effect in firn diffusion. *Physics of Ice Core*  
825 *Records*, (159), 121–140, doi: 10.7916/D8KW5D4X
- 826 Kilbourne, K. H., T. M. Quinn, F. W. Taylor, T. Delcroix, and Y. Gouriou (2004), El Niño-  
827 Southern Oscillation-related salinity variations recorded in the skeletal geochemistry of a  
828 *Porites* coral from Espiritu Santo, Vanuatu, *Paleoceanography*, *19*(4),  
829 doi:10.1029/2004PA001033.
- 830 Lawman, A. E., T. M. Quinn, J. W. Partin, K. Thirumalai, F. W. Taylor, C. C. Wu, et al. (2020), A  
831 century of reduced ENSO variability during the Medieval Climate Anomaly.  
832 *Paleoceanography and Paleoclimatology*, doi: 10.1029/2019PA003742.
- 833 LeGrande, A. N., and G. A. Schmidt (2006), Global gridded data set of the oxygen isotopic  
834 composition in seawater, *Geophys. Res. Lett.*, *33*(12), 15833–5, doi:10.1029/2006GL026011.
- 835 Linsley, B. K., A. Kaplan, and Y. Gouriou (2006), Tracking the extent of the South Pacific  
836 Convergence Zone since the early 1600s, *Geochem. Geophys. Geosyst.*, *7*,  
837 doi:10.1029/2005GC001115.
- 838 Lough, J. M. (2004), A strategy to improve the contribution of coral data to high-resolution  
839 paleoclimatology. *Palaeogeography, Palaeoclimatology, Palaeoecology*, *204*(1-2), 115–  
840 143, doi: 10.1016/S0031-0182(03)00727-2.
- 841 Lough, J. M. (2010), Climate records from corals, *WIREs Clim Change*, *1*(3), 318–331,  
842 doi:10.1002/wcc.39.
- 843 Okumura, Y. M., T. Sun, and X. Wu (2017), Asymmetric Modulation of El Niño and La Niña and  
844 the Linkage to Tropical Pacific Decadal Variability, *J. Climate*, *30*(12), 4705–4733,  
845 doi:10.1175/JCLI-D-16-0680.1.

- 846 Otto-Bliesner, B. L., E. C. Brady, J. Fasullo, A. Jahn, L. Landrum, S. Stevenson, N. Rosenbloom,  
847 A. Mai, and G. Strand (2016), Climate Variability and Change since 850 CE: An Ensemble  
848 Approach with the Community Earth System Model, *Bull. Amer. Meteor. Soc.*, *97*(5), 735–754,  
849 doi:10.1175/BAMS-D-14-00233.1.
- 850 Partin, J. W., T. M. Quinn, C. C. Shen, J. Emile-Geay, F. W. Taylor, C. R. Maupin, et al. (2013),  
851 Multidecadal rainfall variability in South Pacific Convergence Zone as revealed by  
852 stalagmite geochemistry. *Geology*, *41*(11), 1143–1146, doi: .10.1130/G34718.1.
- 853 Parzen, E. (1962), On estimation of a probability density function and mode, *Ann. Math. Stat.*,  
854 *33*(3), 1065–1076, doi: 10.1214/aoms/1177704472.
- 855 Pearson, K. (1920), Notes on the history of correlation, *Biometrika*, *13*(1), 25,  
856 doi:10.2307/2331722.
- 857 Quinn, T. M., and D. E. Sampson (2002), A multiproxy approach to reconstructing sea surface  
858 conditions using coral skeleton geochemistry, *Paleoceanography*, *17*(4), 14–1–14–11,  
859 doi:10.1029/2000PA000528.
- 860 Ren, L., B. K. Linsley, G. M. Wellington, D. P. Schrag, and O. Hoegh-guldberg (2003),  
861 Deconvolving the  $\delta^{18}\text{O}$  seawater component from subseasonal coral  $\delta^{18}\text{O}$  and Sr/Ca at  
862 Rarotonga in the southwestern subtropical Pacific for the period 1726 to 1997, *Geochim.*  
863 *Cosmochim. Acta*, *67*(9), 1609–1621, doi:10.1016/S0016-7037(02)00917-1.
- 864 Roden, J. S., G. Lin and J. R. Ehleringer (2000), A mechanistic model for interpretation of  
865 hydrogen and oxygen isotope ratios in tree-ring cellulose. *Geochimica Et Cosmochimica*  
866 *Acta*, *64*(1), 21–35, doi: 10.1016/S0016-7037(99)00195-7.
- 867 Ropelewski, C. F., and M. S. Halpert (1987), Global and regional scale precipitation patterns  
868 associated with the El Niño/Southern Oscillation, *Mon. Weather Rev.*, *115*, 1606–1626,  
869 doi:10.1175/1520-0493(1987)115<1606:GARSPP>2.0.CO;2.
- 870 Russon, T., A. W. Tudhope, M. C. G. Research, 2015 (2015), Inferring changes in ENSO amplitude  
871 from the variance of proxy records, *Geophys. Res. Lett.*, *42*(4), 1197–1204,  
872 doi:10.1002/(ISSN)1944-8007.
- 873 Sayani, H. R., K. M. Cobb, K. DeLong, N. T. Hitt, and E. R. M. Druffel (2019), Intercolony  $\delta^{18}\text{O}$   
874 and Sr/Ca variability among *Porites* spp. corals at Palmyra Atoll: Towards more robust coral-  
875 based estimates of climate, *Geochem. Geophys. Geosyst.*, *20*, doi:10.1029/2019GC008420.
- 876 Schmidt, G. A. et al. (2014), Using palaeo-climate comparisons to constrain future projections in  
877 CMIP5, *Clim. Past*, *10*(1), 221–250, doi:10.5194/cp-10-221-2014.
- 878 Schrag, D. P. (1999), Rapid analysis of high-precision Sr/Ca ratios in corals and other marine  
879 carbonates, *Paleoceanography*, *14*(2), 97–102, doi:10.1029/1998PA900025.
- 880 Shen, C.-C. et al. (2012), High-precision and high-resolution carbonate  $^{230}\text{Th}$  dating by MC-ICP-  
881 MS with SEM protocols, *Geochim. Cosmochim. Acta*, *99*(C), 71–86,  
882 doi:10.1016/j.gca.2012.09.018.

- 883 Smith, S. V., R. W. Buddemeier, R. C. Redalje, and J. E. Houck (1979), Strontium-calcium  
884 thermometry in coral skeletons, *Science*, 204(4391), 404–407,  
885 doi:10.1126/science.204.4391.404.
- 886 Stevenson, S., B. S. Powell, M. A. Merrifield, K. M. Cobb, J. Nusbaumer, and D. Noone (2015),  
887 Characterizing seawater oxygen isotopic variability in a regional ocean modeling framework:  
888 Implications for coral proxy records, *Paleoceanography*, 30, 1573–1593,  
889 doi:10.1002/2015PA002824.
- 890 Stevenson, S., H. V. McGregor, S. J. Phipps, and B. Fox-Kemper (2013), Quantifying errors in  
891 coral-based ENSO estimates: Toward improved forward modeling of  $\delta^{18}\text{O}$ , *Paleoceanography*,  
892 28(4), 633–649, doi:10.1002/palo.20059.
- 893 Stevenson, S., B. Fox-Kemper, M. Jochum, B. Rajagopalan, and S. G. Yeager (2010), ENSO model  
894 validation using wavelet probability analysis. *Journal of Climate*, 23(20), 5540–5547, doi:  
895 10.1175/2010JCLI3609.1.
- 896 Sun, T., and Y. M. Okumura (2019), Role of Stochastic Atmospheric Forcing from the South and  
897 North Pacific in Tropical Pacific Decadal Variability, *J. Climate*, 32(13), 4013–4038,  
898 doi:10.1175/JCLI-D-18-0536.1.
- 899 Thompson, D. M., T. R. Ault, M. N. Evans, J. E. Cole, and J. Emile-Geay (2011), Comparison of  
900 observed and simulated tropical climate trends using a forward model of coral  $\delta^{18}\text{O}$ , *Geophys.*  
901 *Res. Lett.*, 38(14), L14706, doi:10.1029/2011GL048224.
- 902 Thyng, K., C. Greene, R. Hetland, H. Zimmerle, and S. DiMarco (2016), True colors of  
903 oceanography: Guidelines for effective and accurate colormap selection, *Oceanog*, 29(3), 9–13,  
904 doi:10.5670/oceanog.2016.66.
- 905 Trenberth, K. E. (1997), The definition of El Niño, *Bull. Amer. Meteor. Soc.*, 78(12), 2771–2777,  
906 doi:10.1175/1520-0477(1997)078<2771:TDOENO>2.0.CO;2.
- 907 Trenberth, K. E., and T. J. Hoar (1996), The 1990–1995 El Niño–Southern Oscillation event:  
908 Longest on record, *Geophys. Res. Lett.*, 23(1), 57–60, doi:10.1029/95GL03602.
- 909 Weber, J. N. (1973), Incorporation of strontium into reef coral skeletal carbonate, *Geochim.*  
910 *Cosmochim. Acta*, 37(9), 2173–2190, doi:10.1016/0016-7037(73)90015-X.
- 911 Weber, J. N., and P. M. J. Woodhead (1972), Temperature dependence of oxygen-18 concentration  
912 in reef coral carbonates, *Journal of Geophysical Research: Oceans*, 77(3), 463–473,  
913 doi:10.1029/JC077i003p00463.
- 914 Wittenberg, A. T. (2009), Are historical records sufficient to constrain ENSO simulations?  
915 *Geophys. Res. Lett.*, 36(12), 3–5, doi:10.1029/2009GL038710.
- 916 Wittenberg, A. T., A. Rosati, T. L. Delworth, G. A. Vecchi, and F. Zeng (2014), ENSO Modulation:  
917 Is It Decadally Predictable? *J. Climate*, 27(7), 2667–2681, doi:10.1175/JCLI-D-13-00577.1.

918 Wong, C. I. and D. O. Breecker (2015), Advancements in the use of speleothems as climate  
919 archives. *Quaternary Science Reviews*, 127, 1–18, doi: 10.1016/j.quascirev.2015.07.019.

920 Wu, X., Y. M. Okumura, and P. N. DiNezio (2019), What controls the duration of El Niño and La  
921 Niña events? *Journal of Climate*, 32(18), 5941–5965, doi: 10.1175/JCLI-D-18-0681.1.

922

## 923 **Figure Captions**

924 **Figure 1.** Coral proxy system model (PSM) schematic. The sea-surface temperature (SST), sea-  
925 surface salinity (SSS), or the oxygen isotopic composition of sea water ( $\delta^{18}\text{O}_{\text{sw}}$ ) environmental inputs  
926 (green box) can come from instrumental observations, climate model output, or reanalysis data [Evans  
927 *et al.*, 2013; Dee *et al.*, 2015]. Here and in all subsequent figures,  $\text{SST}_{\text{Sr/Ca}}$  refers to SST derived from  
928 coral Sr/Ca. The coral  $\delta^{18}\text{O}$  sensor model [Thompson *et al.*, 2011] accounts for sensitivity to SST and  
929  $\delta^{18}\text{O}_{\text{sw}}$  (SSS). The growth rate archive model (purple box) describes how an environmental signal  
930 may be emplaced or transformed in the coral archive due to variable growth rates. The coral  
931 observation models (blue boxes) include the combined effect of analytical and calibration errors, as  
932 well as age model uncertainties that arise from transforming the coral geochemical from the depth to  
933 the time domain. Arrows shows possible permutations of the archive and observation sub-models to  
934 yield pseudocoral output perturbed by the coral PSM (gray boxes). The full coral PSM refers to  
935 consecutively perturbing the environmental inputs with the variable growth rate, analytical and  
936 calibration, and age-model algorithms.

937

938 **Figure 2.** Simulated annual coral growth rates (cm/year). (a) A randomly generated realization of  
939 simulated growth rates for 100 pseudocoral annual density bands. The growth rates are simulated  
940 using an autoregressive order 2, AR(2), model with lag coefficients and variance parameters  
941 determined from measured *Porites* corals from the southwest Pacific (Section 2.4). This figure shows  
942 one randomly generated realization of the AR(2) simulated growth rates. We note that the variable  
943 growth rate model could be run multiple times to generate  $n$  realizations that are subsequently used  
944 to stretch and compress the original input to the coral PSM. (b) Histogram of modeled pseudo *Porites*  
945 annual growth rates ( $1.2 \pm 0.2$  cm/year,  $\pm 1\sigma$ ). The pseudocoral annual growth rates are used to stretch  
946 and compress the environmental inputs to mimic how equal sampling in the depth domain can yield  
947 to unequal sampling in the time domain.

948

949 **Figure 3.** Impact of variable growth rates and analytical and calibration errors on environmental  
950 signals. (a-d) Blue curves depicts the original SST (a, c) and  $\Delta\delta^{18}\text{O}_{\text{pseudocoral}}$  (b, d) inputs transformed  
951 from the time to the depth domain using a realization of the AR(2) variable growth rate model. Gray  
952 curves indicate the original inputs transformed to the depth domain using a constant transformation  
953 of 1.2 cm/year (i.e., no variable growth rates) for the model grid points closest to Kiritimati (a, b) and  
954 Vanuatu (c, d). Model output in this and all subsequent figures are from the CESM-LME 850 control  
955 [Otto-Bliesner *et al.*, 2016] (Section 2.1).  $\Delta\delta^{18}\text{O}_{\text{pseudocoral}}$  in this and all subsequent figures is generated  
956 using the sensor model of Thompson *et al.* [2011] (Section 2.3.1). (e, g) Pseudocoral  $\text{SST}_{\text{Sr/Ca}}$   
957 perturbed with the combined effect of analytical and calibration errors ( $\pm 0.30^\circ\text{C}$ ,  $2\sigma$ ; Section 2.5.1)  
958 at the model grid points closest to Kiritimati (e) and Vanuatu (g). (f, h)  $\Delta\delta^{18}\text{O}_{\text{pseudocoral}}$  perturbed  
959 with analytical error ( $\pm 0.20\%$ ,  $2\sigma$ ; Section 2.5.1) for Kiritimati (f) and Vanuatu (h). Black line in (e-h)  
960 indicates the unperturbed environmental inputs for the selected sites, and the blue shading represents  
961 the spread of forward modeled pseudocoral time series ( $n = 1000$ ). For illustrative purposes, each  
962 panel includes a 20-year subset of the 850 control to show how variable growth rates and  
963 analytical/calibration errors impact the original inputs.



964

965 **Figure 4.** Age modeling of pseudocoral SST at Vanuatu. Climatology (black)  $\pm 1\sigma$  (shading) for the  
 966 original (a) and age modeled (d) SST output for the grid point nearest Vanuatu in the CESM-LME  
 967 850 control ( $n = 1156$  years). Histogram of the warmest (red bars) and coolest (blue bars) month for  
 968 each individual year in the (b) 850 control and the (e) age modeled SST output. The climatological  
 969 warmest/coolest months are indicated with dashed vertical lines in (b, e). (c) 10 years of the (c)  
 970 unperturbed monthly SST and the (f) age modeled monthly SST at Vanuatu. Triangles in (a, c, d, f)  
 971 indicate the climatological warmest (Feb.) and coolest (Aug.) months. The black circles in (c) indicate  
 972 the peak/troughs identified by the age model algorithm, and the adjacent text labels indicate the  
 973 calendar month at each critical point. (g) Monthly SSTA for the original input (black) and age  
 974 modeled pseudocoral SST (teal). In this and all subsequent figures, anomalies are with respect to the  
 975 climatology of the full-length control run. The warmest/coolest month distributions in (b) and (e) are  
 976 wider than a single month, and is directly related to a loss of interannual variance in (g).  
 977

978 **Figure 5.** Age modeling of pseudocoral SST at Kiritimati. Same as Figure 4 except for the grid point  
 979 nearest to Kiritimati. Triangles in (a, c, d, f) indicate the climatological warmest (Jun.) and coolest  
 980 (Oct.) months. Years with strong El Niño events (e.g. model years 8 and 9) have a reduced annual  
 981 cycle and a small and/or absent trough during boreal winter, leading to incorrect month assignment  
 982 in (f) that results in a reduction in interannual variance in anomaly space (g).  
 983

984 **Figure 6.** Pseudocoral SST<sub>Sr/Ca</sub> and  $\delta^{18}\text{O}$  changes in interannual variance. (a) Standard deviation (SD)  
 985 of monthly SSTA in the LME 850 control. Warm colors highlight regions with the largest interannual  
 986 signal. (b) Percent difference in SD between pseudocoral SST<sub>Sr/Ca</sub> anomalies perturbed with analytical  
 987 and calibration errors and the SD of the unperturbed SST anomalies. (c) Amplitude of the annual SST  
 988 cycle in the LME 850 control. (d) Percent change in SD between age modeled pseudocoral SST<sub>Sr/Ca</sub>  
 989 anomalies and the original, unperturbed SST anomalies. (e) SD of monthly forward modeled  
 990  $\Delta\delta^{18}\text{O}_{\text{pseudocoral}}$ . (f) Percent difference in SD between pseudocoral  $\delta^{18}\text{O}$  anomalies perturbed with  
 991 analytical errors and the SD of the unperturbed  $\Delta\delta^{18}\text{O}_{\text{pseudocoral}}$  anomalies. (g) Amplitude of the annual  
 992  $\Delta\delta^{18}\text{O}_{\text{pseudocoral}}$  cycle in the 850 control. (h) Percent change in SD between age modeled pseudocoral  
 993  $\Delta\delta^{18}\text{O}$  anomalies and the original, unperturbed  $\Delta\delta^{18}\text{O}$  anomalies. The percent difference in SD for the  
 994 full-length time series ( $\sim 1156$  years) is reported. The SD for the coral PSM output is the median of  
 995 1000 realization in (b, f) and 1 realization of the deterministic age model (d, h). The Niño 3.4 region  
 996 is outlined by a white box (a-h). The changes in interannual variance from analytical/calibration errors  
 997 (b, f) is inversely related to the magnitude of the interannual signal (a, e), whereas the change in  
 998 variance from age modeling (d, h) is linked to the amplitude of the annual cycle (c, g). Colormaps in  
 999 this and all subsequent maps use the cmocean: colormaps for oceanography toolbox [Thyng *et al.*,  
 1000 2016].  
 1001

1002 **Figure 7.** Changes in interannual variance for the full coral PSM. Percent difference in SD between  
 1003 pseudocoral (a) SST<sub>Sr/Ca</sub> and (b)  $\Delta\delta^{18}\text{O}$  anomalies perturbed with variable growth rates,  
 1004 analytical/calibration errors, and the age modeling algorithm, and the original, unperturbed  
 1005 environmental input ( $n = 100$  realizations). Selected sites at Kiritimati ( $2^\circ\text{N}$ ,  $157^\circ\text{W}$ ) in the central  
 1006 Pacific, and Vanuatu ( $16^\circ\text{S}$ ,  $167^\circ\text{E}$ ) in the southwest Pacific are indicated with gold stars. The white  
 1007 box outlines the Niño 3.4 region. The percent change in SD for the full coral PSM reveals the tradeoff  
 1008 between interannual variability and the amplitude of the annual cycle (Figure 6).  
 1009

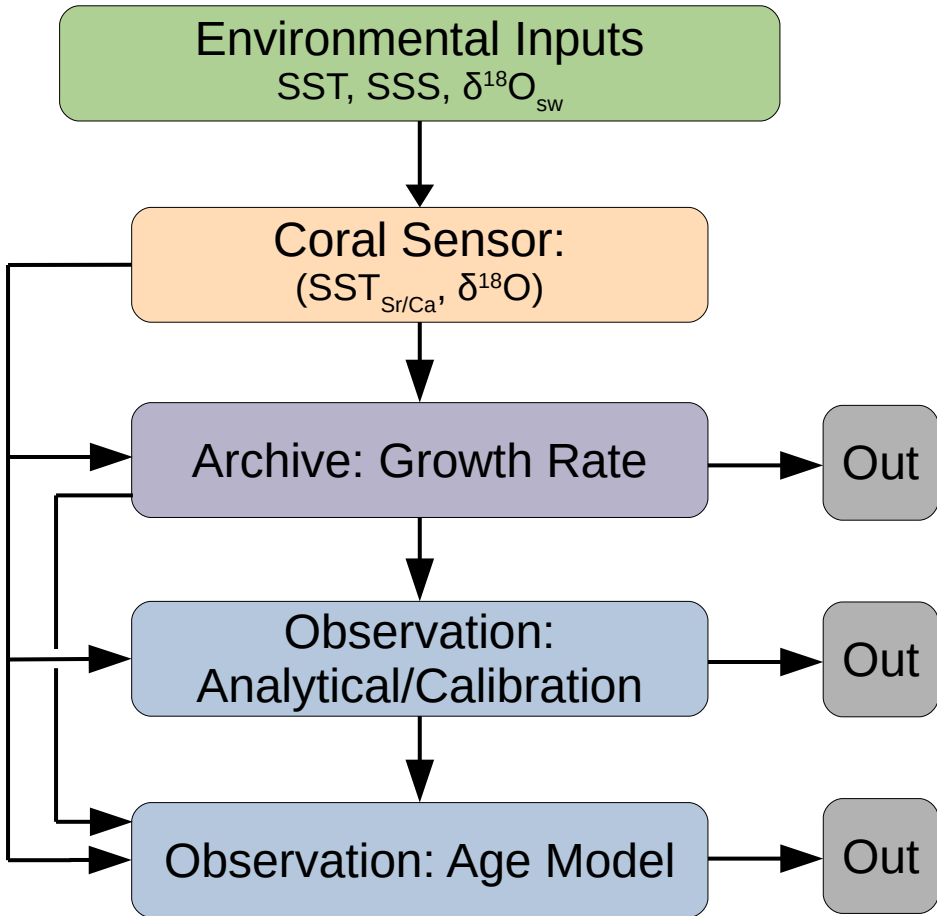
1010 **Figure 8.** Quantifying changes in internal ENSO variability. (a) Monthly SSTA averaged across the  
 1011 Niño 3.4 region in the 850 control (200-yr subset shown for clarity). Distribution of Niño 3.4 SSTA  
 1012 depicted as a histogram/PDF (b) and box plot (c) for the full-length control (1156 years). (d) 20-yr  
 1013 running standard deviation of Niño 3.4 monthly SSTA ( $\sigma_{\text{Niño3.4-SSTA}}$ ). Shaded portions in (a, d)  
 1014 highlight two intervals with more (red) and less (blue) internal ENSO variability. Distribution of  
 1015  $\sigma_{\text{Niño3.4-SSTA}}$  values depicted as a histogram/PDF (e) and box plot (f). Higher SD values indicate  
 1016 increased ENSO variability, whereas lower SD values indicate decreased variability. PDFs in (b, e)  
 1017 are based on a kernel density estimation method [Parzen, 1962]. The lower and upper bounds of the  
 1018 boxes in (c, f) correspond to the 25<sup>th</sup> and 75<sup>th</sup> percentiles and the center line indicates the median. The  
 1019 whiskers in (c, f) represent the 1.5 x inter-quartile range (IQR). Outliers greater than 1.5xIQR are  
 1020 omitted for clarity. The running SD of monthly anomalies (f) is a metric for decadal+ changes in  
 1021 interannual variability.

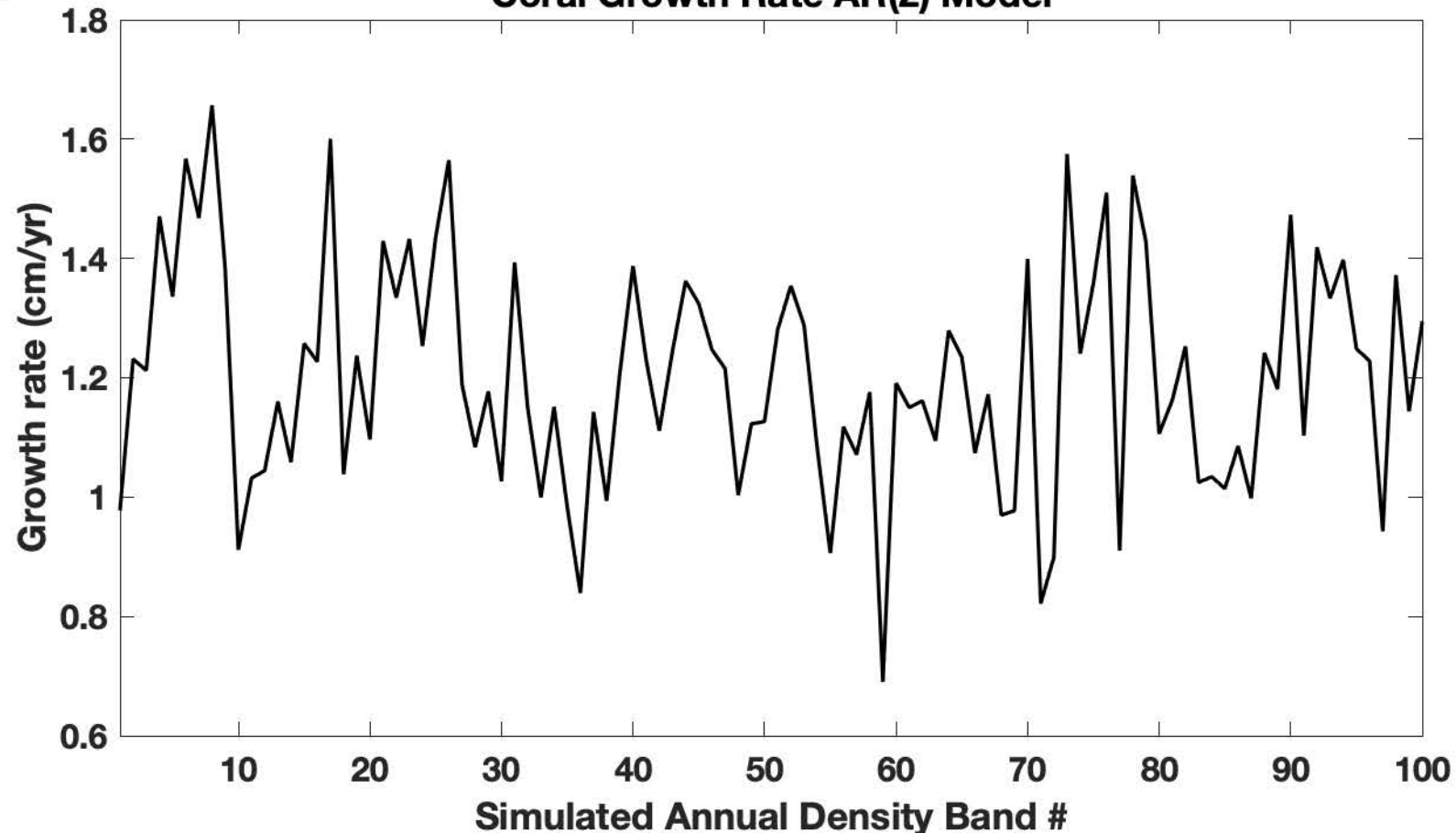
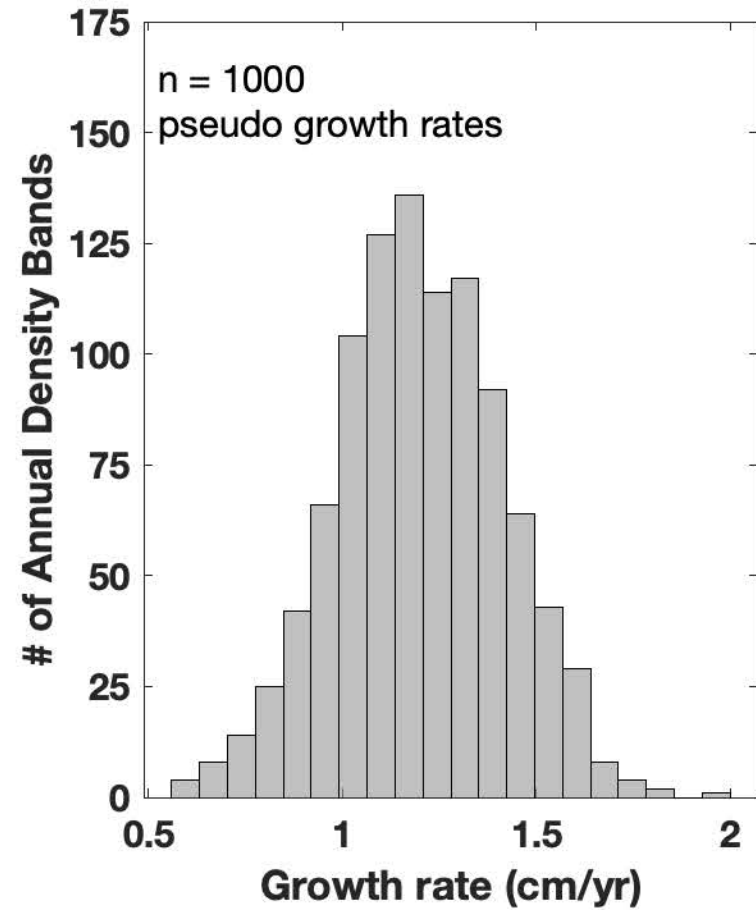
1022  
 1023 **Figure 9.** The impact of coral PSM uncertainties on interannual variance. Box plots showing the  
 1024 distribution of 20-yr running standard deviation values for pseudocoral SST<sub>Sr/Ca</sub> (a, c) and  $\delta^{18}\text{O}$  (b, d)  
 1025 anomalies across all pseudocoral realizations for the Kiritimati (a, b) and Vanuatu (c, d) grid points.  
 1026 The growth rate and age model (GR & AM), analytical/calibration, and full PSM include the results  
 1027 for 1000 realizations. The deterministic age modeled results are shown for 1 realization. The full PSM  
 1028 is determined by consecutively running the growth rate algorithm, applying analytical/calibration  
 1029 error, and then age modeling all 1000 pseudocoral SST<sub>Sr/Ca</sub> or  $\Delta\delta^{18}\text{O}_{\text{pseudocoral}}$  realizations. The lower  
 1030 and upper bounds of the boxes correspond to the 25<sup>th</sup> and 75<sup>th</sup> percentiles and the center line indicates  
 1031 the 50<sup>th</sup> percentile. The whiskers represent 1.5xIQR. Outliers greater than 1.5 x IQR are omitted for  
 1032 clarity. Dashed horizontal gray lines indicate the median SD for the original environmental inputs.  
 1033 The median 20-year running standard deviation of SST<sub>Sr/Ca</sub> and  $\Delta\delta^{18}\text{O}_{\text{pseudocoral}}$  anomalies illustrates  
 1034 how the various PSM subcomponents systematically increase or decrease interannual variance. The  
 1035 length of the box and whiskers encapsulates information about the range of simulated internal  
 1036 variability.

1037  
 1038 **Figure 10.** Changes in interannual variance for the full coral PSM. Percent difference in the median  
 1039 20-year running standard deviation between pseudocoral SST<sub>Sr/Ca</sub> (a) and  $\Delta\delta^{18}\text{O}$  (b) anomalies  
 1040 perturbed with variable growth rates, analytical/calibration errors, and the age modeling algorithm,  
 1041 and the original, unperturbed environmental input (n = 100 realizations). Gold stars indicate select  
 1042 sites at Kiritimati and Vanuatu. The white box indicates the Niño 3.4 region. The percent change in  
 1043 standard deviation for the full coral PSM reveals the tradeoff between interannual variability and the  
 1044 amplitude of the annual cycle. The patterns displayed here are similar to those of Figure 6, indicating  
 1045 that the two variability metrics yield consistent results.

1046  
 1047 **Figure 11.** Correlation between Niño 3.4 SSTA and values at each grid point. Monthly Niño 3.4  
 1048 correlated with monthly values for SSTA (a) and monthly values of forward modeled pseudocoral  
 1049  $\Delta\delta^{18}\text{O}_{\text{pseudocoral}}$  (b). The 20-yr running SD of Niño 3.4 SSTA ( $\sigma_{\text{Niño3.4-SSTA}}$ ) with the 20-yr running SD  
 1050 of SSTA (c) and  $\Delta\delta^{18}\text{O}_{\text{pseudocoral}}$  anomalies (d). The 20-yr running SD of Niño 3.4 SSTA with the 20-yr  
 1051 running standard deviation of SSTA (e) and  $\Delta\delta^{18}\text{O}_{\text{pseudocoral}}$  anomalies (f) perturbed by the full coral  
 1052 PSM. Colormap in (e, f) is the median correlation coefficient for 100 full PSM realizations. The Niño  
 1053 3.4 region is outlined by a white box (a-f). The correlation coefficient averaged across all grid points  
 1054 within the Niño 3.4 region (white box) is indicated with a gold diamond in (c-f). Colormaps provide  
 1055 the Pearson correlation coefficient [Pearson, 1920].  $\Delta\delta^{18}\text{O}_{\text{pseudocoral}}$  is generated using the sensor  
 1056 model of Thompson *et al.* [2011] (Section 2.3.1). Stippling indicates statistically significant

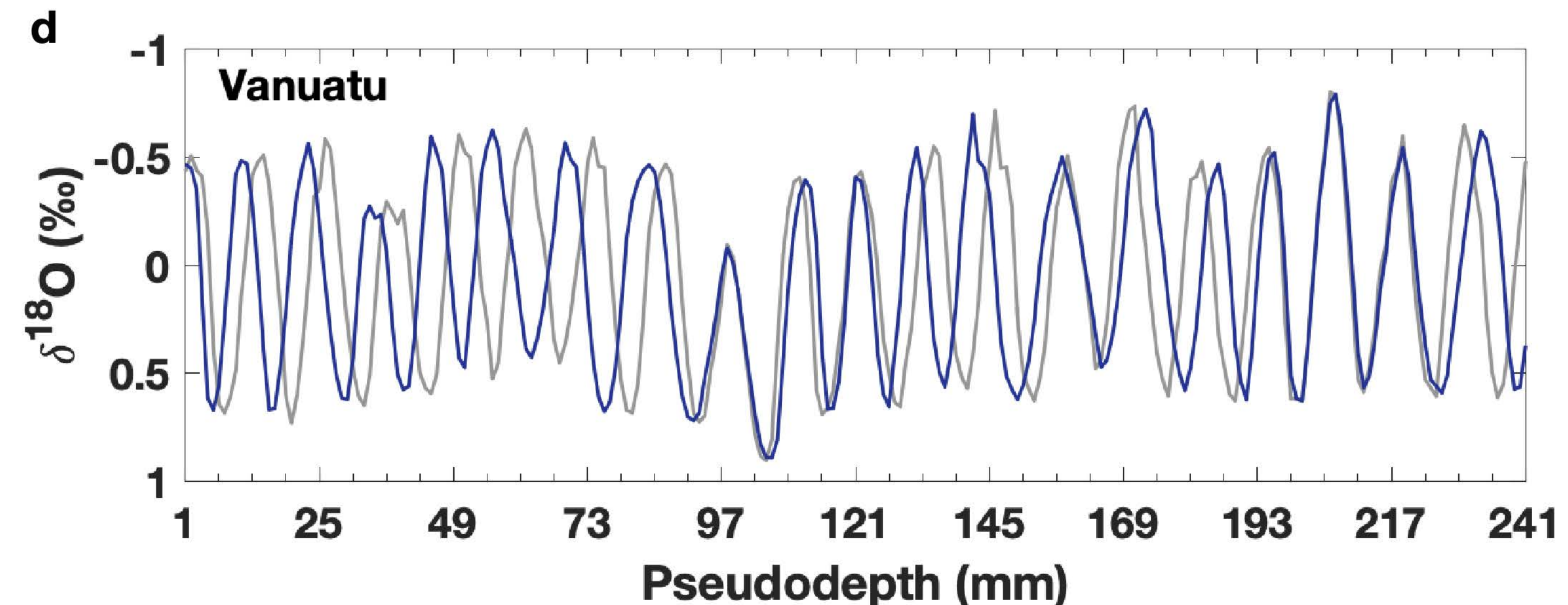
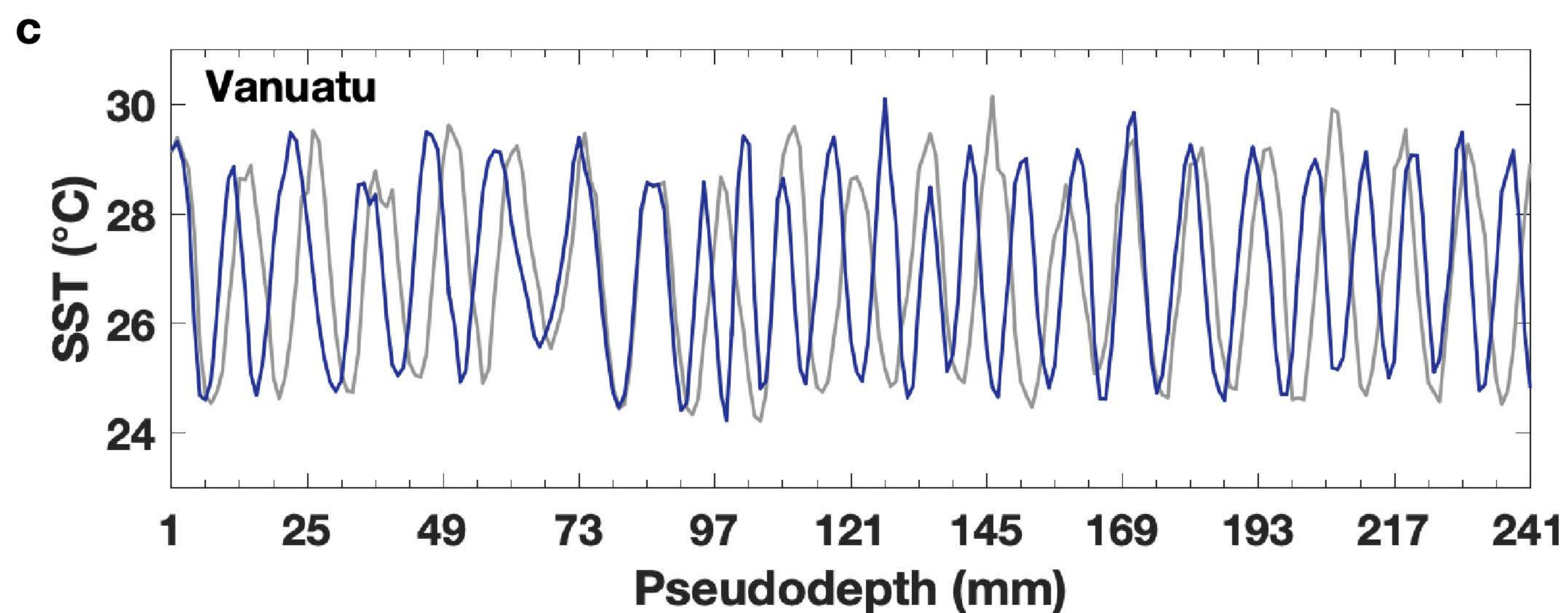
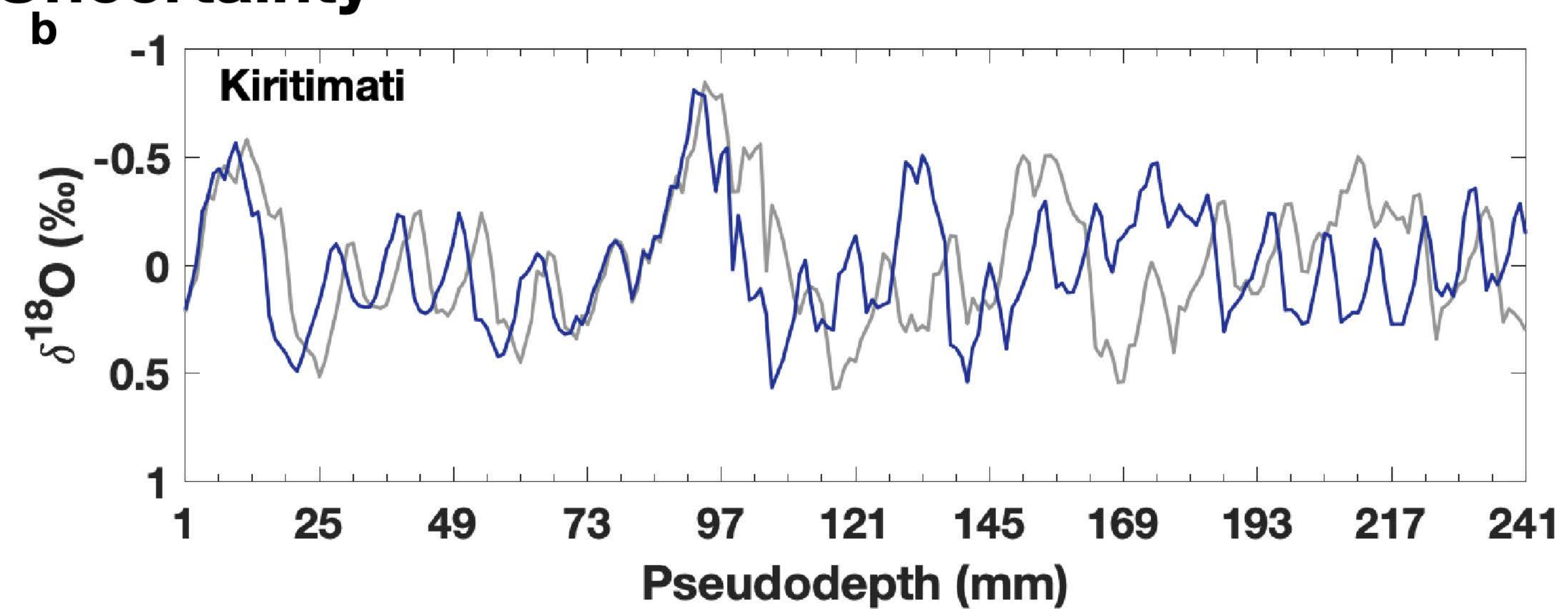
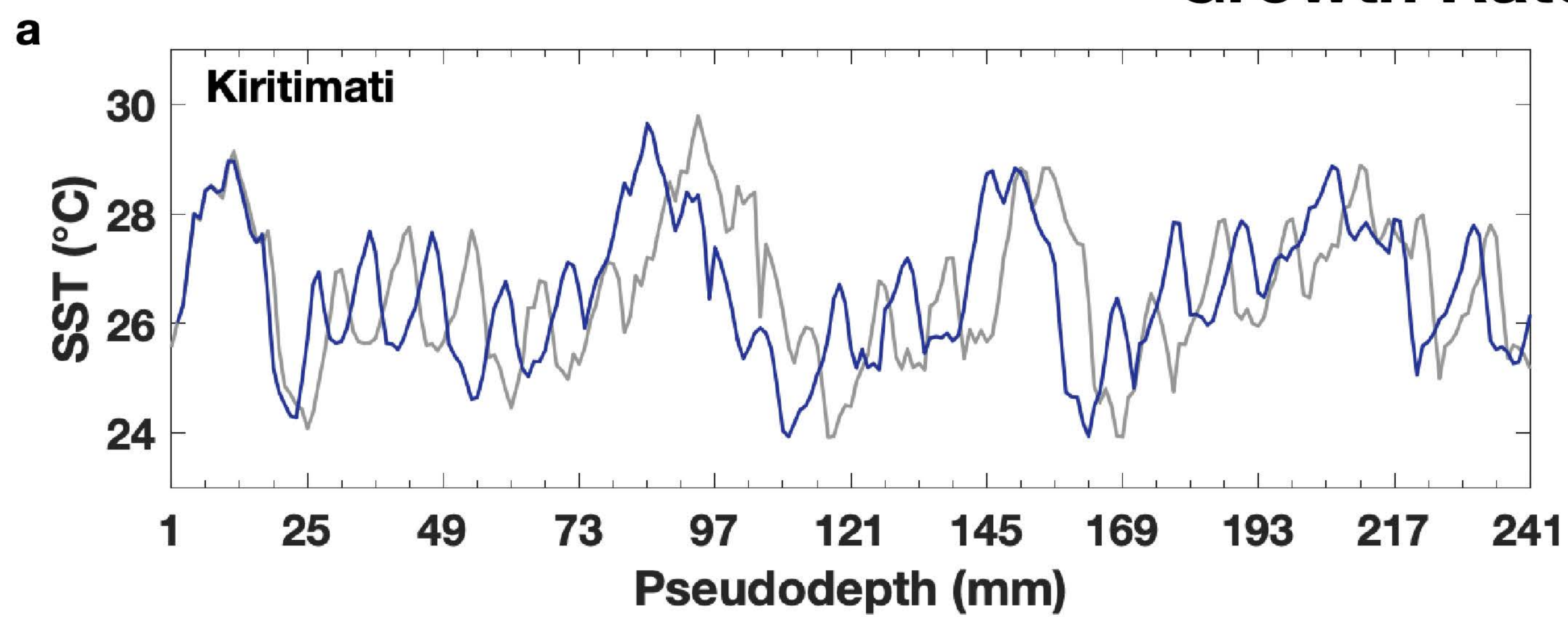
1057 correlations ( $p < 0.01$ ) that accounts for autocorrelation in the time series [*Dawdy and Matalas*, 1964;  
1058 *Hu et al.*, 2017]. Gold stars indicate select sites at Kiribati and Vanuatu. Decadal+ changes in  
1059 forward-modeled interannual SST<sub>Sr/Ca</sub> and  $\delta^{18}\text{O}$  variability are positively correlated with  $\sigma_{\text{Niño3.4-SSTA}}$   
1060 across much of the tropical Pacific (**e, f**) even with the added uncertainties in our PSM, indicating that  
1061 these processes do not obscure the target climate signal of decadal+ changes in ENSO variability.



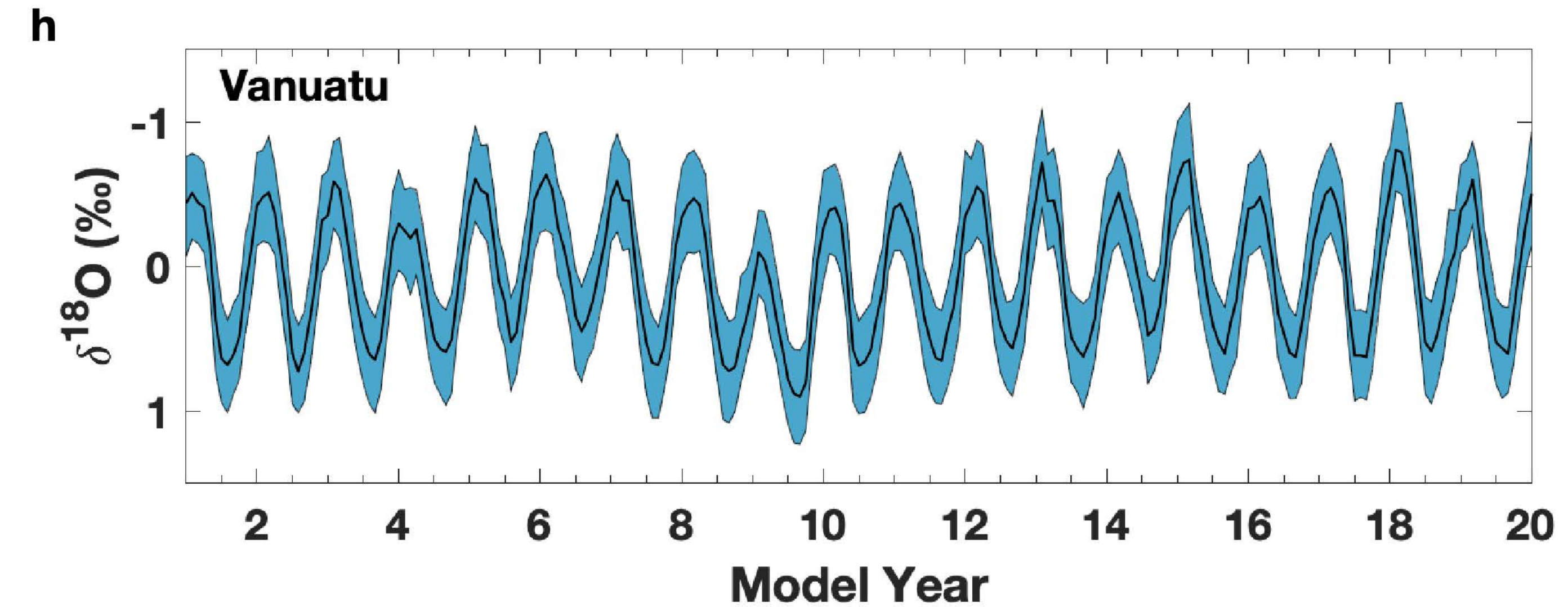
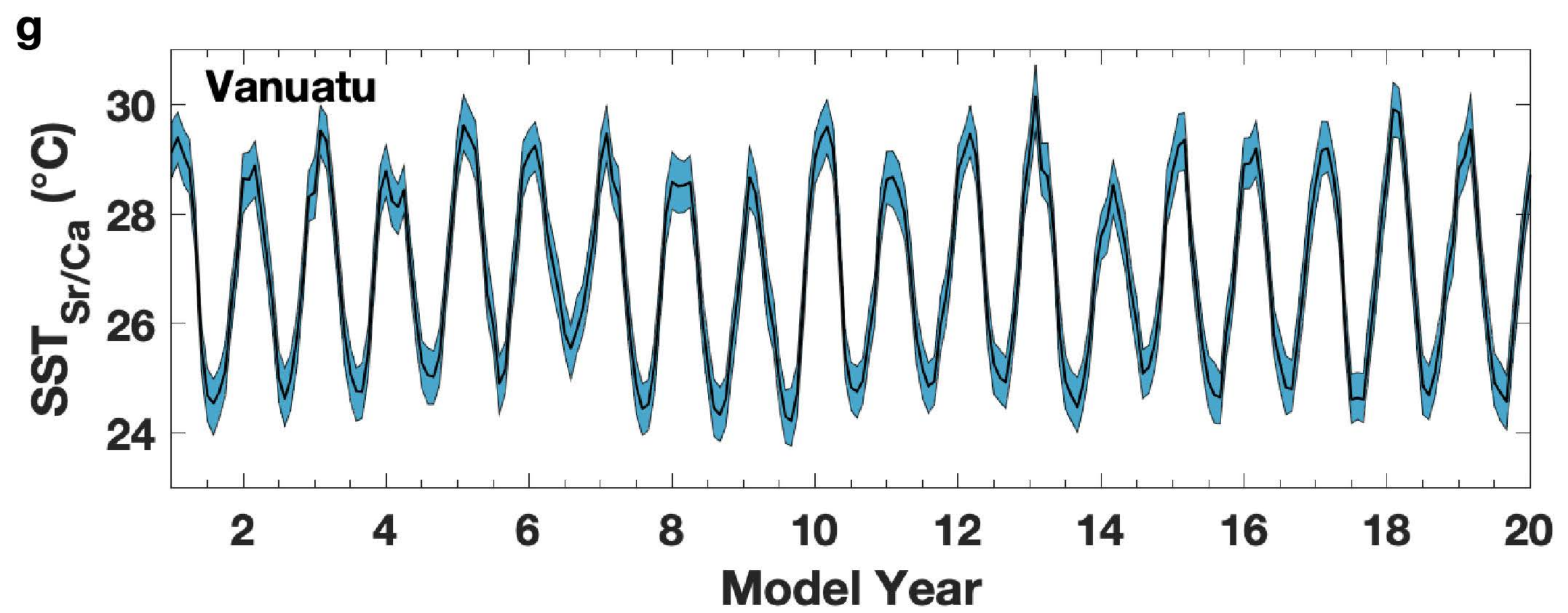
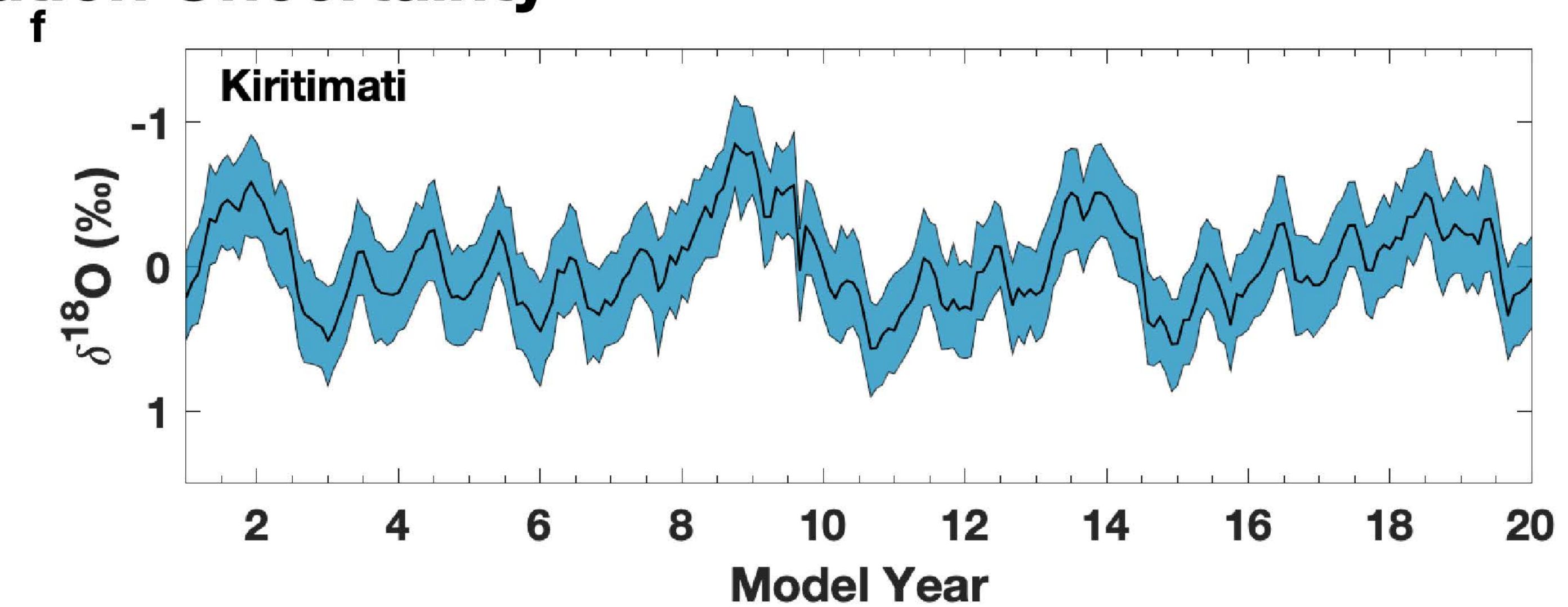
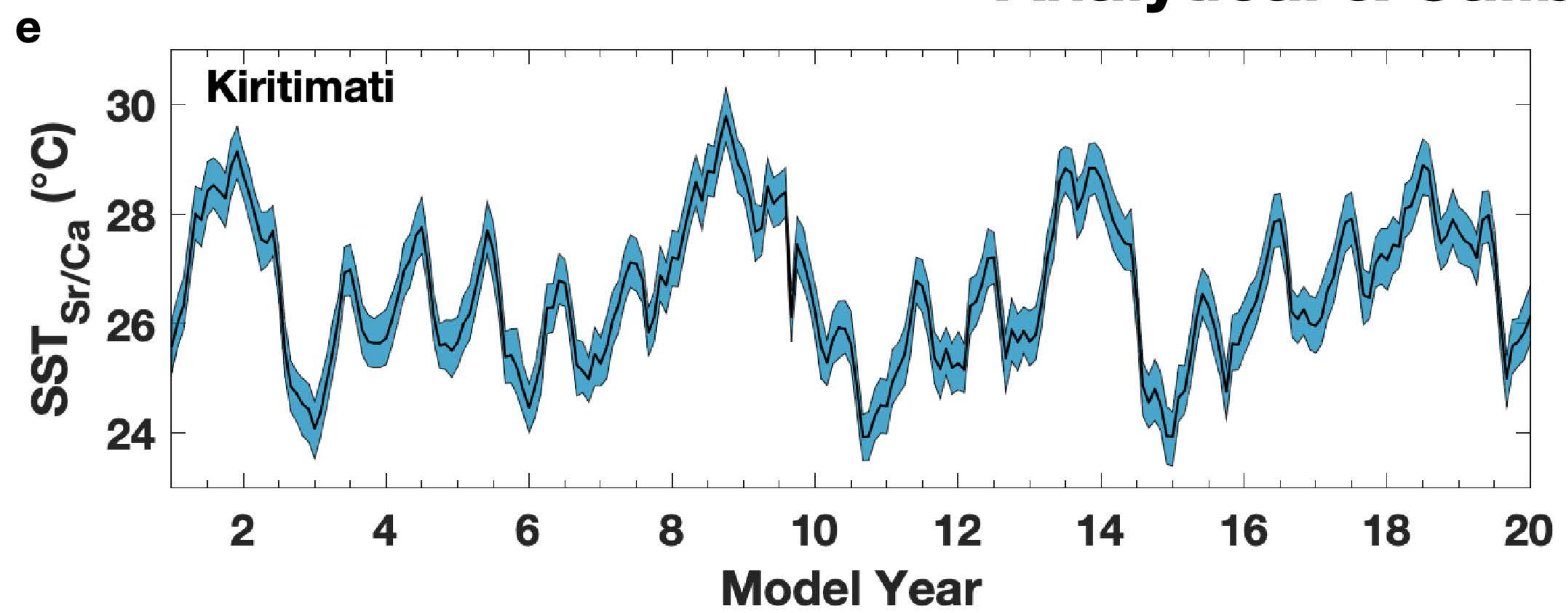
**a****Coral Growth Rate AR(2) Model****b**



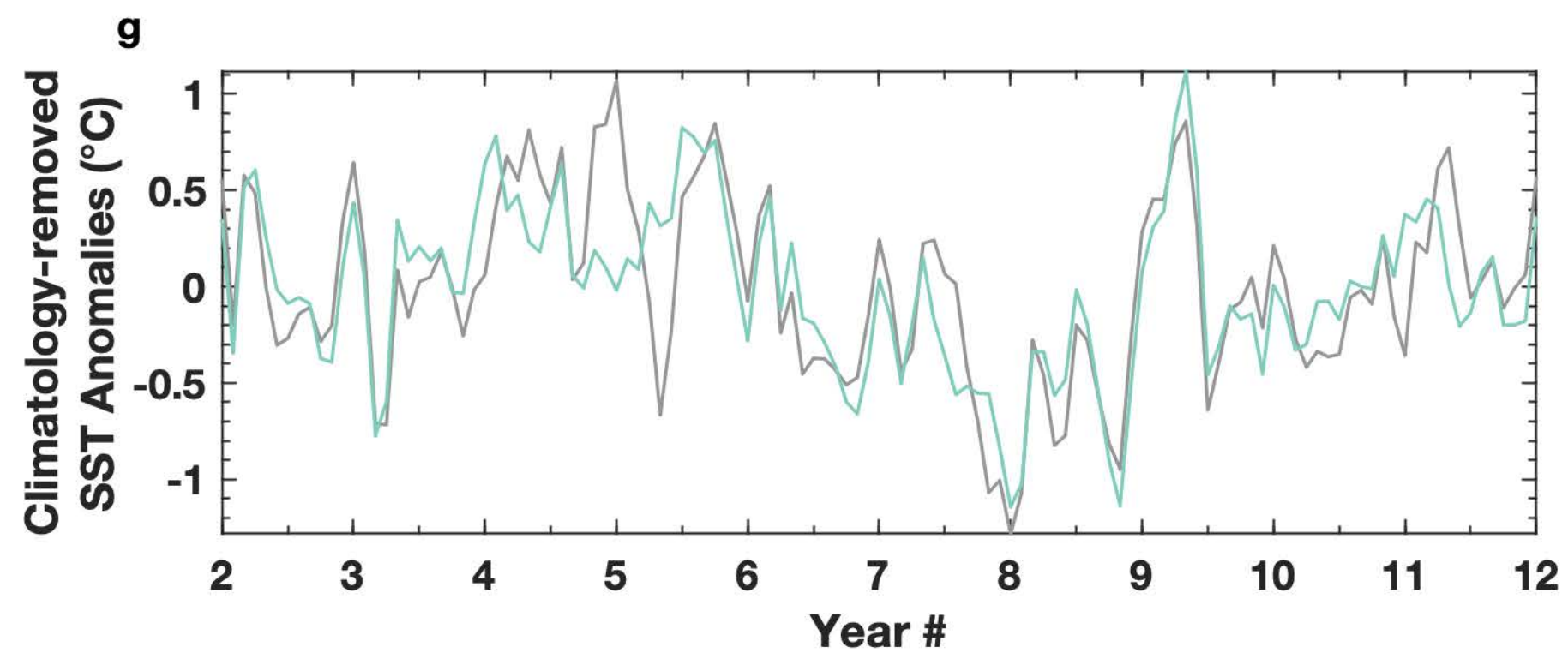
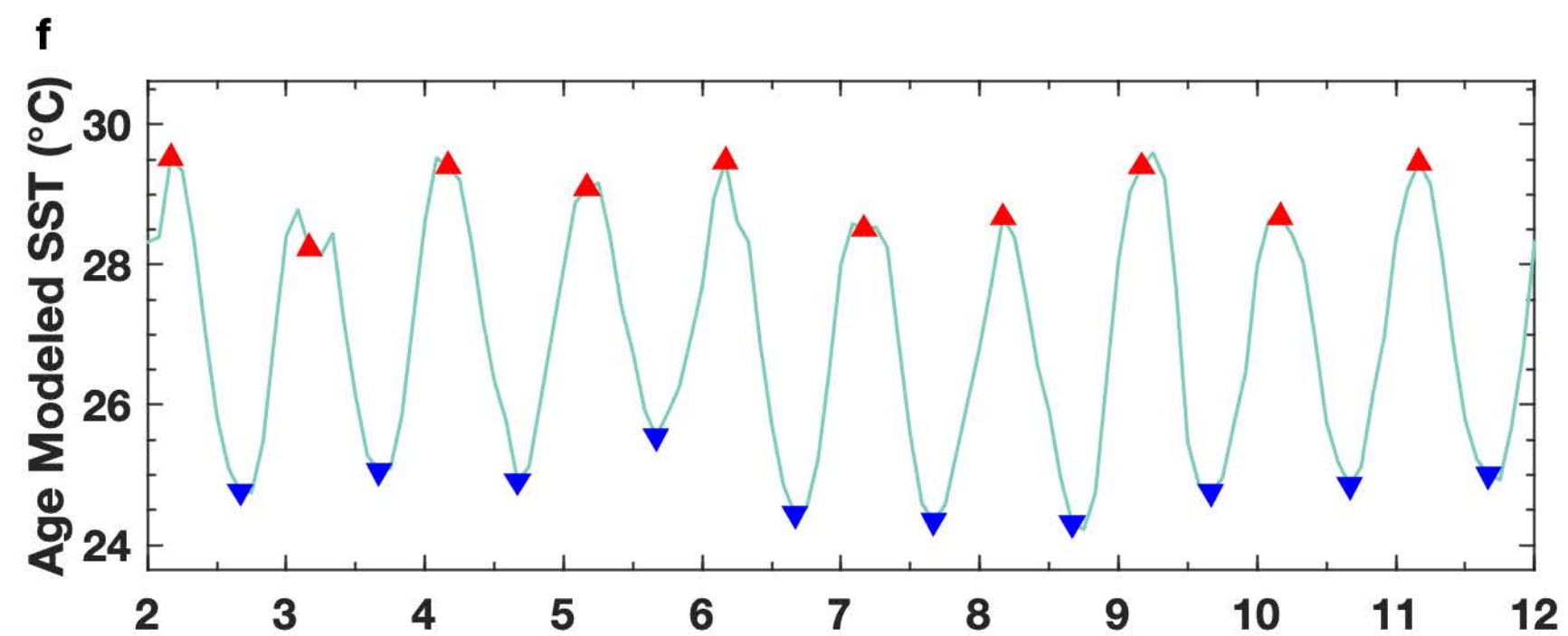
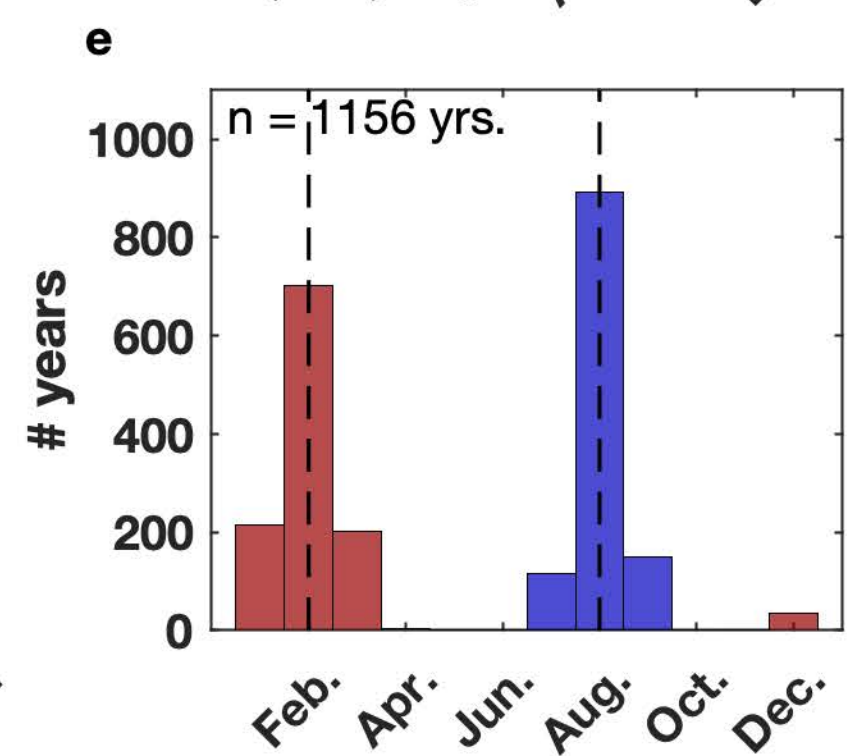
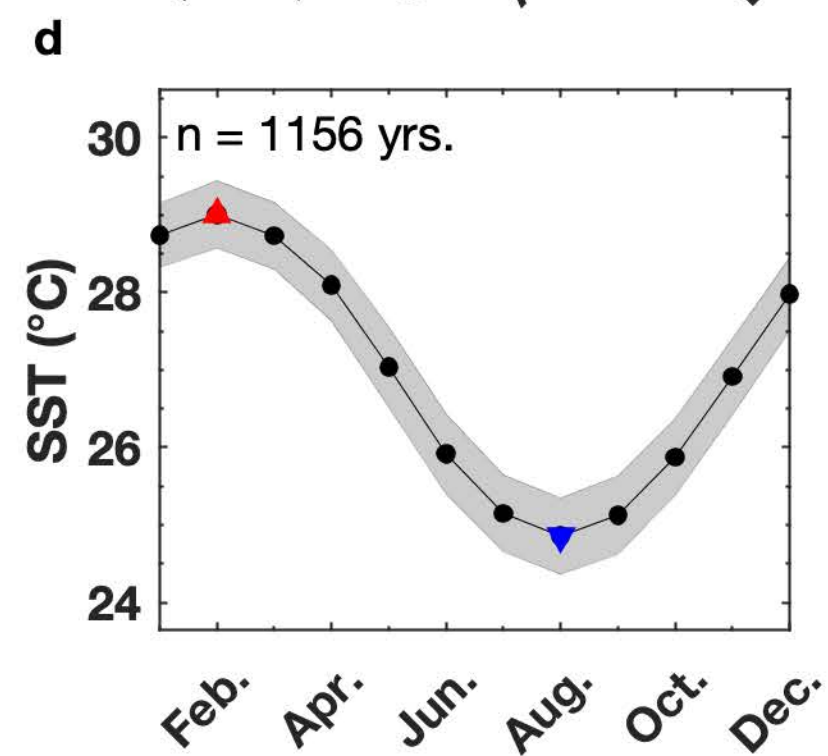
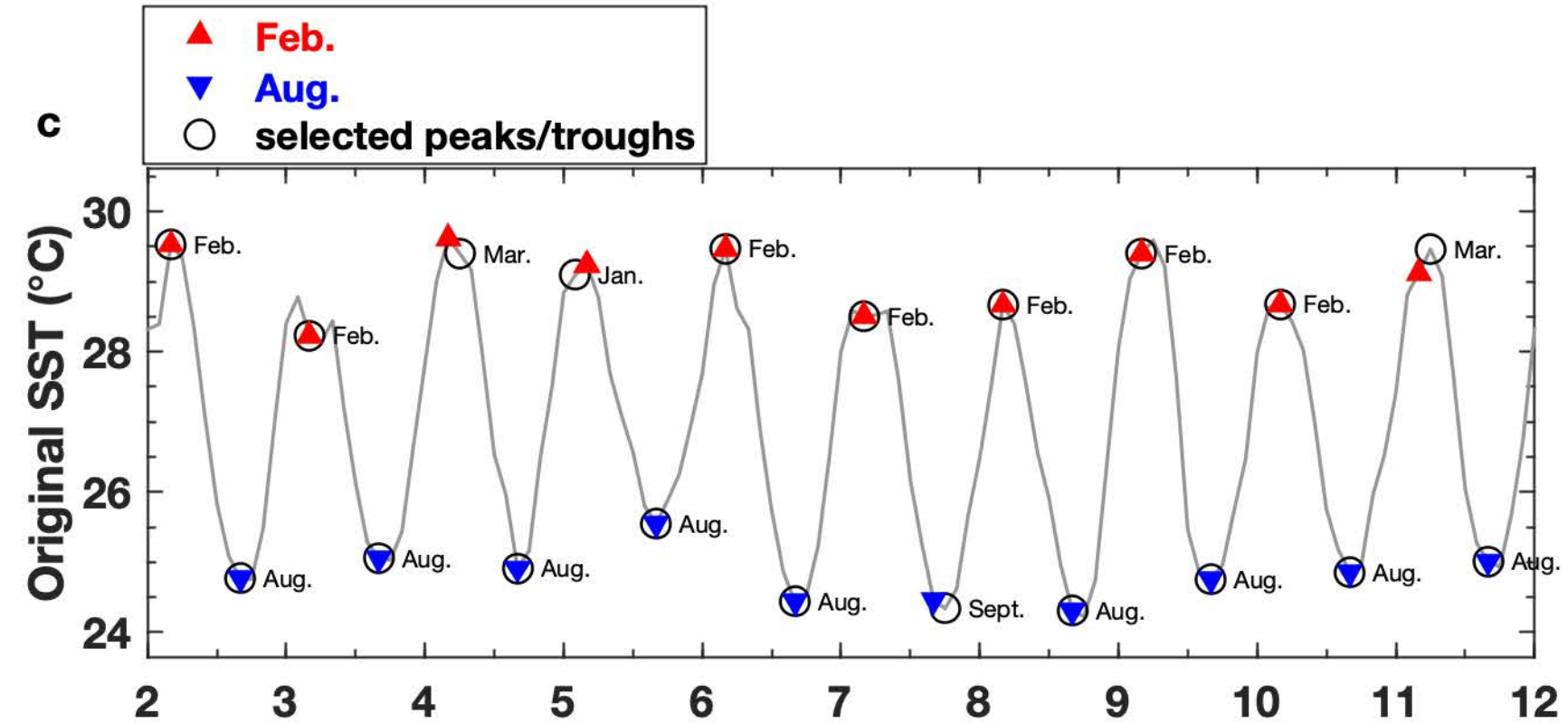
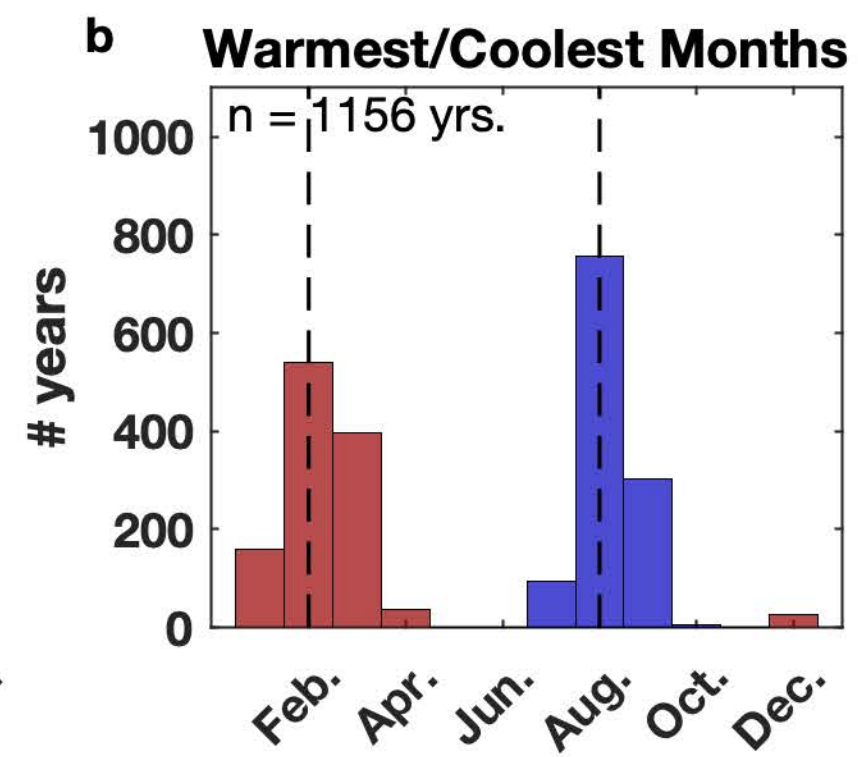
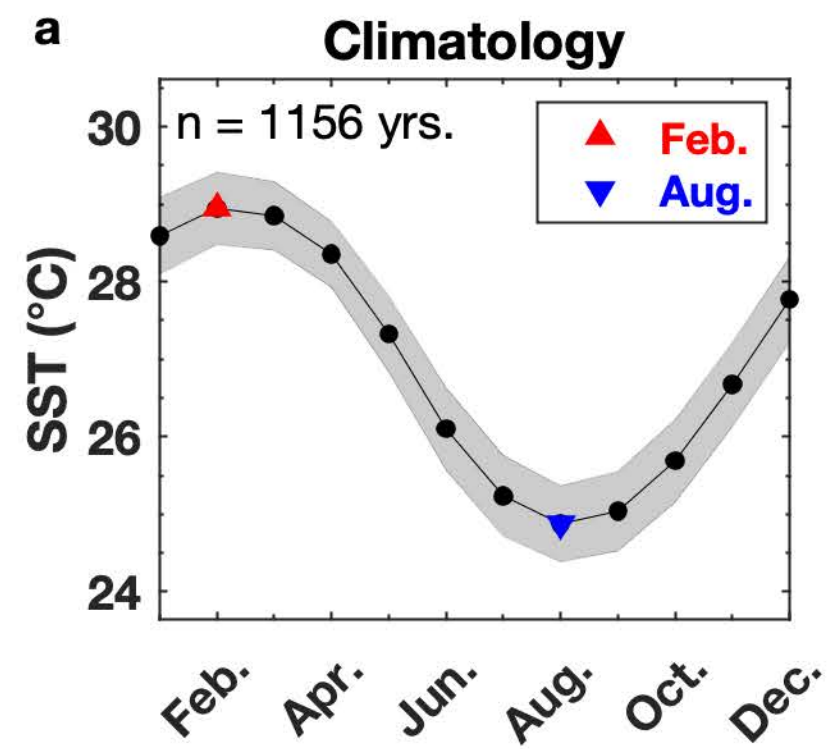
# Growth Rate Uncertainty

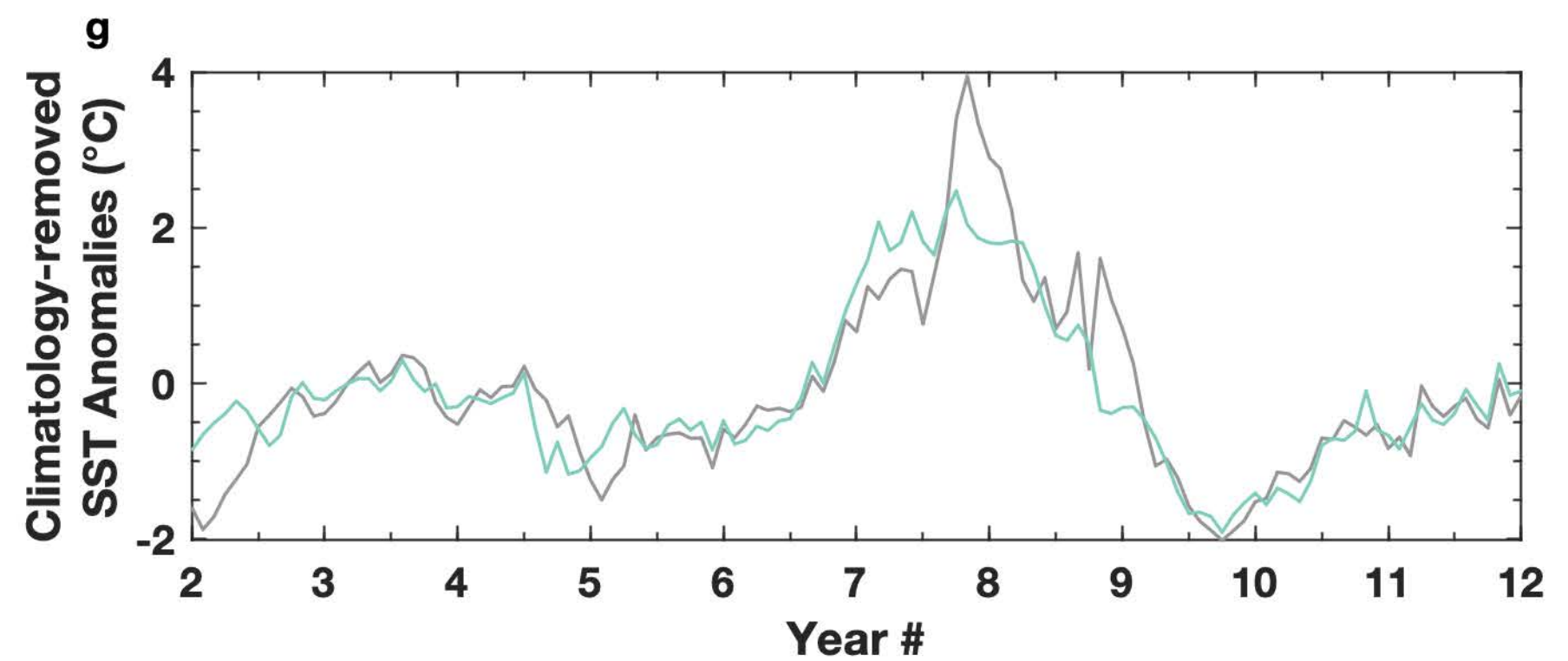
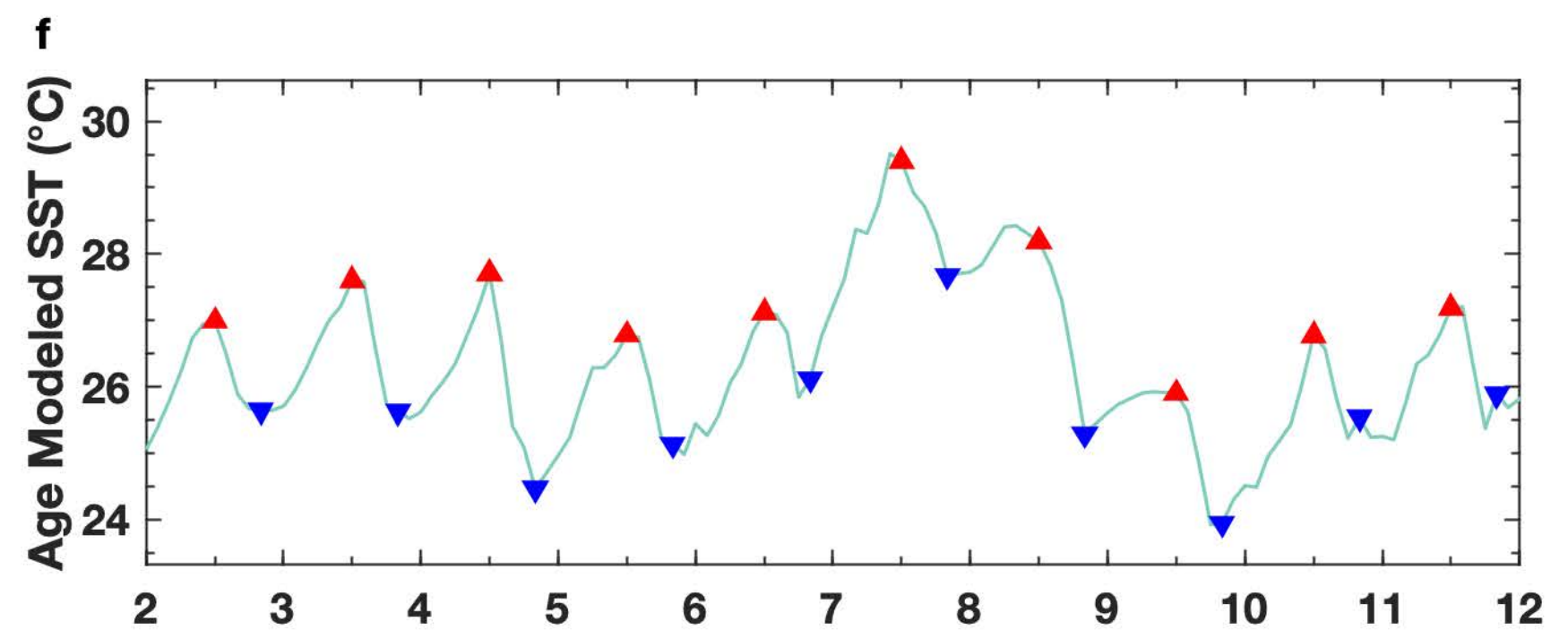
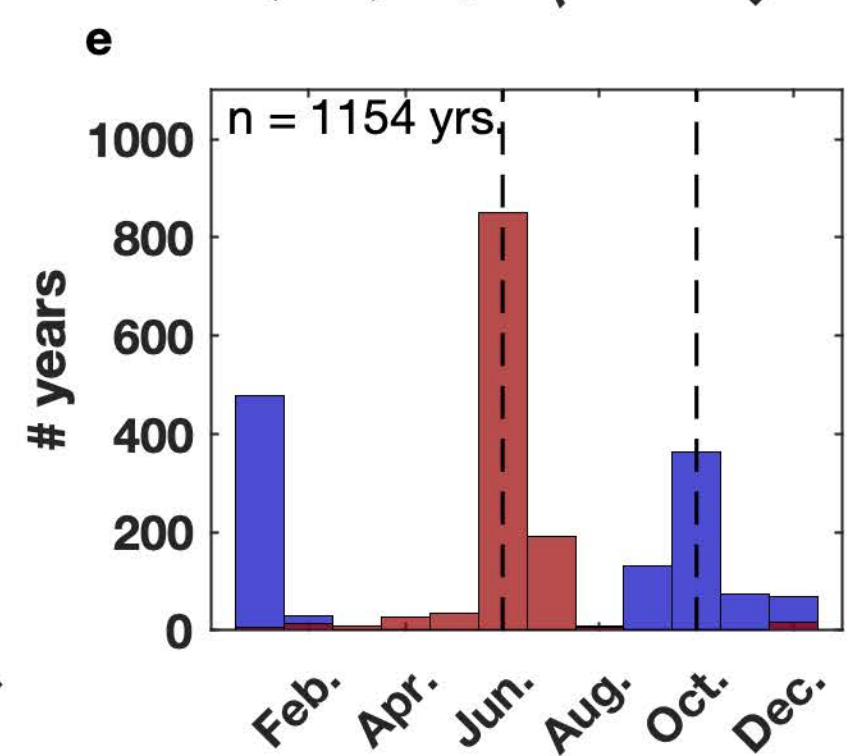
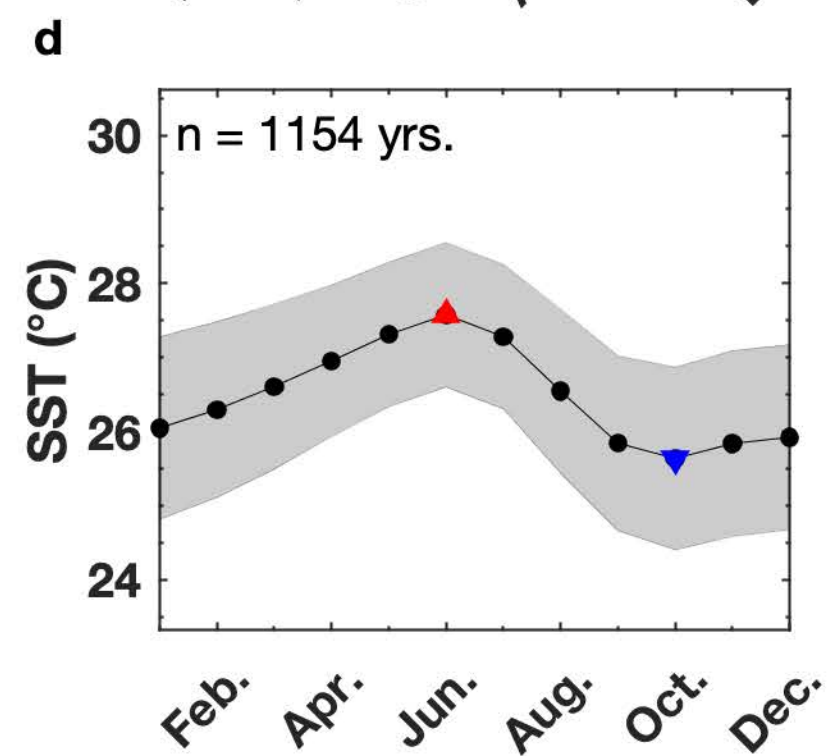
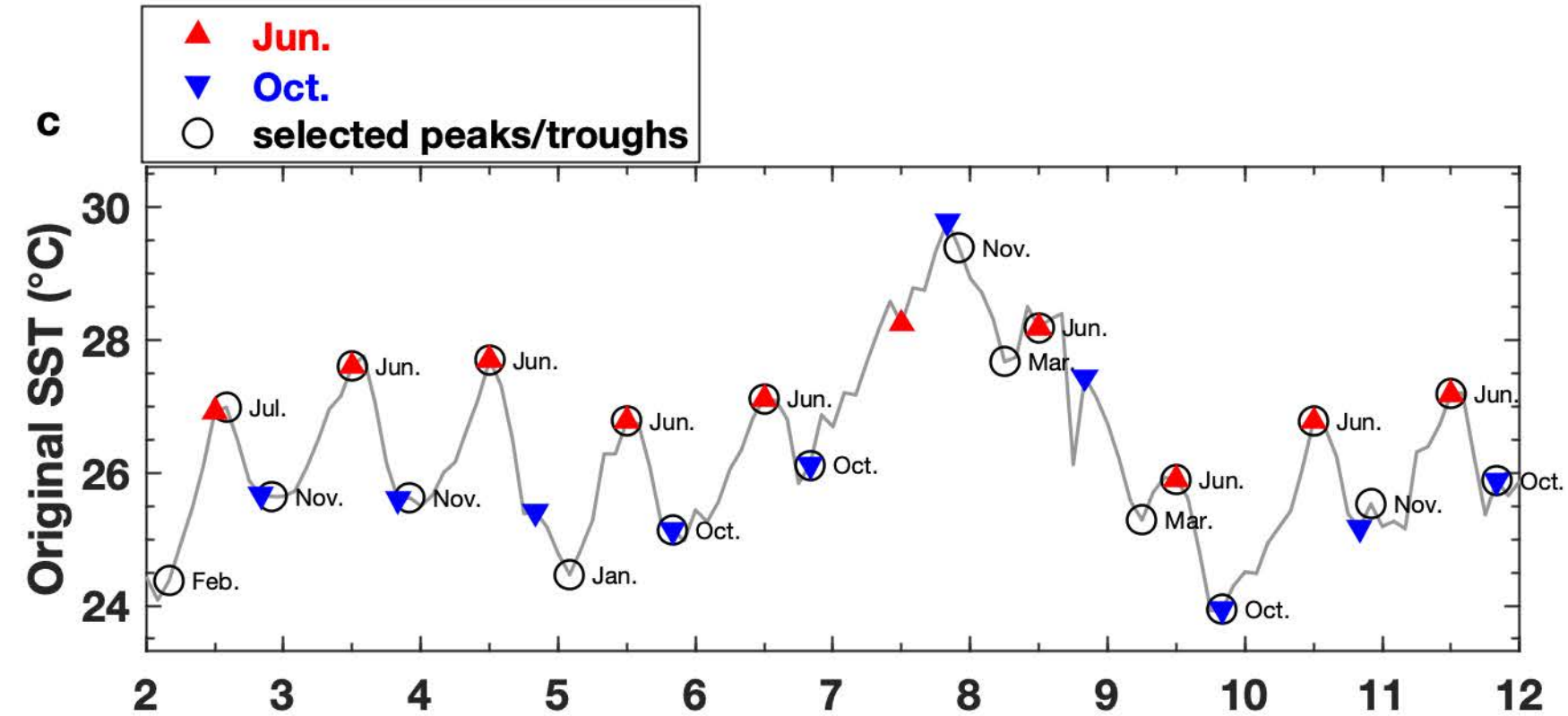
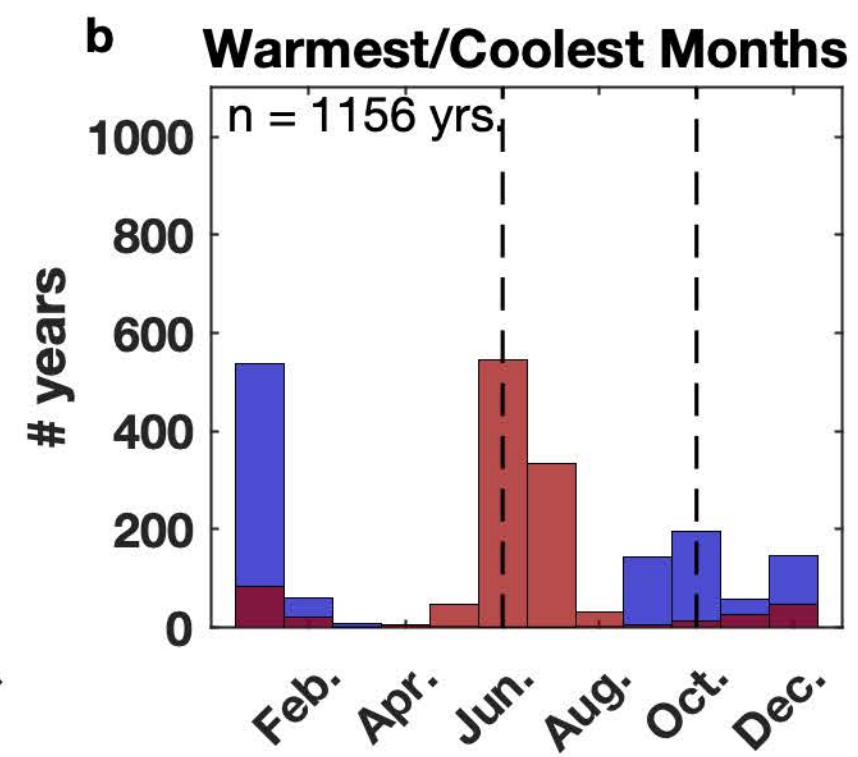
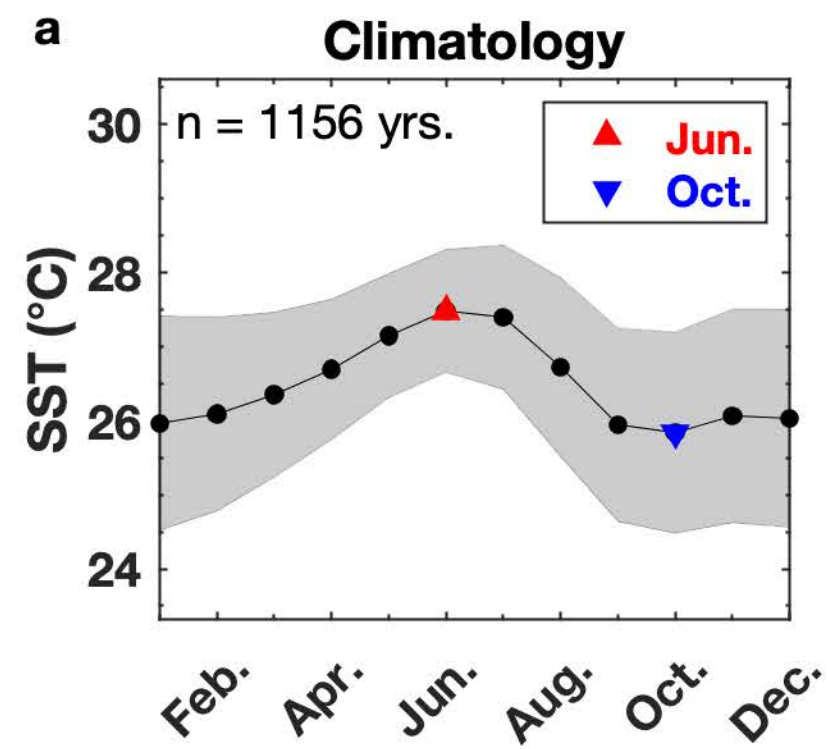


# Analytical & Calibration Uncertainty

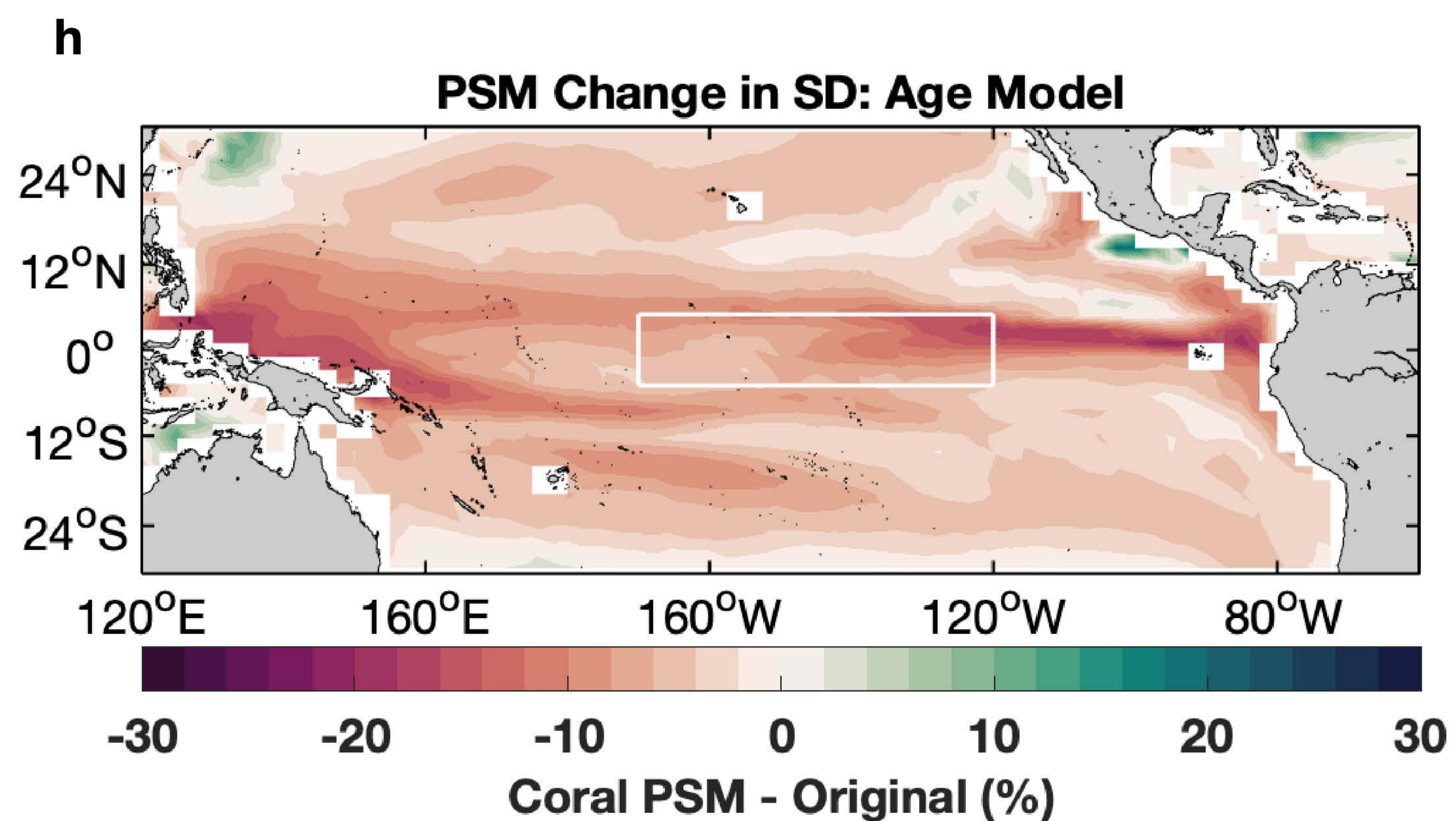
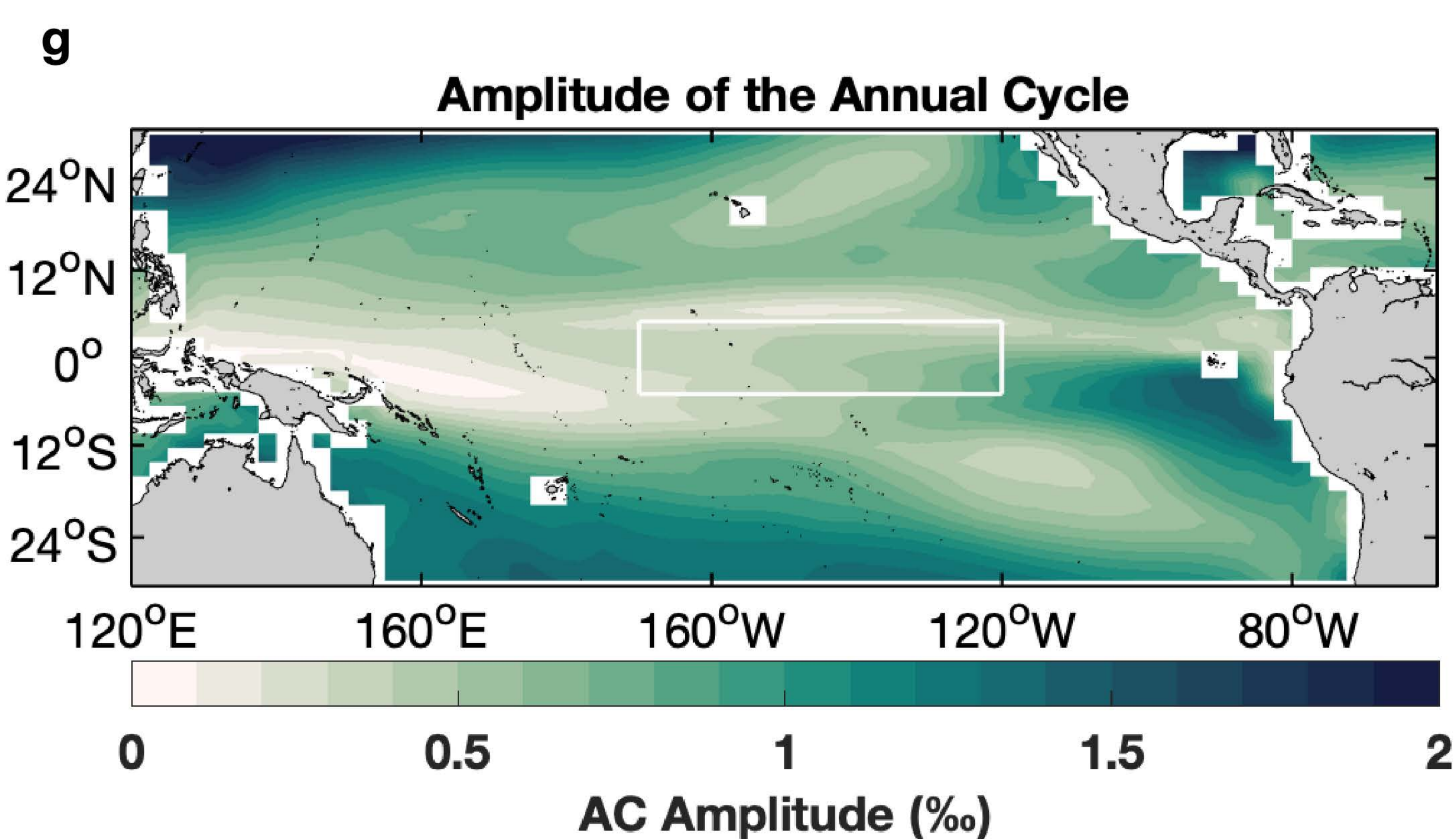
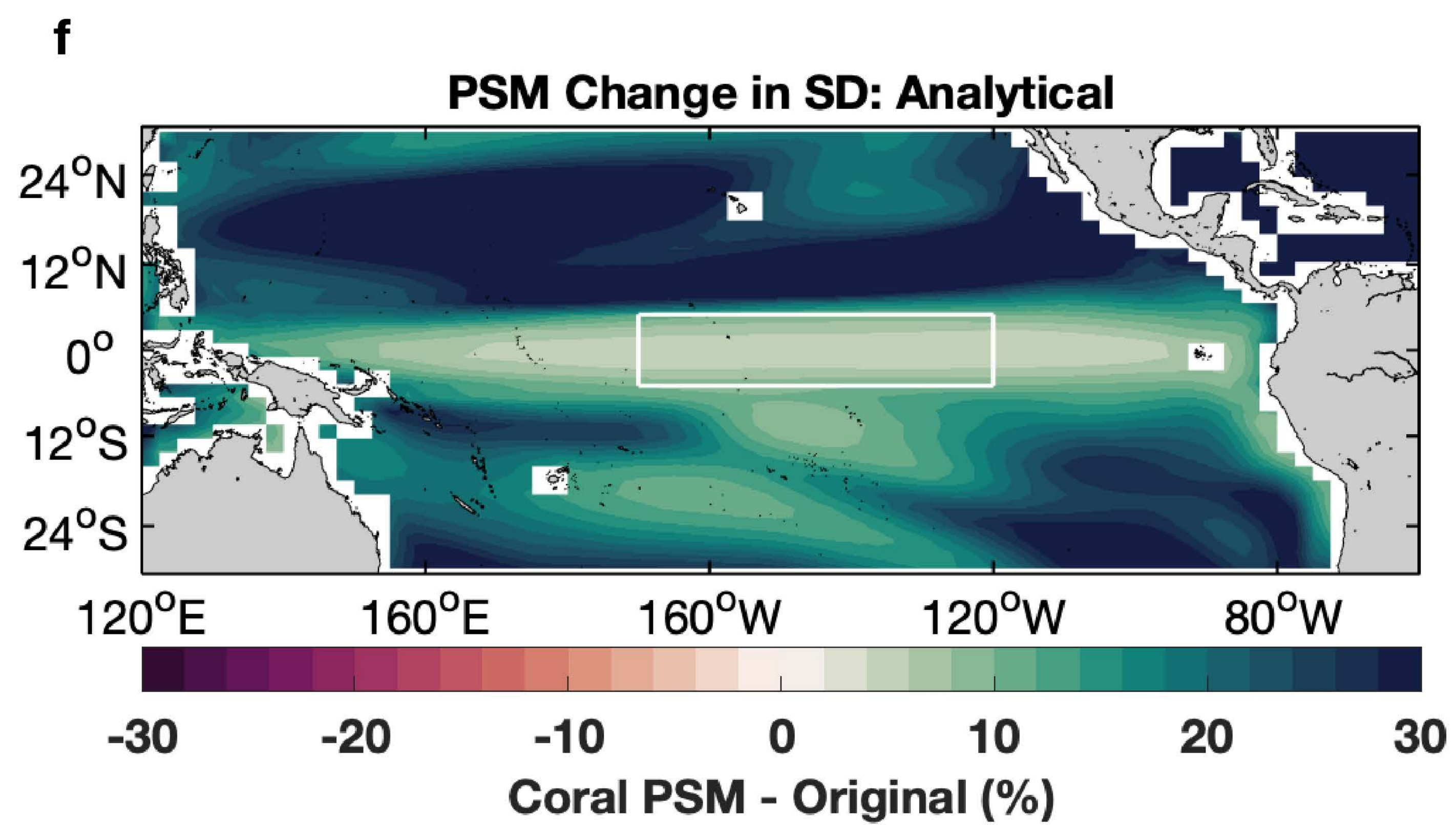
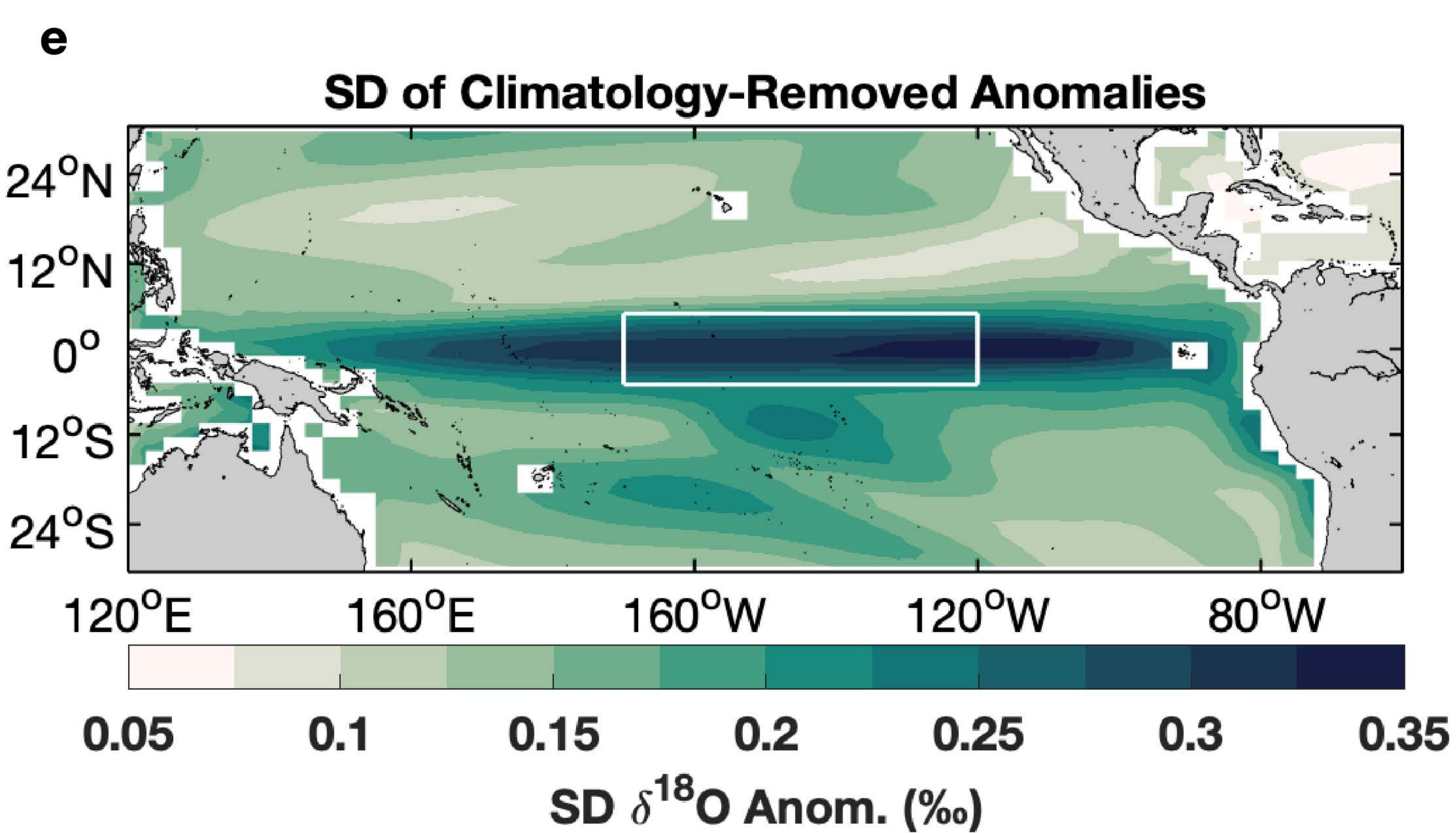
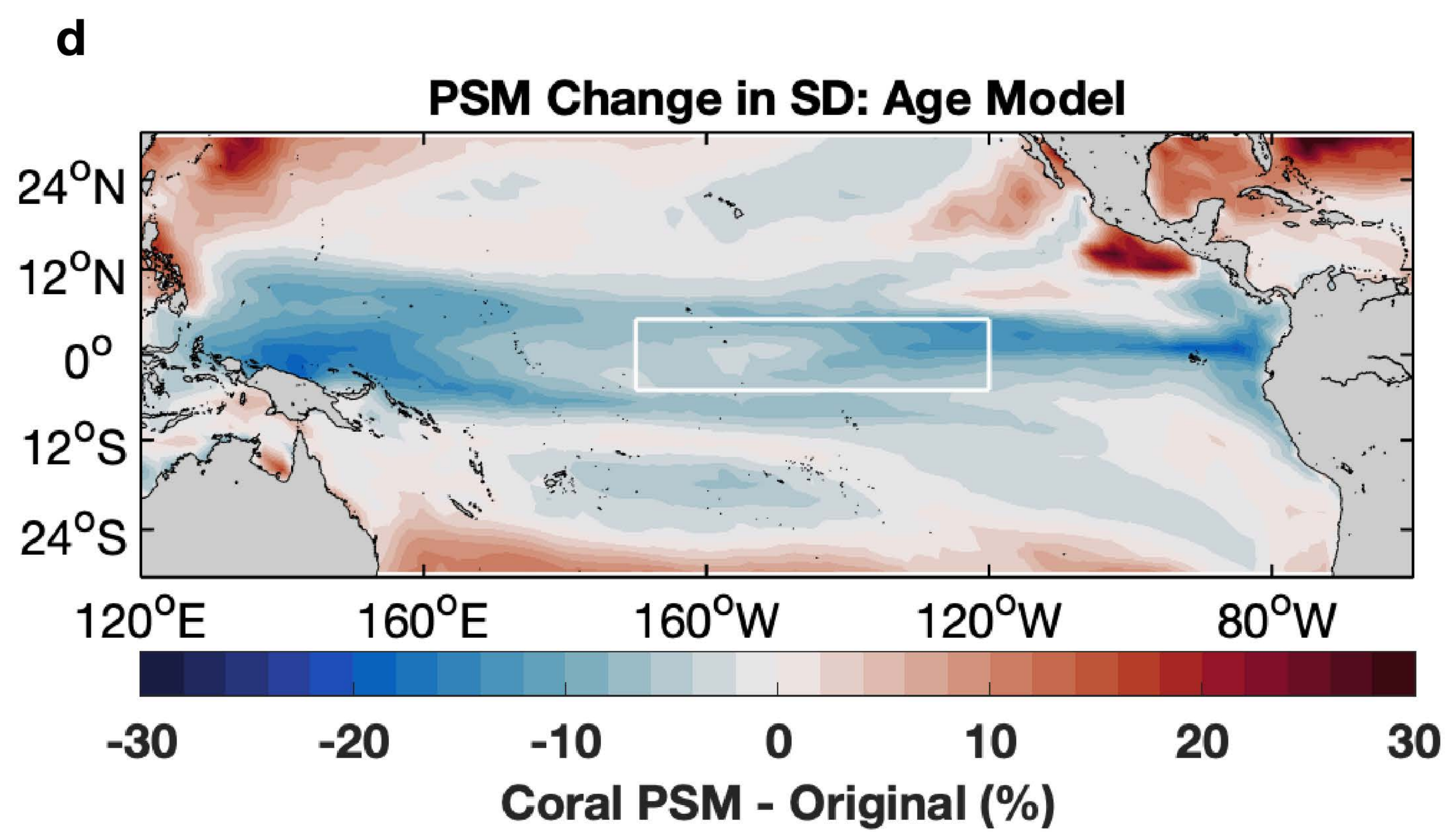
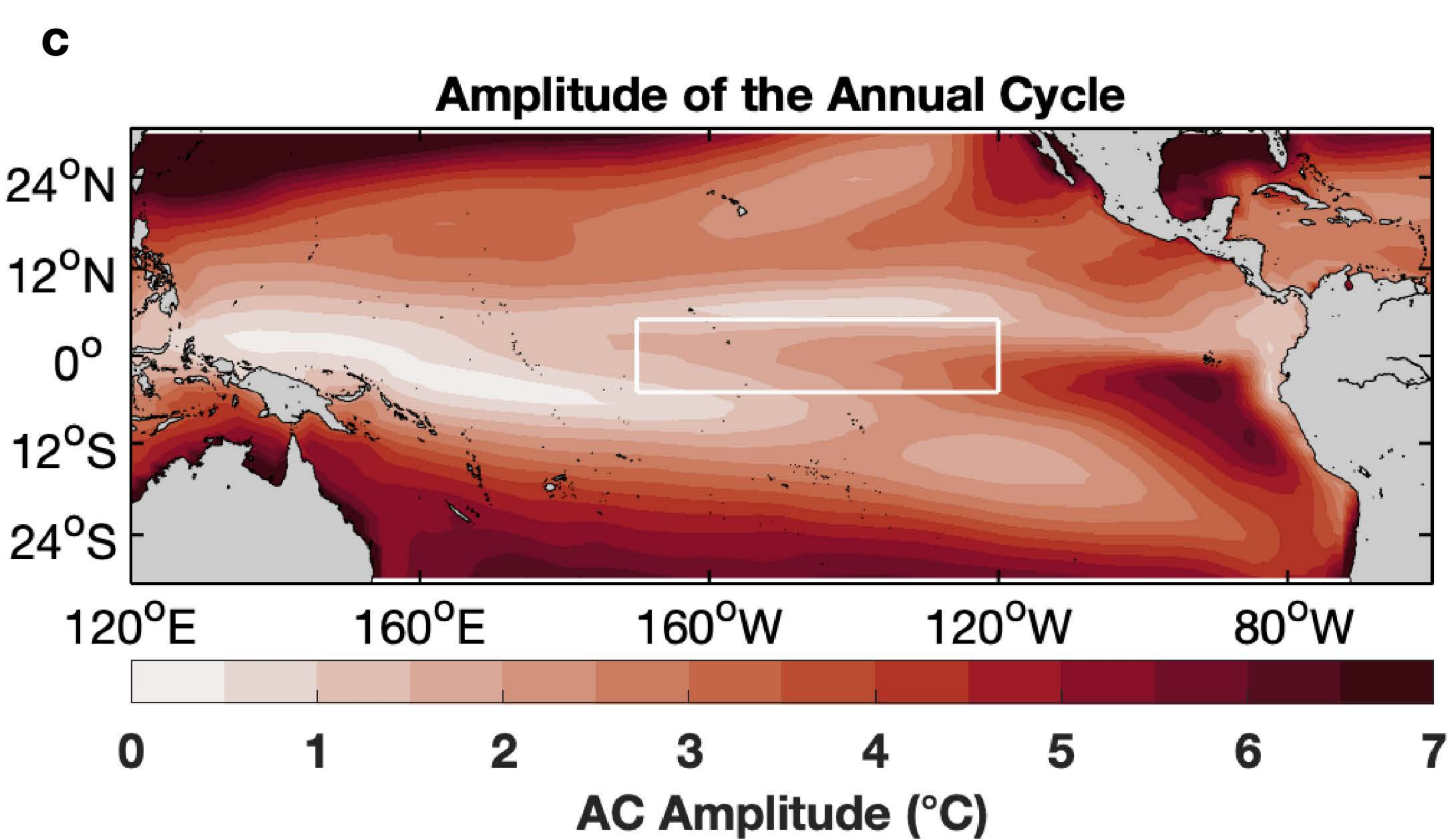
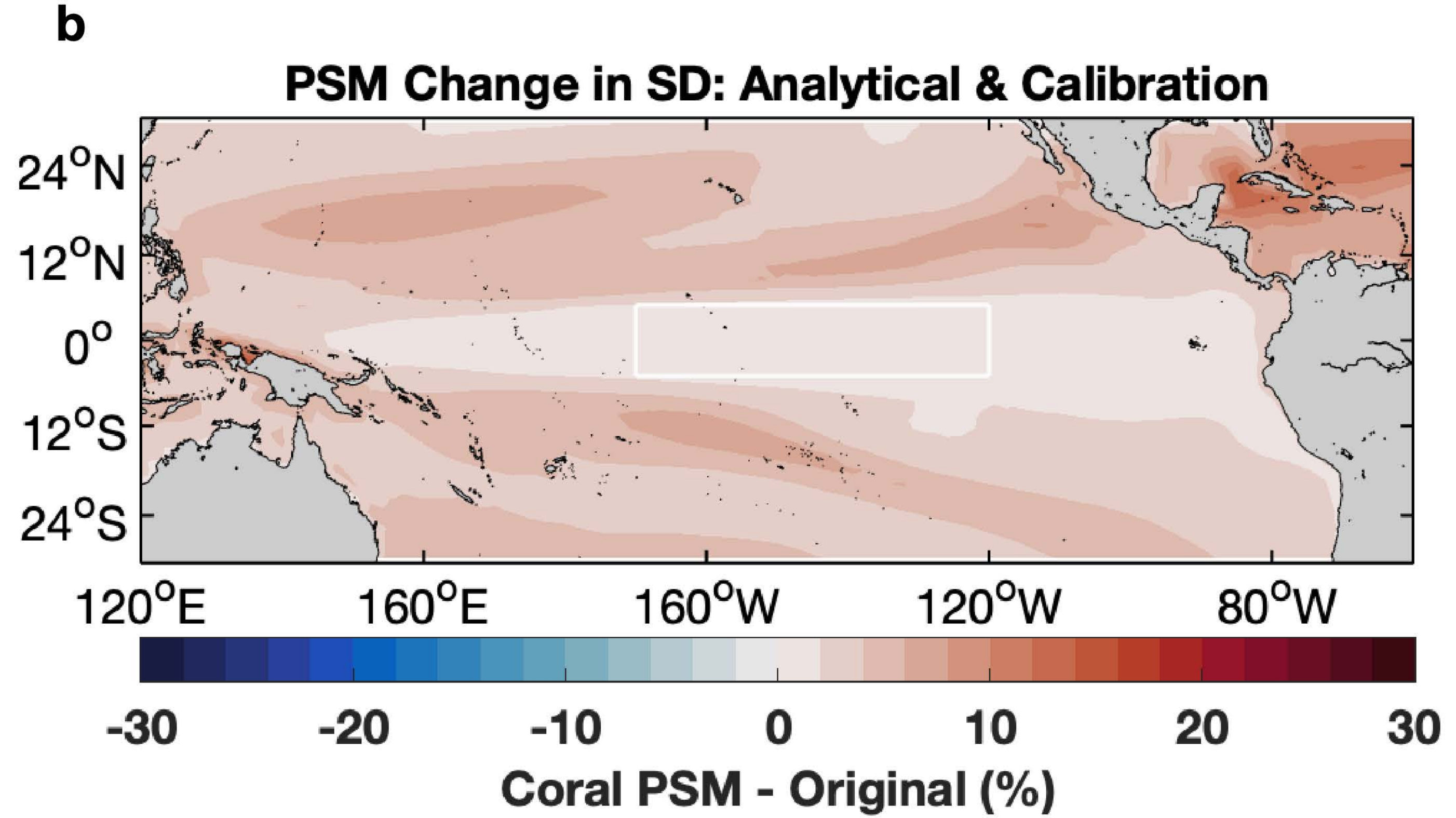
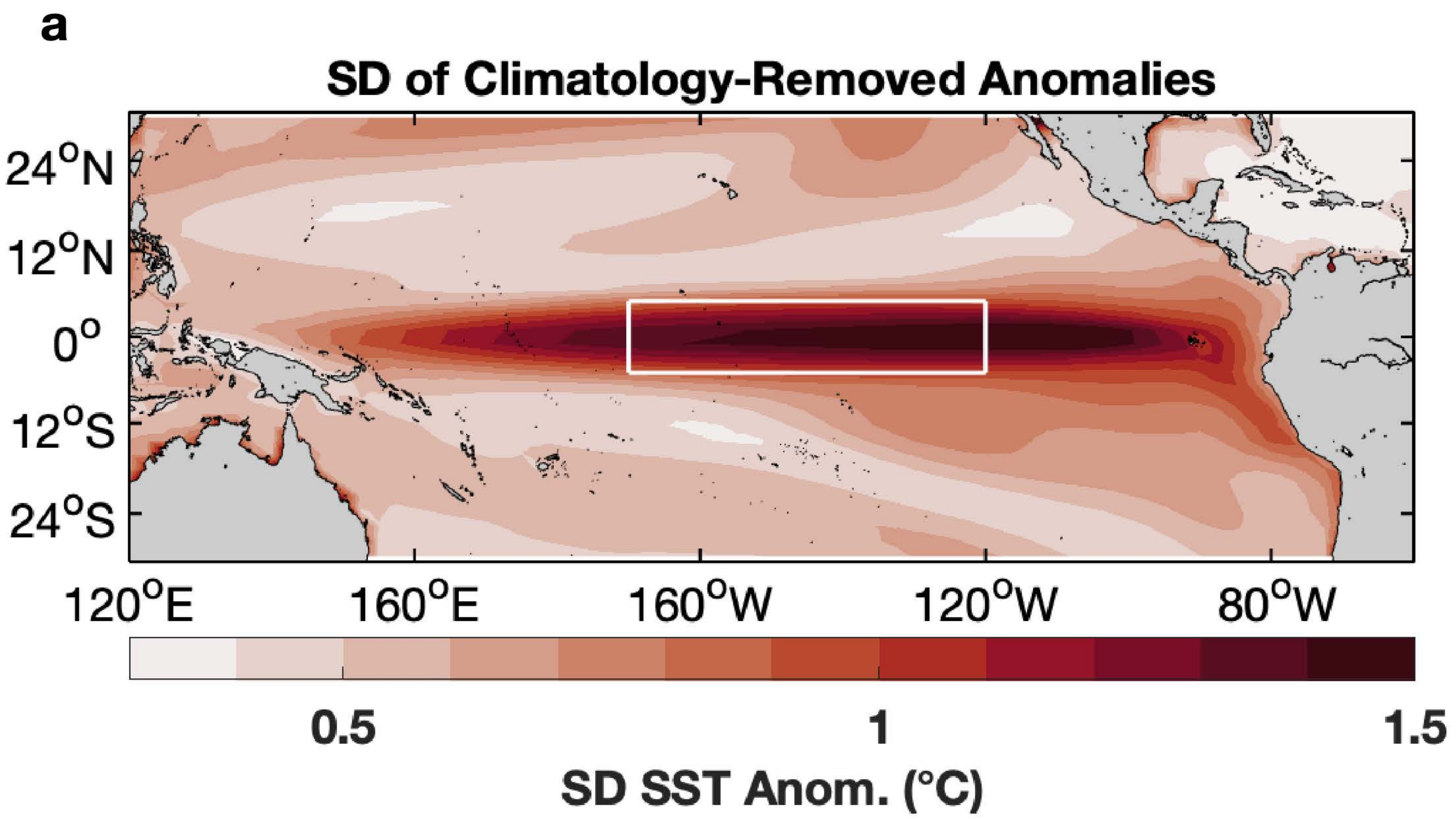








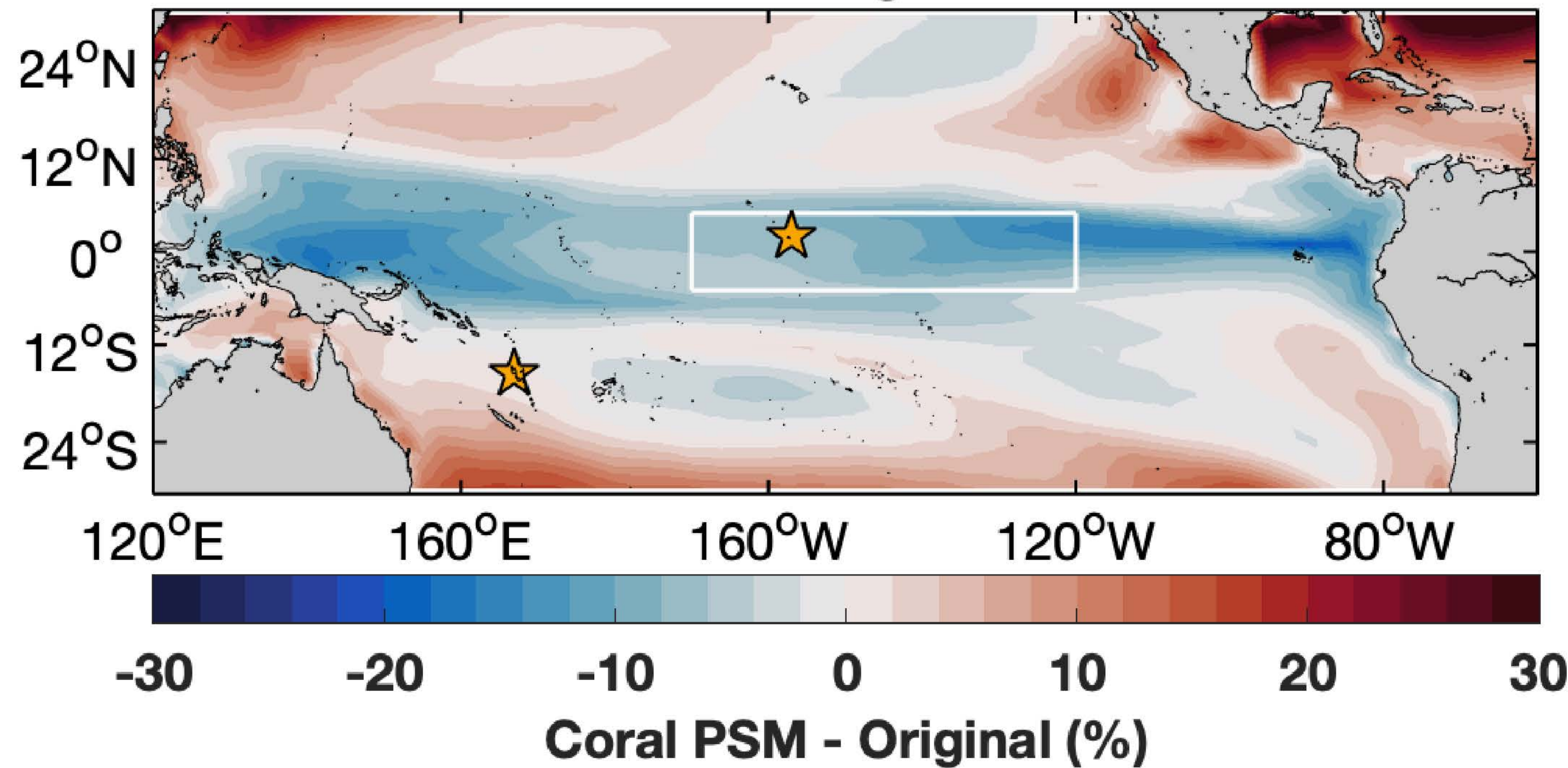






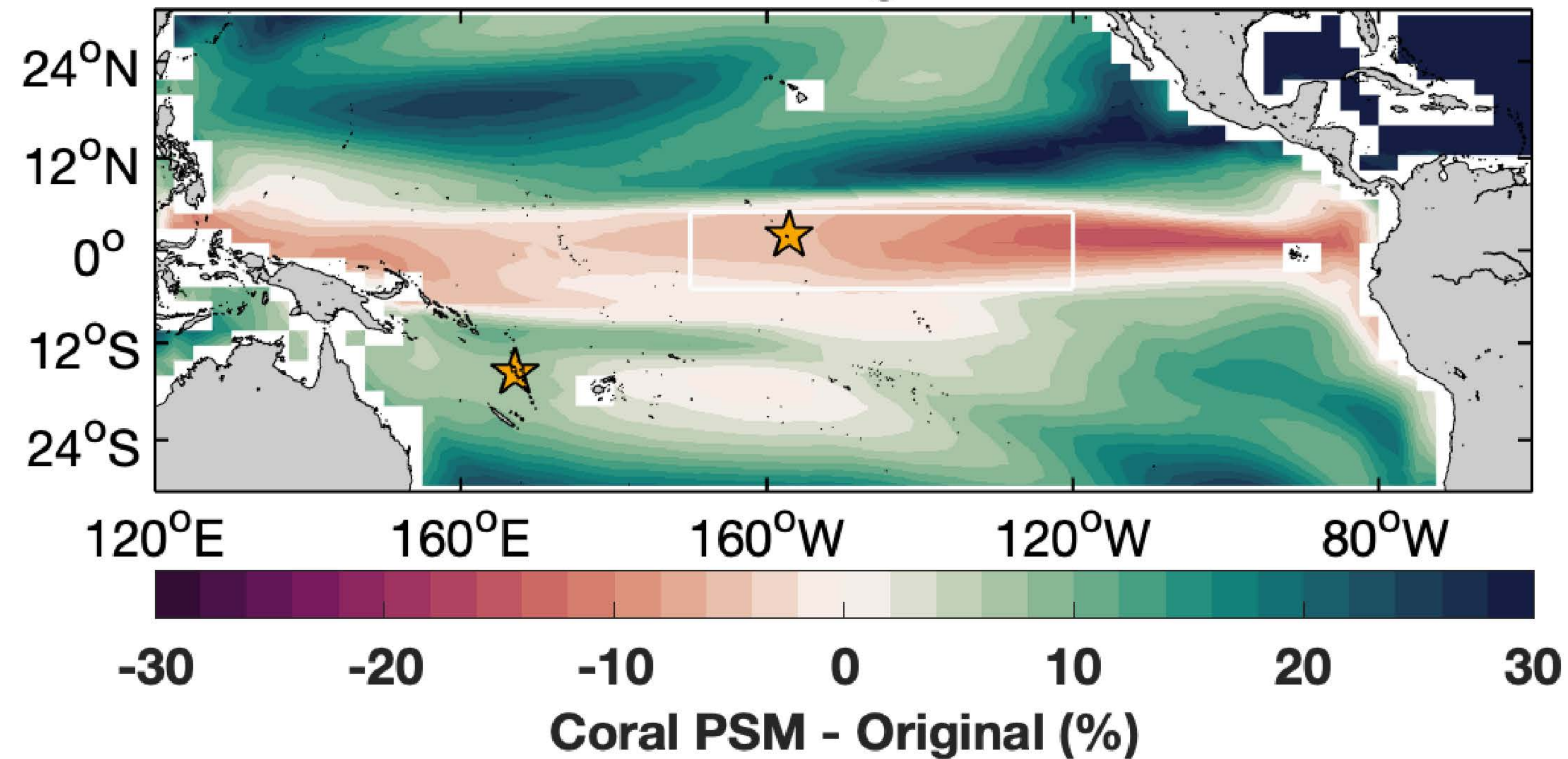
a. SST<sub>Sr/Ca</sub>

PSM Change in SD

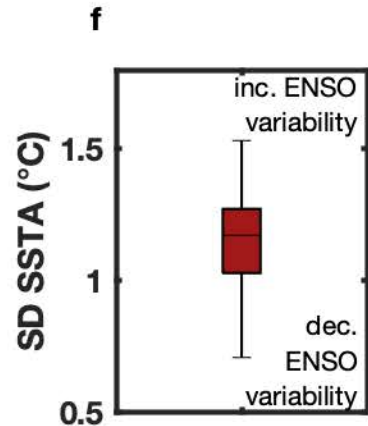
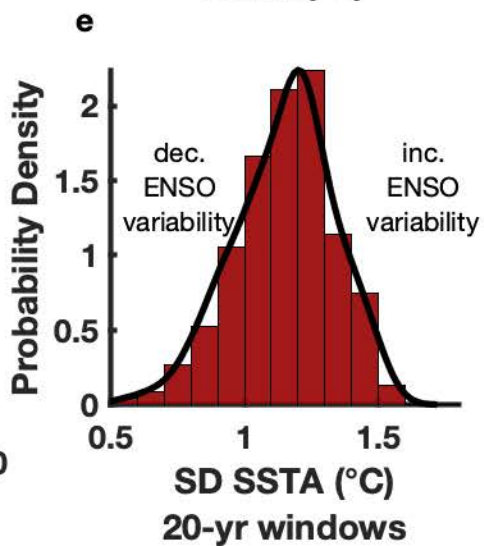
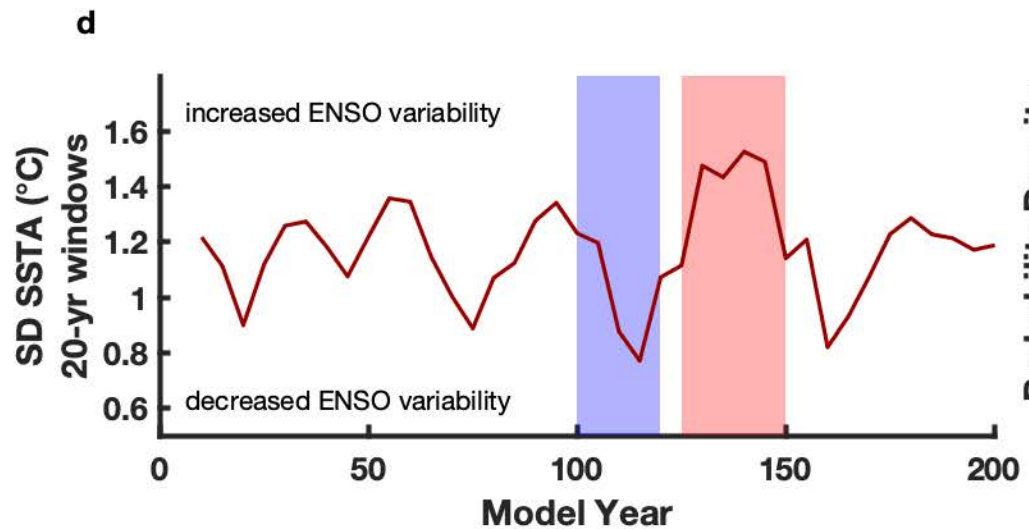
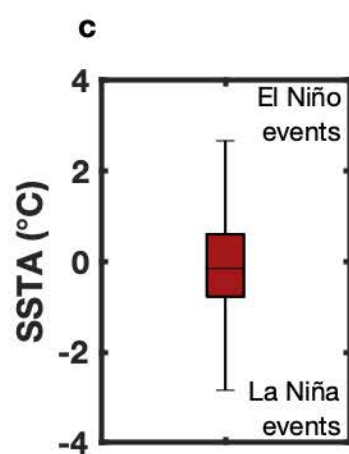
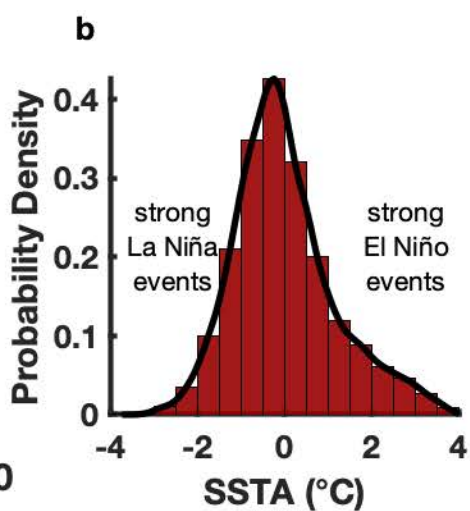
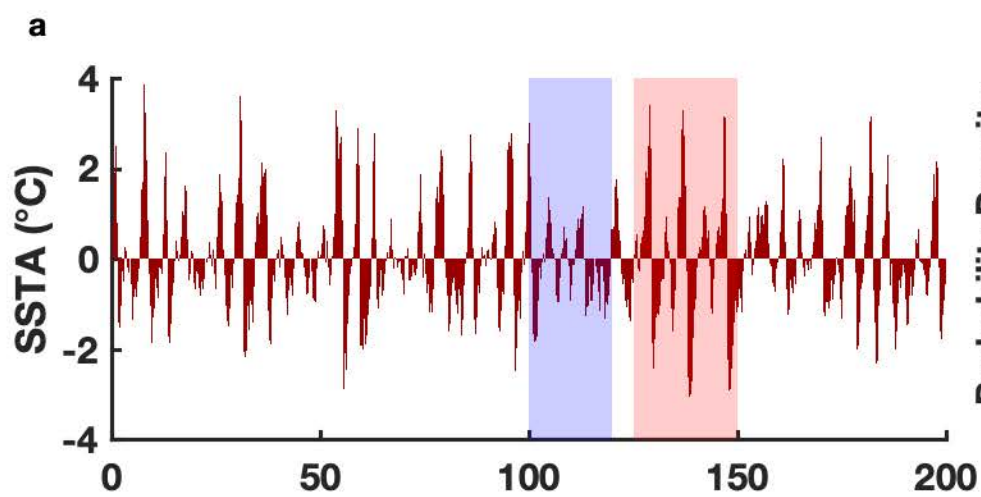


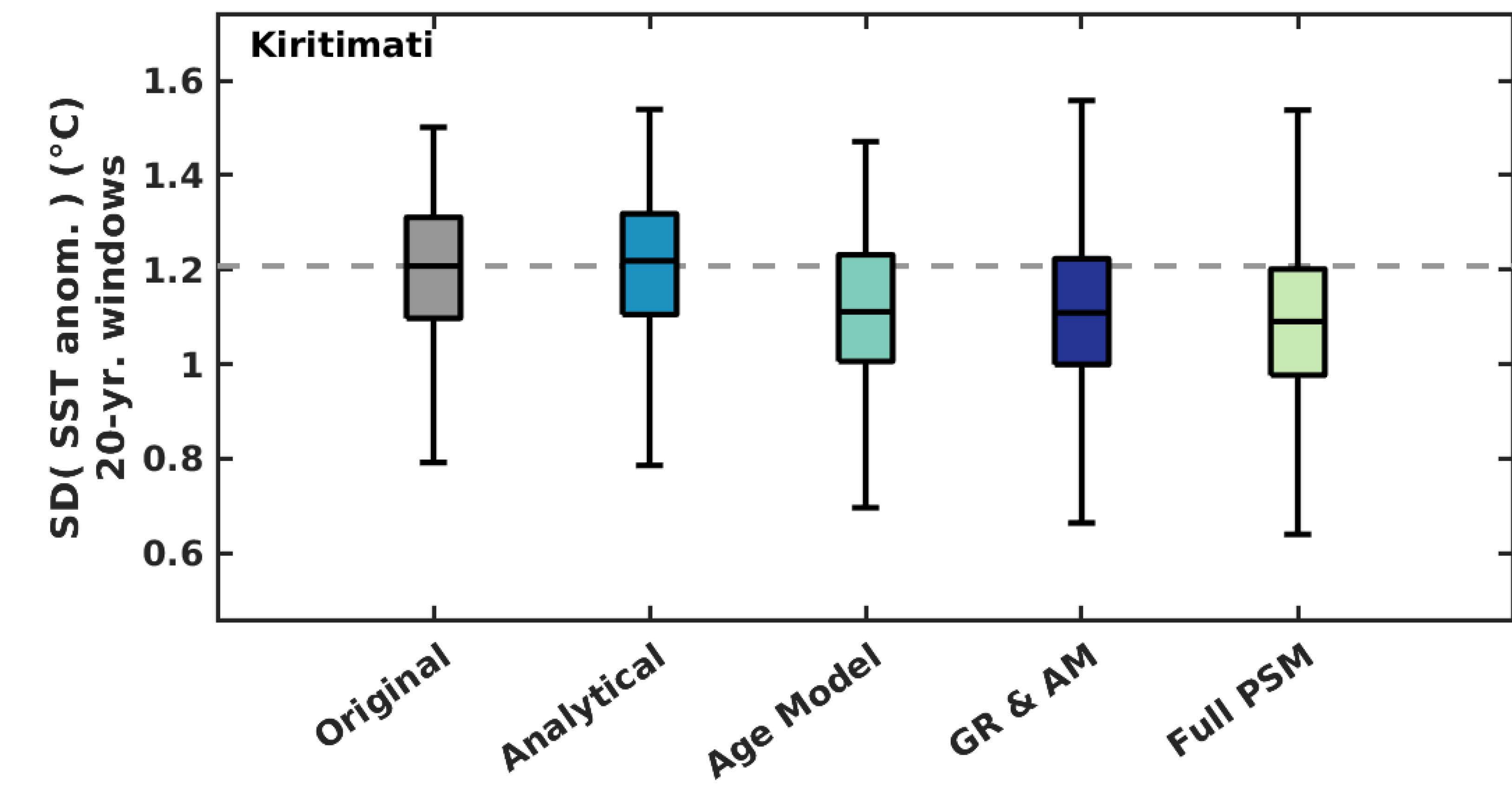
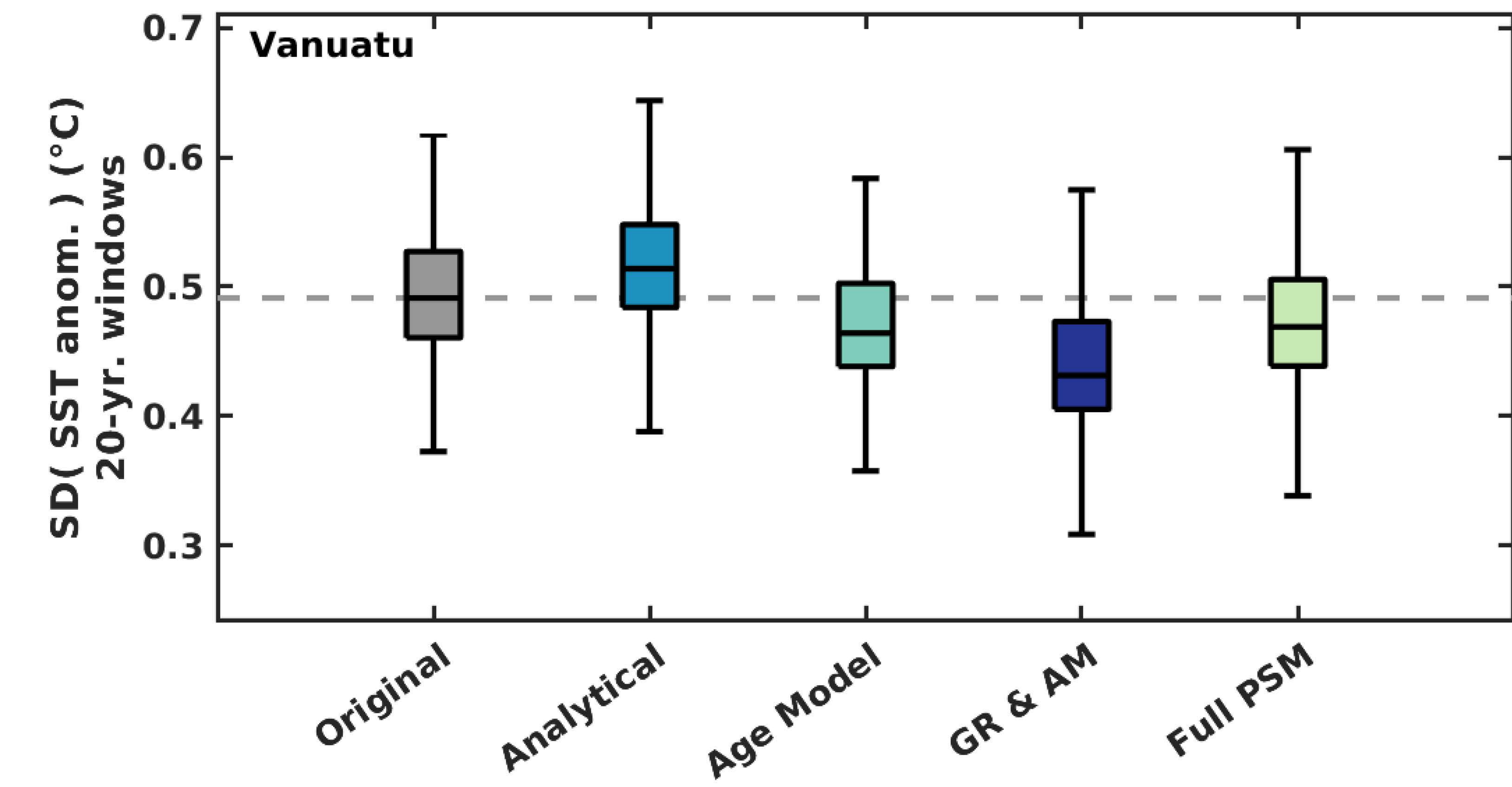
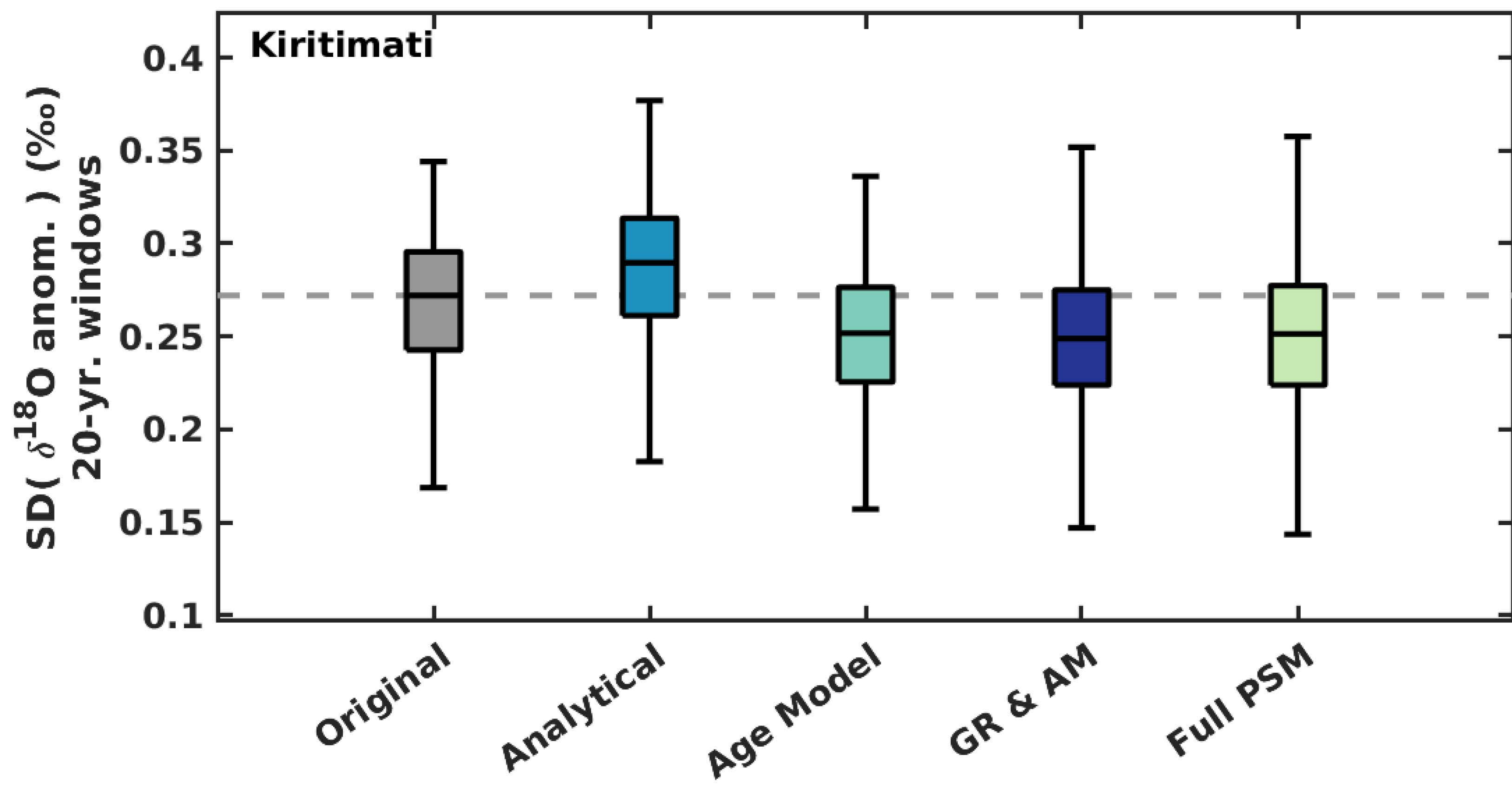
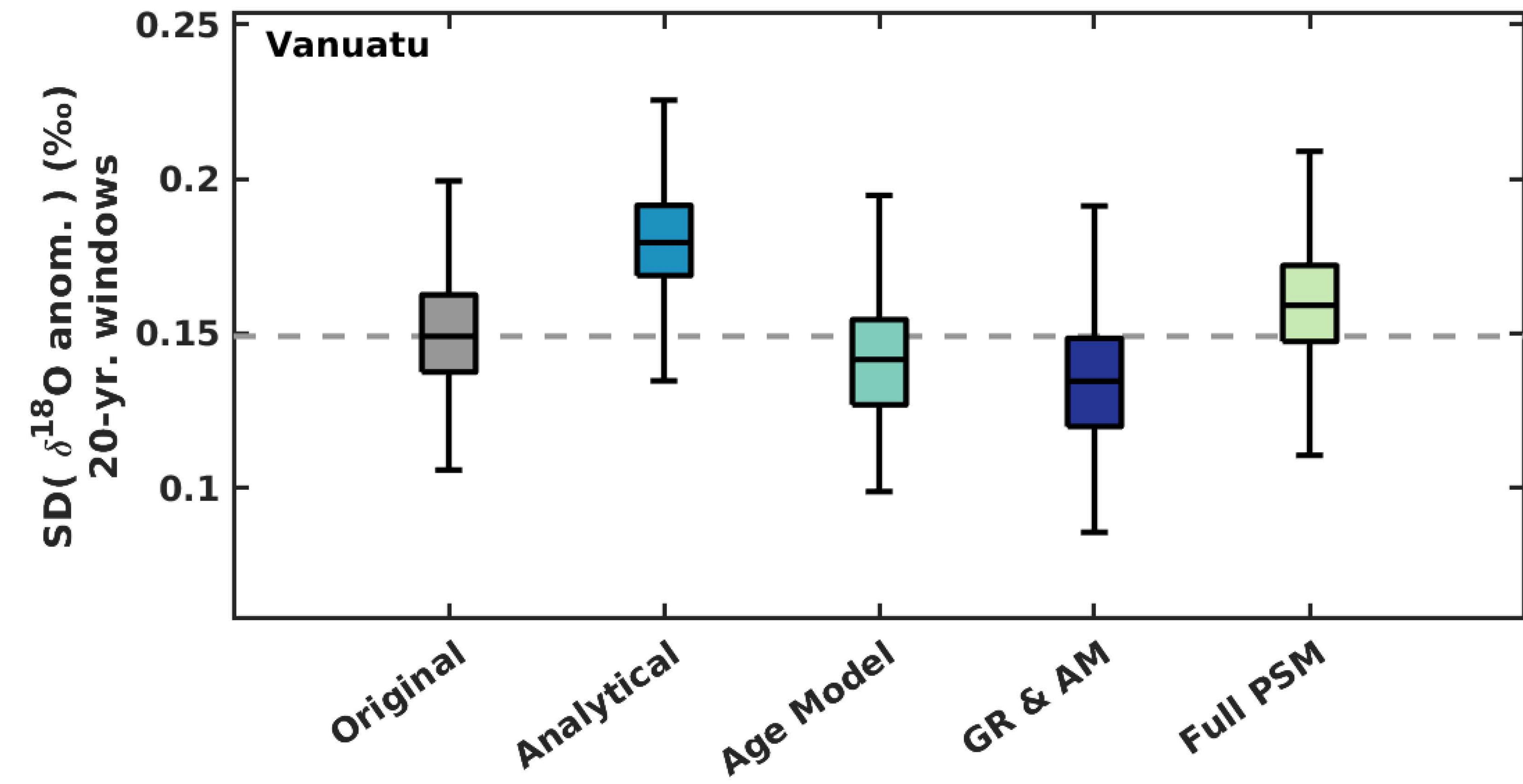
b.  $\Delta\delta^{18}\text{O}$

PSM Change in SD





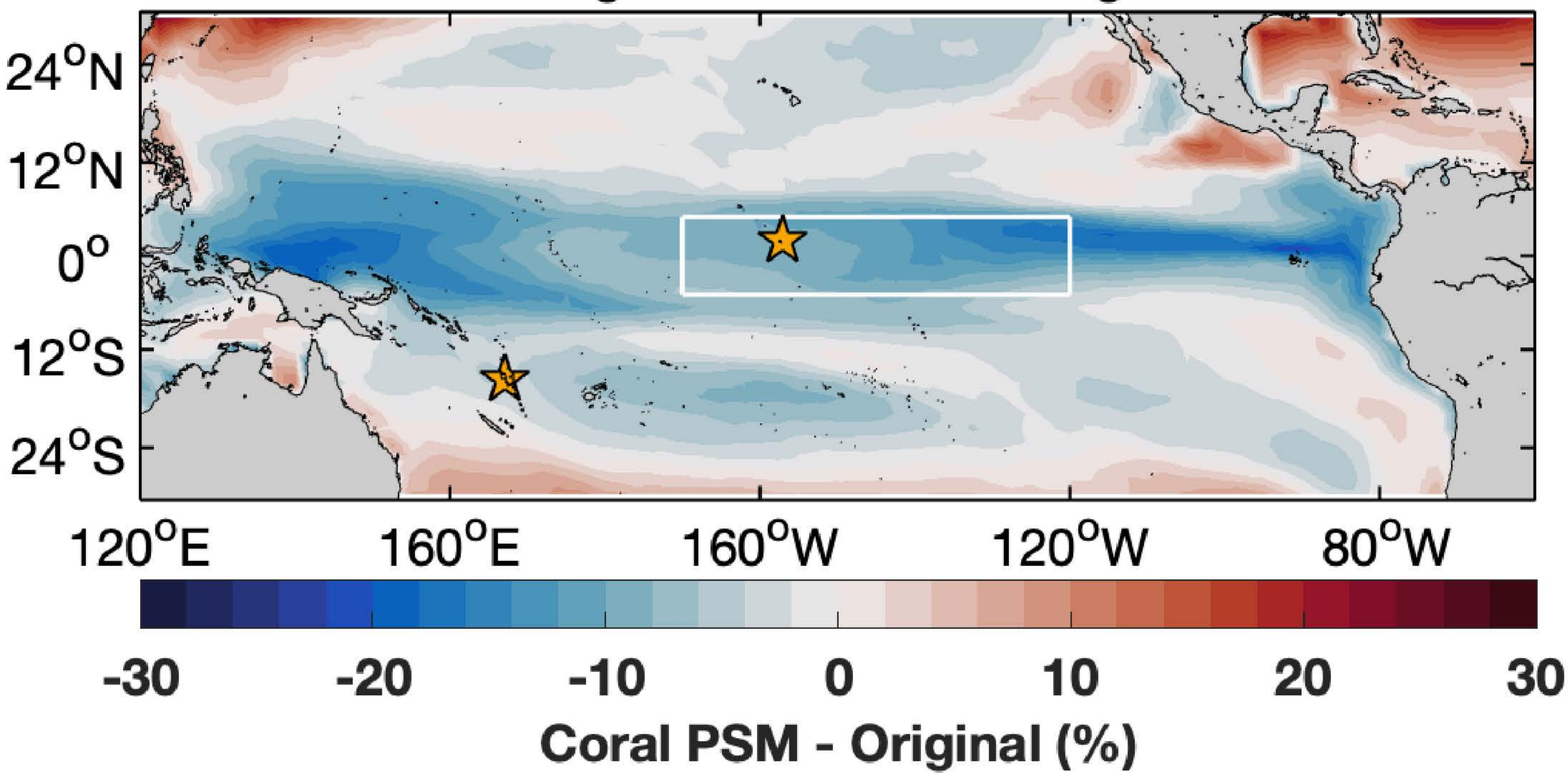


**a****b****c****d**



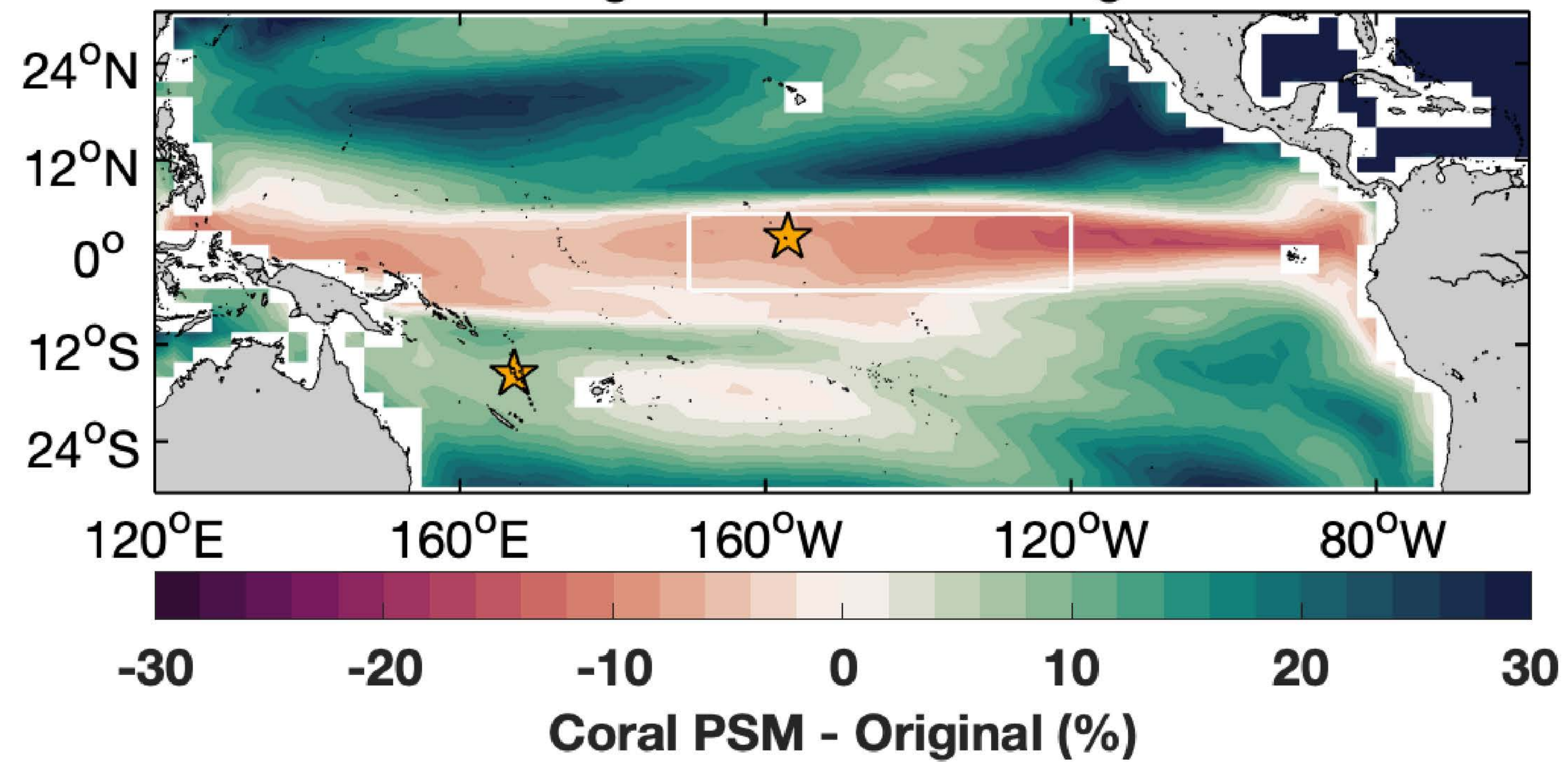
a. SST<sub>Sr/Ca</sub>

Change in Median Running SD

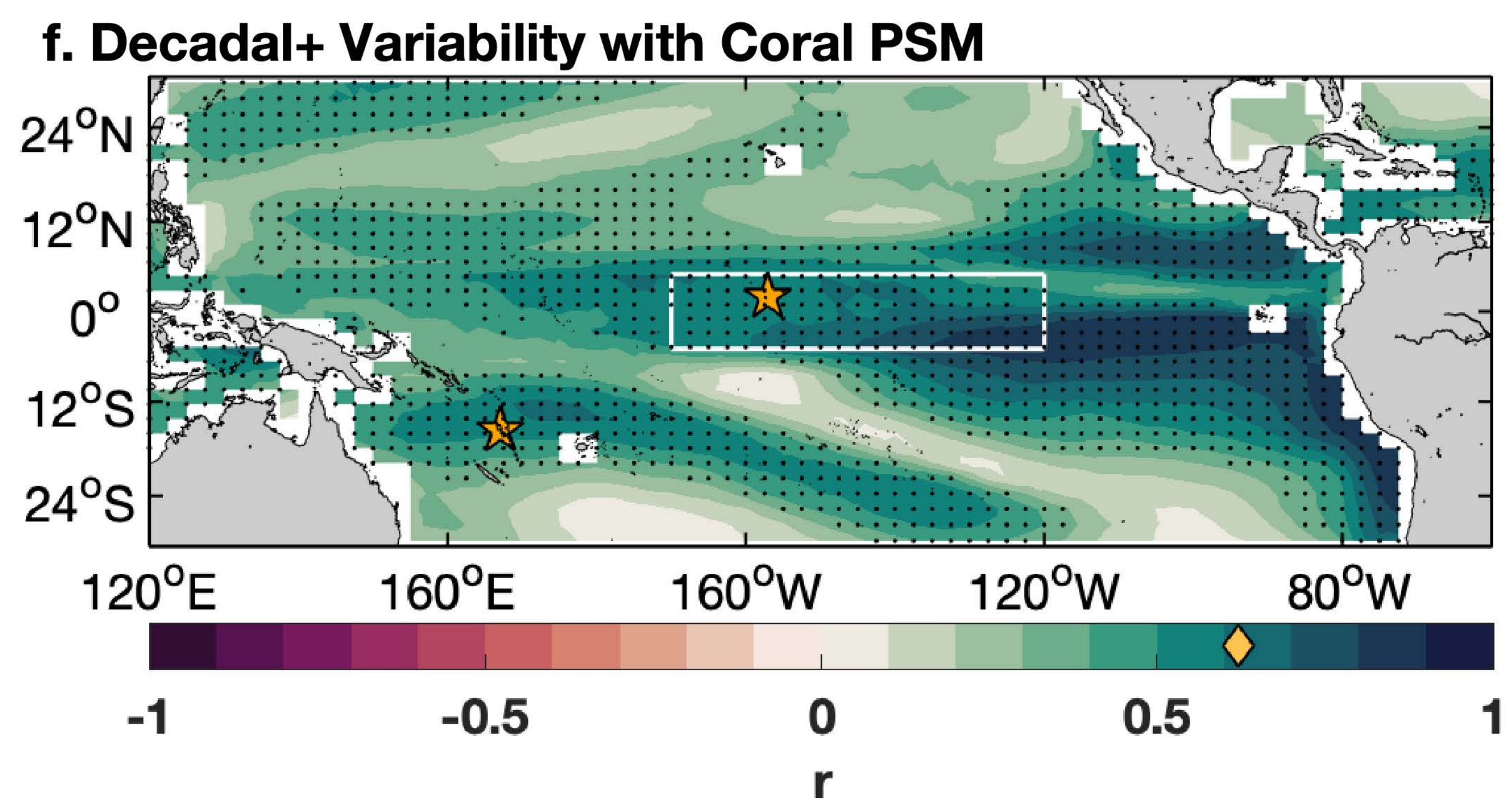
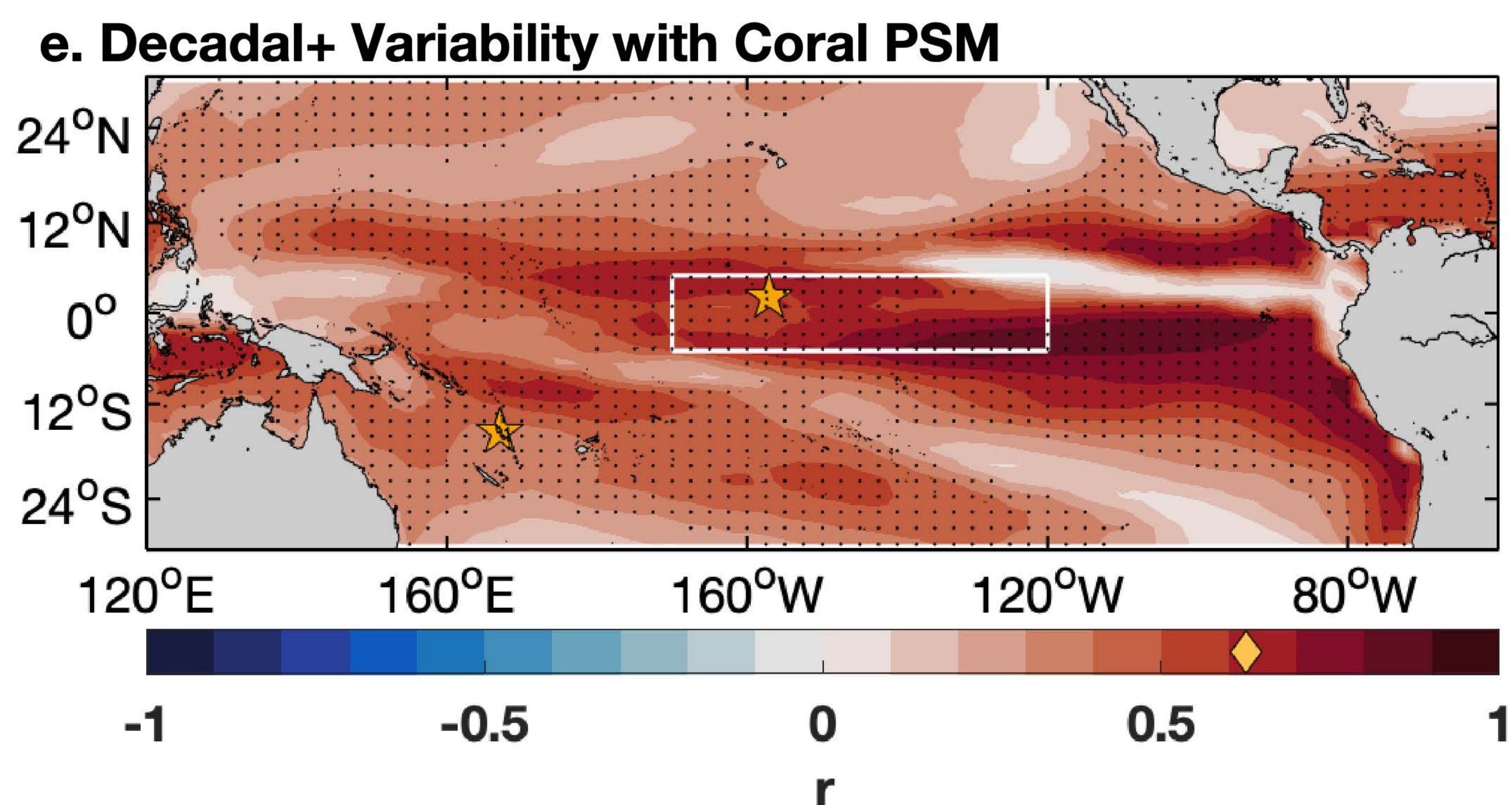
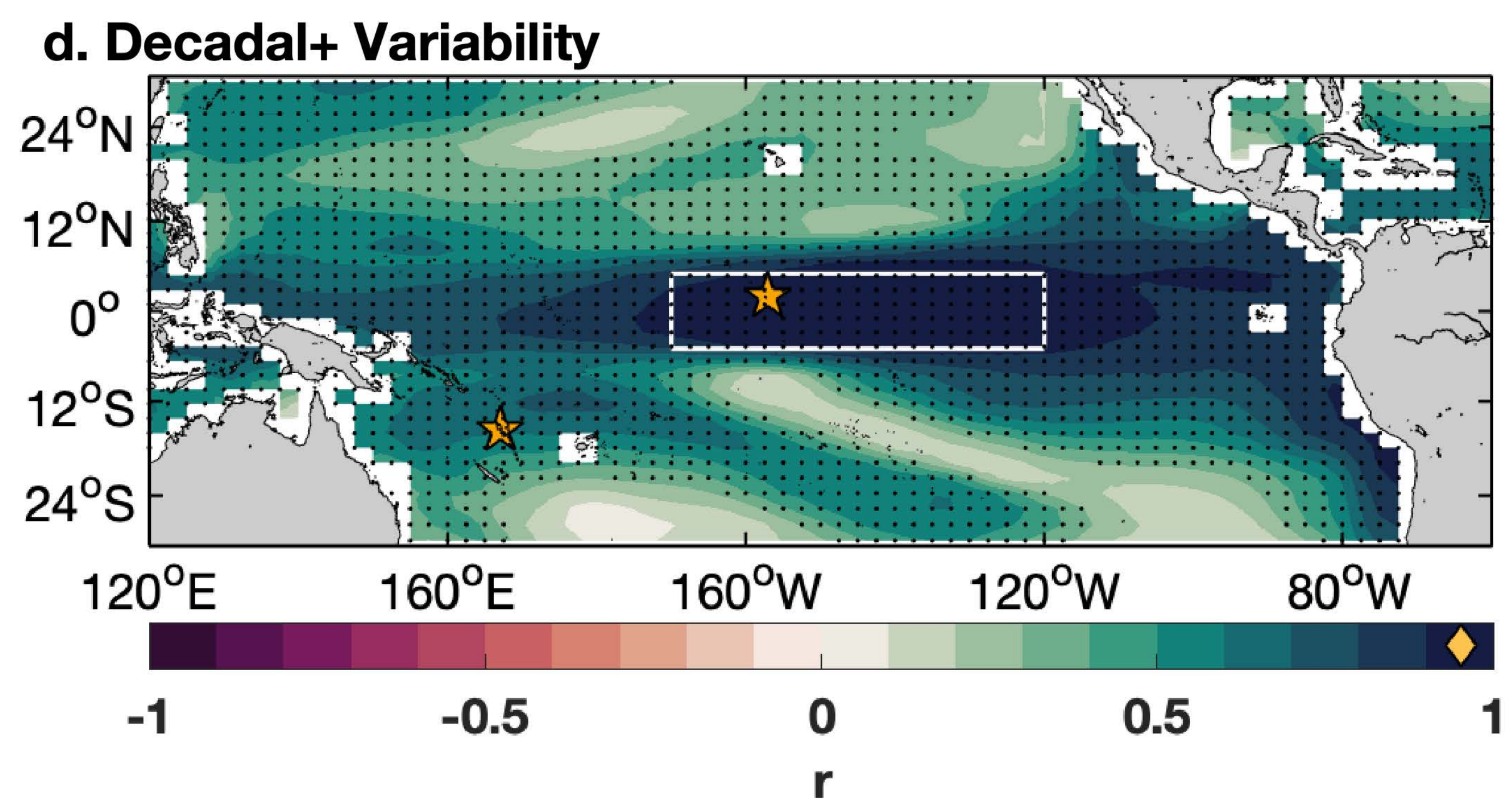
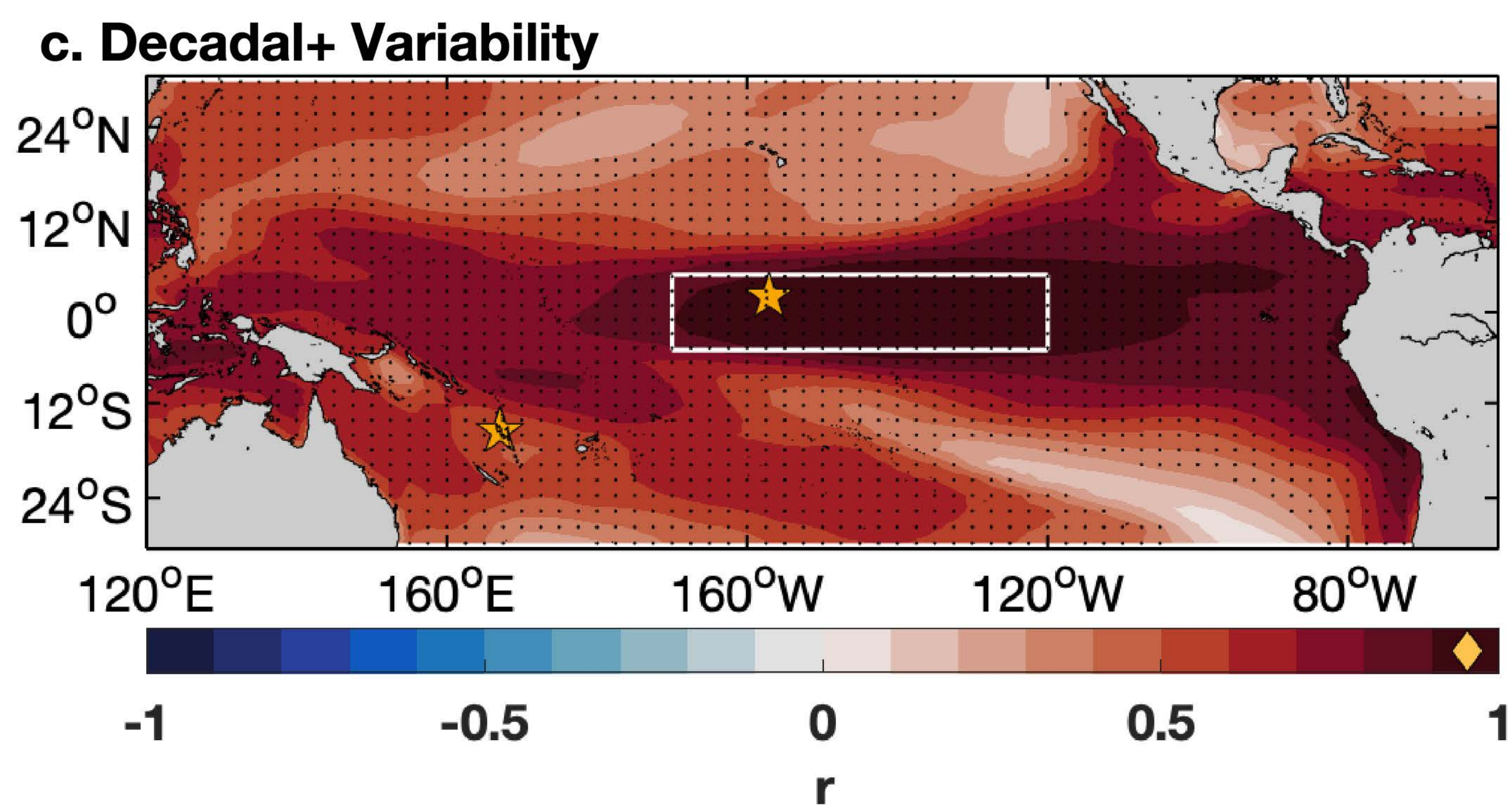
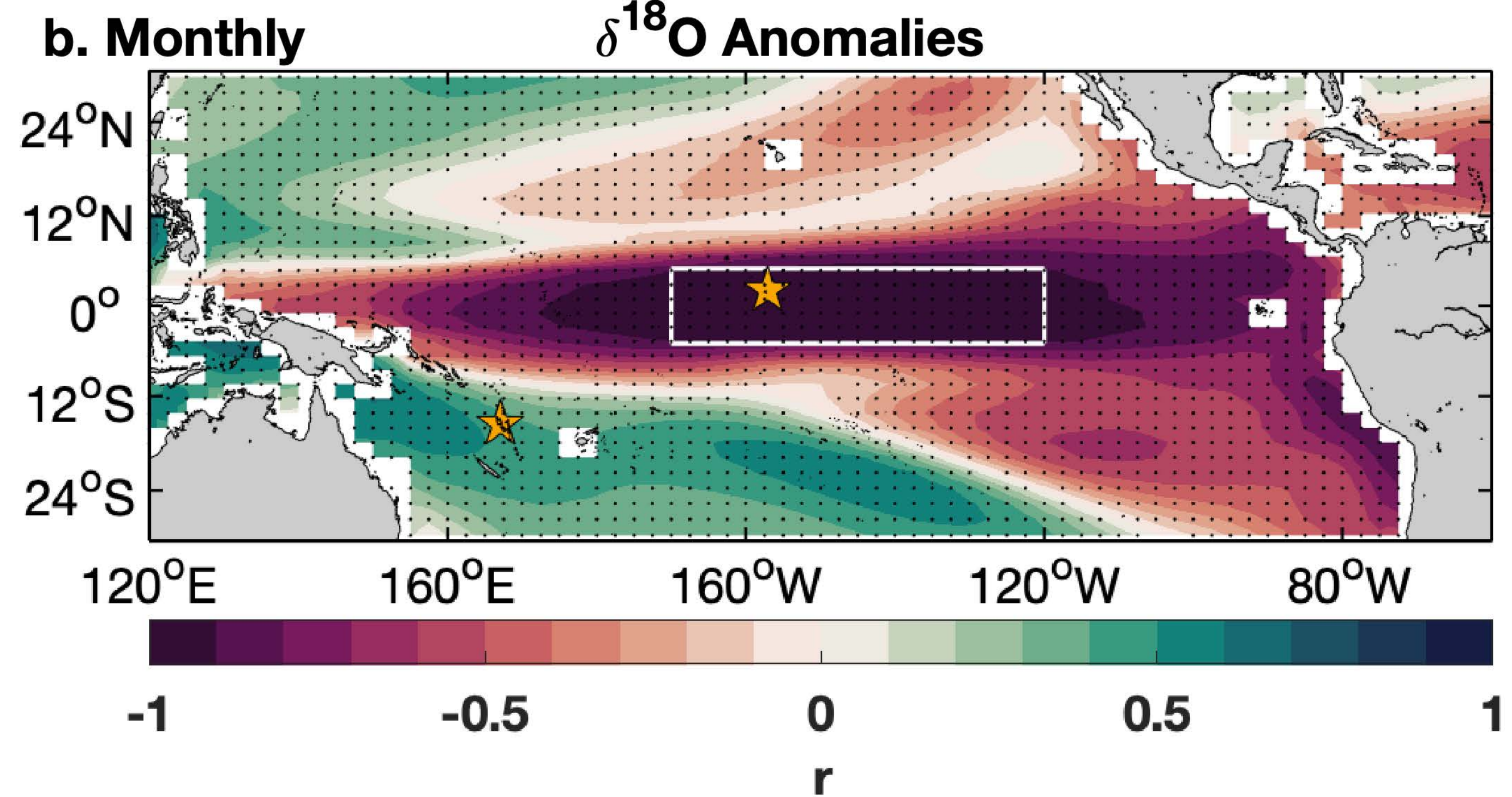
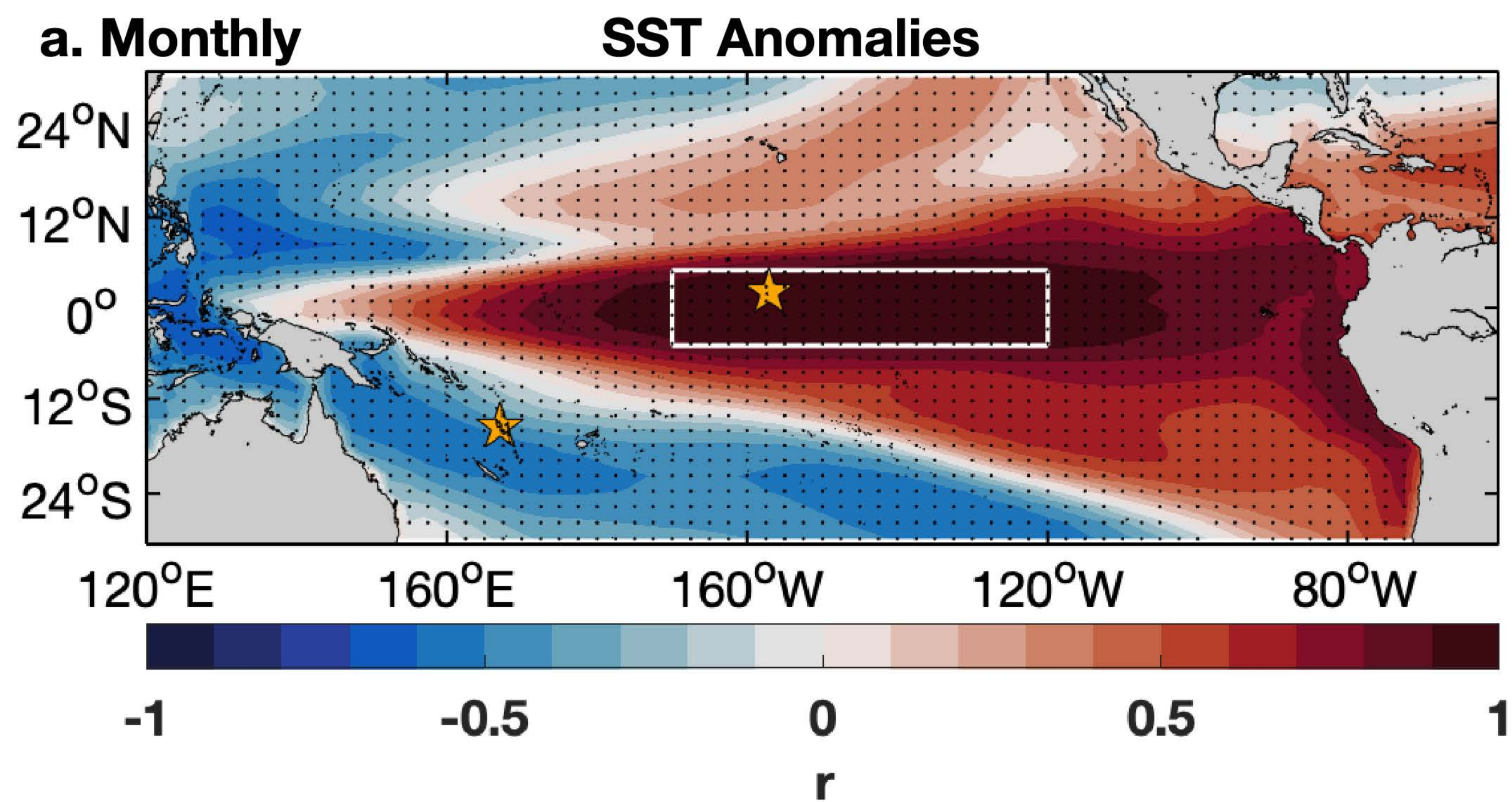


b.  $\Delta\delta^{18}\text{O}$

Change in Median Running SD









**Developing a coral proxy system model to compare coral and climate model estimates of changes in paleo-ENSO variability**

A. E. Lawman<sup>1,2\*</sup>, J. W. Partin<sup>1</sup>, S. G. Dee<sup>3</sup>, C. A. Casadio<sup>1</sup>, P. Di Nezio<sup>1</sup>, T. M. Quinn<sup>1,2</sup>

<sup>1</sup>Institute for Geophysics, Jackson School of Geosciences, The University of Texas at Austin, Austin, TX, USA.

<sup>2</sup>Department of Geological Sciences, Jackson School of Geosciences, The University of Texas at Austin, Austin, TX, USA. <sup>3</sup>Department of Earth, Environmental and Planetary Sciences, Rice University, Houston, TX, USA.

**Contents of this file**

Figures S1 to S2

**Introduction**

The supporting information includes two figures that demonstrate the age model algorithm (Section 2.5.2) for mean-removed pseudocoral  $\delta^{18}\text{O}$  ( $\Delta\delta^{18}\text{O}_{\text{pseudocoral}}$ ). Selected sites include Kiritimati in the central equatorial Pacific (2°N, 157°W) and Vanuatu in the southwest Pacific (16°S, 167°E). Pseudocoral  $\delta^{18}\text{O}$  is forward modeled as a linear combination of sea-surface temperature and salinity using the coral sensor model of *Thompson et al.* [2011] (Section 2.3.1). Surface temperature and salinity data come from the CESM Last Millennium Ensemble 850 control [*Otto-Bliesner et al.*, 2016] (Section 2.1). Refer to the Section 2.5.2 in the main text for age modeled SST derived from coral Sr/Ca ( $\text{SST}_{\text{Sr/Ca}}$ ).



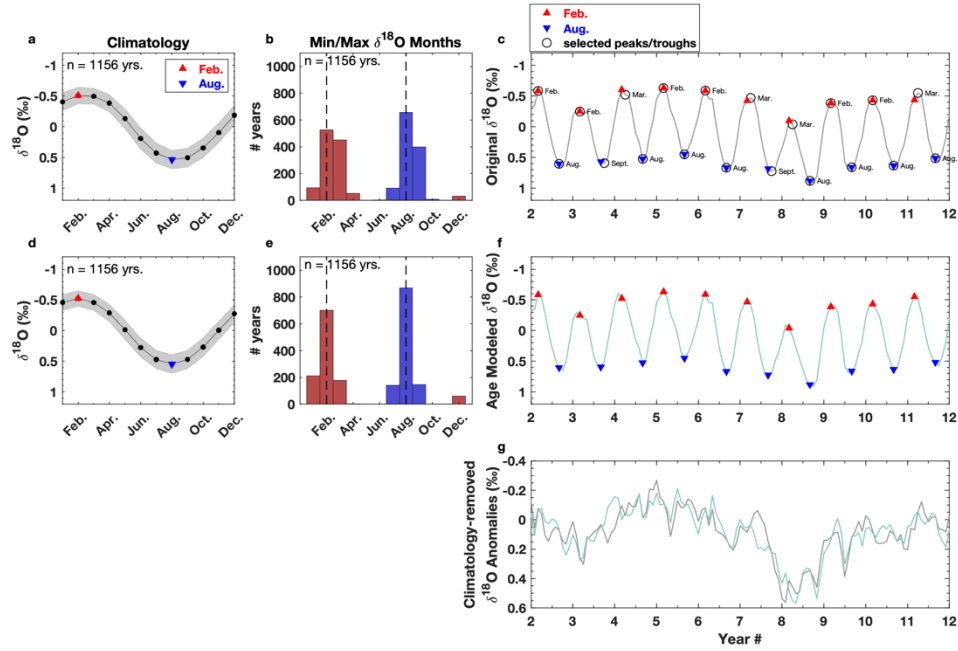


**Figure S1.** Age modeling  $\Delta\delta^{18}\text{O}_{\text{pseudocoral}}$  at Vanuatu. Same as Figure 4 in the main text except for forward modeled  $\Delta\delta^{18}\text{O}_{\text{pseudocoral}}$  at the model grid point closest to Vanuatu. The histograms in (b) and (e) indicate the months of the minimum (red bars) and maximum (blue bars)  $\Delta\delta^{18}\text{O}_{\text{pseudocoral}}$  values for each individual year in the (b) original (unperturbed) and the (e) age modeled  $\Delta\delta^{18}\text{O}_{\text{pseudocoral}}$  output.

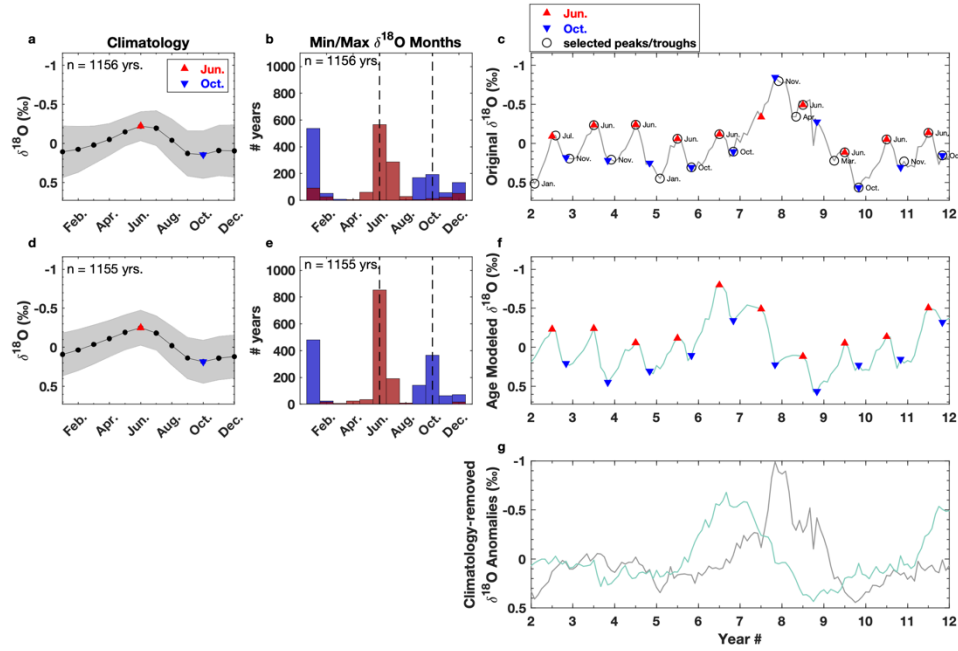


**Figure S2.** Age modeling  $\Delta\delta^{18}\text{O}_{\text{pseudocoral}}$  at Kiritimati. Same as Figure 4 in the main text except for forward modeled  $\Delta\delta^{18}\text{O}_{\text{pseudocoral}}$  at the model grid point closest to Kiritimati. The histograms in (b) and (e) indicate the months of the minimum (red bars) and maximum (blue bars)  $\Delta\delta^{18}\text{O}_{\text{pseudocoral}}$  values for each individual year in the (b) original (unperturbed) and the (e) age modeled  $\Delta\delta^{18}\text{O}_{\text{pseudocoral}}$  output.